ELASTIC SURFACE WAVES GUIDED BY A RECTANGULAR OVERLAY

C.C. Tu, B.S. (Nat. Chekiang U.), M.S. (U. of Conn.)

ELASTIC SURFACE WAVES GUIDED BY A RECTANGULAR OVERLAY

by

Cheng Chun Tu,
B.S. (National Chekiang Univ.), M.S. (Univ. of Connecticut)

A thesis submitted to the Faculty of Graduate Studies and Research
in partial fulfillment of the requirements for the degree of
Doctor of Philosophy.

Department of Electrical Engineering,
McGill University,
Montreal, Quebec.

July, 1972.

ABSTRACT

An analytical method of solution has been developed for elastic surface waveguides where the guiding structure consists of an overlay of rectangular cross section superimposed on the surface of an infinite substrate. When the overlay is thin with respect to the wavelength various perturbation techniques can be used to determine the dispersion curves of such guides. Here two kinds of generalization are implemented : one concerns geometry in that the thickness of the overlay as well as the width can be arbitrary , thus allowing an investigation of the effects of overlay thickness on the dispersion curves and on the displacement distributions in the overlay and in the substrate ; the other concerns materials in that the material combination of overlay and substrate can be freely chosen under the guiding requirement that the shear velocity of the overlay must be lower than or equal to that of the substrate.

The polynomial variational approaches for plates and rectangular rods and the exponentially-crested surface waves are employed in the analysis together with a new procedure which treats the boundary conditions at the interface. The infinite series introduced into the displacement distribution can be truncated at different orders depending on the accuracy desired and on the tolerable computational complexity. Two different orders of truncation are discussed and numerical results for several modes are presented showing the dispersion and displacement behaviour for several pairs of materials with a detailed discussion of the results for a gold overlay on a fused quartz substrate. Results are in very good agreement with the infinite layered geometry, the thin-film guide and the topographic ridge guide, all of which can be considered as limiting cases of the analysis and all of which have extensive experimental verification.

ACKNOWLEDGEMENTS

The author wishes to express his sincere gratitude to Dr. G.W. Farnell for his supervision of the study and for his help in the preparation of the thesis.

Special thanks are due to Dr. M.S. Kharusi for the Calcomp program to plot the distortion of the waveguides, to the staff of the McGill Computing Centre for cooperation, to Messrs. M.S. Hsieh, C.C. Huang and M.F. Yen for assistance of programming, to Mr. J. Martucci for a reading of the final draft and to Mrs. P. Hyland for typing most of the chapters.

The research fellowships awarded by the National Research Council and the Northern Electric Company are gratefully acknowledged.

TABLE OF CONTENTS

PREFACE

LIST OF SYMBOLS

Notations	Description
(Part 1. Subscripts and Superscripts)	
a,b,c,d	= 1 and 3 (for coordinate subscripts)
i,j,k,l	= 1, 2, 3 (for coordinate subscripts)
I,J,K,L	= 1,2,3,4,5 (for labels of eigenvalues)
n,m,p,q	= 0,1,2, ... (for specified orders of terms of a serie
N,M	= 1,2, ... 15 (for labels of homogeneous equations)
(Part 2. General Notations)	
a	Prefix to mode designation for "antisymmetric"
$a_i^{(n)}$, a_J	Weighting factors
$A_i^{(n)}$	Amplitudes of the polynomial (plate) displacements $u_i^{(n)}$
$\hat{A}_i^{(n,m)}$	Amplitudes of the polynomial (bar) displacements $\hat{u}_i^{(n,m)}$
A_{IJ}	Eigenvectors
$\hat{A}_N$	Column-vector notation for $\hat{A}_i^{(n,m)}$, antisymmetric moc
$\hat{b}_i$	Group notations, Equations (6.4) and (6.6)
c_{ijkl}, $\hat{c}_{ijkl}$	Elastic tensors of the substrate and overlay respectively
C_n	Legendre polynomial constants of integration
d_{jk}	Group notations (Appendix A)

D_{ni}	Group notations (Appendix A)
$E, E^{(n)}$	Abbreviations, Equations (2.1) and (2.5)
f_A, f_S	Partial matrices of the antisymmetric and symmetric modes respectively
f_{NM}	Elements of the partial matrix f_A or f_S
$(f_A)_{NM}, (f_S)_{NM}$	Elements of the matrices f_A and f_S respectively
$F_{2j}^{(n)}$	Polynomial tractions for Region II
$\hat{F}_{2j}^{(n,m)}, \hat{F}_{3j}^{(n,m)}$	Polynomial tractions for the overlay
g_A, g_S	Partial matrices of the antisymmetric and symmetric modes respectively
g_{NM}	Elements of the partial matrix g_A or g_S
$(g_A)_{NM}, (g_S)_{NM}$	Elements of the matrices g_A and g_S respectively
$G_{3j}^{(n)}$	Polynomial stresses
G_J	Column-vector notation for $G_{3j}^{(n)}$
h_2, h_3	Semi-width and semi-thickness of the overlay
H_2, H_3	Width parameter $k\,h_2$ and thickness parameter $k\,h_3$
i	$\sqrt{-1}$
I_n	Increments of $k_t h_3$ for 1 % increase of r_n
$J_{jk}^{(n)}, J'_{jk}$	Group notations, Equation (7.21)

k	Propagation real phase constant
k_t	$\omega / v_t = 2\pi / \lambda_t$
L	Notation of Love-like mode
$m_{ij}^{(n)}$, m'_{jk}	Eigenvectors of the (1,1) - approximation
$M_{jk}^{(n)}$, M'_{jk}	Submatrices of the equations of motion of the (1,1) - approximation
P_n	Legendre polynomial of the transverse coordinate, order n
Q_n	Legendre polynomial of the vertical coordinate, order n
R	Notation of Rayleigh-like mode
r_n	Adjustment parameters
s	Prefix to mode designation for "symmetric"
S_{ij}	Strain tensor
$S_{ij}^{(n)}$	Polynomial (plate) strains
$\hat{S}_{ij}^{(n,m)}$	Polynomial (bar) strains
$\hat{S}_M$	Column-vector notation of $\hat{A}_i^{(n,m)}$, symmetric mode
t	Temporal coordinate
$t_{jk}^{(n)}$, t'_{jk}	Coefficients of the polynomial stresses $G_{3j}^{(n)}$ in terms of $a_i^{(n)}$ in the (1,1) - approximation
T_{ij}, $\bar{T}_{ij}$, $\hat{T}_{ij}$	Stresses of Regions II, III and I respectively

$T_{ij}^{(n)}$	Polynomial (plate) stresses
$\hat{T}_{ij}^{(n,m)}$	Polynomial (bar) stresses
u_i , $\hat{u}_i$, $\bar{u}_i$ $(\pm)$	Displacement vectors of Regions II, I and III $(\pm)$ respectively
$u_{i,j}$	$= \partial u_i / \partial x_j$
$\ddot{u}_i$	$= \partial^2 u_i / \partial t^2$
$u_i^{(n)}$	Polynomial (plate) displacements of the substrate, order n
$\hat{u}_i^{(n,m)}$	Polynomial (bar) displacements of the overlay, order n,m
v	Phase velocity
v_t , $\hat{v}_t$	Shear velocities of the substrate and overlay respectively
V_n	Adjusted normalized velocity for the substrate
V_{nm}	Adjusted normalized velocity for the overlay
x_i	Cartesian coordinates (see Figure 1)
X	Exponential propagation function
$Y_{(\pm)}$	Exponential decay factor along the transverse directions
Z, Z_J , $\bar{Z}_{n}$ (j)	Exponential decay factors down to the depth of the substrate

(Part 3. Greek Notations)

α, α_J , α_{ni}	Attenuation constants down to the depth of the substrate
β	Attenuation constant along the transverse direction in Region III

γ_{11} , γ_{12}	Group notations, Equation (7.7)
δ , $\hat{\delta}$	$= (\lambda + 2\mu)/\mu$, $(\hat{\lambda} + 2\hat{\mu})/\hat{\mu}$ respectively
δ_{ij} , δ_{nm}	Kronecker deltas
ϵ_{ni}	Group notations, Equation (3.7)
θ_n	Group notations, Equation (3.6)
λ , $\hat{\lambda}$	Lamé constants of the substrate and overlay respectively
λ, λ_t , λ_R	Wavelength, shear wavelength and Rayleigh wavelength
μ, $\hat{\mu}$	Lamé constants of the substrate and overlay respectively
ζ	$= \delta - 1$
ρ , $\hat{\rho}$	Densities of the substrate and overlay materials respectively
$\tau_{jk}^{(n)}$, τ_{jk}'	Coefficients of the polynomial stresses $G_{3j}^{(n)}$ in terms of $\hat{A}_j^{(n,m)}$ in the (1,1) - approximation
φ_n	Group notations, Equation (7.18)
ω	Angular velocity

CHAPTER I

INTRODUCTION

1. General Background

Interest in microwave acoustics (or simply microsonics) has increased markedly in recent years and the reason for this great surge is both physical and technological. Acoustic waves propagate with velocities typically of five orders of magnitude slower than electromagnetic waves so that acoustic components such as resonators, filters and delay circuits using such waves can be 10^5 times smaller in size than their electromagnetic counterparts for the same frequency. For example, a centimeter length of crystal can provide a delay path at a frequency of 3 GHz of approximately 10^4 wavelengths. For some time, devices employing the propagation of elastic bulk waves in solids have been constructed for the generation and delay of signals, and in the mid-1960's a number of signal-processing applications could be performed because of the discovery of new bulk-wave phenomena involving semiconductors (White, 1962) and magnetic materials (Eshback, 1962) and acoustooptical interactions (Gordon, 1966). But it is clearly elastic surface waves which have aroused the greatest interest and provide the key to certain miniature signal processing systems. Such surface waves possess inherent advantages in that they are accessible to be tapped, guided or amplified on the surface of the substrate and in that the fabrication techniques can be a duplication of those used for integrated circuitry. A review article by White (1970) provides a general survey and a comprehensive bibliography of the whole field of elastic surface waves. In considering these signal-processing devices, he indicated that it might be most advantageous to do a variety of signal-processing steps in a single package once the signals were in elastic form and envisioned a receiver having the entire processing from RF input to IF output performed with surface waves on a single crystal plate with suitable overlays.

Recently, progress has been reported in many aspects of surface-wave technology. For example, by the addition of internal surface-wave amplifiers to long-path delay circuit, the time delay available is extended into the 10 millisecond range with frequencies of 100 MHz and higher (Shaw , 1971). Monolithic surface-wave amplifiers (Goldren, 1971) have been constructed with measured electronic gains of 50 dB/ cm up to 2 GHz and good agreement with the theory.

For the development of the microwave acoustic circuits envisaged by Stern (1969), elastic waveguides are of fundamental importance. Oliner (1971 a) has also noted that the full potential of the elastic surface waves will be realized only when the surface waveguides are thoroughly understood and exploited. This thesis deals with the propagation characteristics of elastic surface waveguides and an analytical method is developed to solve for these characteristics in the most fundamental type of such waveguides.

Generally speaking, guided elastic waves are transmitted by bound media which contain free surfaces or interfaces forming reflecting walls, or a particular region where the velocity of the waves is slower than in the surroundings. The velocity of such guided waves depends upon the frequency of excitation, the mode of transmission, the elastic constants of the materials and the size and geometry of the medium. From this broad view, the fundamental example of a guided elastic wave is the Rayleigh surfave wave in a half-space, a single-mode, non-dispersive and non-radiating wave which is concentrated near the free surface because its velocity is lower than the velocities of the bulk waves in the medium. Rayleigh gave the theory for this mode of propagation in 1887.

A second waveguide example is the infinite plate in which the waves are confined and guided by two parallei free surfaces. In this geometry there are many different modes and they can be classified as shear-horizontal (SH) and longitudinal and shear-vertical (L + SV). The dispersion relation of the (L + SV) family, commonly known as the Rayleigh-Lamb equations (Rayleigh, 1889 ; Lamb, 1917), are quite complex and have usually been evaluated by numerical methods.

Another example of guided waves is provided by the layered geometry (Achenbach and Epstein, 1967 ; Farnell and Adler, 1972), i.e., a half-space substrate overlaid by a solid layer (infinite plate) of a different material. Depending upon the material combination and the layer thickness, Rayleigh modes, Love modes and Stoneley waves are possible. The last reference gives a review of the characteristics of these modes of propagation in thin layers and some are considered below in numerical examples as limiting cases of the analysis here.

In all the above cases, the waves propagate in a form somewhat like uniform sheets that extend to infinity, ideally, in the direction transverse to that of propagation and parallel to the boundary surface or surfaces. Mathematically, all the above can be formulated by an exact approach though numerical techniques may be required for the actual solutions. In a real guided wave, however, most of the energy of the waves must be confined to only a finite portion of the above sheet. Exact solutions are available for wave propagation in circular rods (Meeker and Meitzler, 1964), and although no exact solutions seem possible for rectangular bars, several workable approximate theories have been developed in recent years (Frazer, 1969 ; Medick, 1966 and 1968 ; Nigro, 1966 to 1969 ; Volterra, 1961) . However, in the desirable frequency range for microsonic applications, say from 10 MHz to 1 GHz, the cross-sectional dimensions of such bars would be of the order of microns and thus they would be too thin and too weak to be self-supporting. When substrates are added for support or as part of the propagation medium, the problem turns to the case we wish to consider in this analysis.

2. Rectangular-Overlay Elastic Surface Waveguides

The elastic surface waveguides of concern here consist of a rectangular overlay of one isotropic solid in welded contact with a substrate of a different material. This type of waveguide owes its guiding action to the presence of the overlay, which is chosen to have a shear velocity lower than that of the substrate. Thereby the region near the overlay has lower phase velocity than the surrounding free surface and thus waves are guided along the overlay.

Various types of elastic surface waveguides have been studied, analytically or experimentally, by Tiersten (1969), Oliner (1969 and 1971 b), Ash et al.

(1969) and Waldron (1969 to 1972). All of these, implying some restrictive simplification either of geometry or of material, as will be seen below, can be considered as limiting cases of the type of waveguide considered here ; while the present analysis is approximate, it has fewer restraints than the earlier analyses.

The thin-film waveguide was proposed by Seidel and White (1967) and analyzed by Tiersten (1969) under the assumption that the overlay was very thin relative to the wavelength so that the entire effect of this thin-film overlay could be treated as a nonzero homogeneous boundary condition at the surface of the substrate, and the variation of the particle displacements in the overlay could be ignored. A complementary analysis using a similar assumption has been given by Adkins and Hughes (1969). No such restriction is used in the analysis here, the thickness of the overlay as well as its width can be arbitrary. It will be shown that this generalization of geometry can be extended to include two extreme cases, the layered configuration which results when the width of the overlay approaches infinity at a finite thickness, and the end-plate problem when the thickness approaches infinity at a finite width. These limiting cases form useful checks for the theory. Oliner (1971 b) has used an analytical approach for elastic surface waveguides, called the microwave network method, but it appears to be valid only for an overlay of very high or very low thickness-to-width ratio and therefore it still belongs to a limiting case of the present problem.

Another generalization in the analysis here concerns materials. The material combination of overlay and substrate is limited only by the guiding requirement that the shear velocity of the overlay must be equal to or lower than that of the substrate, and can be freely chosen without imposing the restriction of a perfectly rigid substrate as introduced by Waldron (1971). However, solutions for the almost perfectly rigid substrates can be obtained from this more general analysis by using artificial substrates of increasing rigidity. Moreover, by using the same material for the overlay and the substrate as a special case of the material combination, the analysis includes the topographic ridge waveguides of Ash et al (1969).

The derivation of the fundamental equations in this analysis is generalized so that they can be directly applied or easily converted for anisotropic materials. However, the detailed exposition and application of the theory here is for materials that are homogeneous, isotropic and linearly elastic solids. Dispersion curves of the first Rayleigh-like mode, the first Love-like mode and some higher modes are obtained and displacement patterns are provided in order to show the mode characteristics, a thorough understanding and complete knowledge of which is obviously the first necessary step toward the study and development of this type of waveguides.

CHAPTER II

PREPARATION OF THE ANALYSIS

1. Fundamental Consideration

Physically there are only two regions of different materials in the wave-guide problem under consideration, namely, a long overlay of rectangular cross-section and a half-space substrate. However, the substrate is further divided for mathematical purposes into the regions I, II, III (+) and III (−) shown in Figure 1. Before proceeding with the analysis of this problem as a whole, it is illustrative and helpful to consider these regions separately in order to grasp some of their basic characteristics as propagation media.

Let us begin with the central Region II. If isolated, Region II alone is a semi-infinite plate with boundaries formed by the two parallel sides and the top edge, and within this Region we can use the two-dimensional variation theory of wave propagation in plates developed by Mindlin and Medick (1959). The particle displacement fields are then chosen to be a product of a series of Legendre polynomials in the x_2 - coordinate and factors decaying exponentially with depth $(-x_3)$.

Since the overlay Region I is essentially a rectangular bar, we can use the one-dimensional variation theory of wave propagation in bars of rectangular cross-section, developed by Medick (1966 and 1968), which is really an extension of the two-dimensional theory of plates. Modification is needed, however, due to the fact that here the bottom boundary is no longer traction-free but constrained because it is in contact with the substrate, a fact that complicates the analysis. The particle dis-

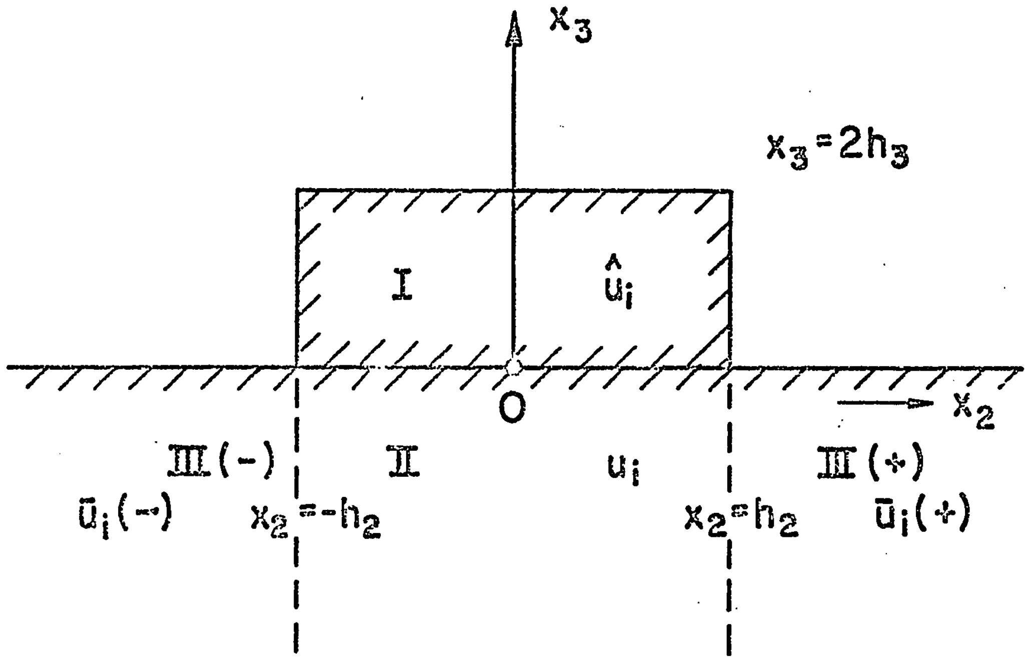

Fig. 1. Geometry for rectangular overlay waveguide. Region I is the overlay, Regions II and III form the substrate. Boundaries at $x_2 = \pm h_2$ are for mathematical convenience.

placement fields for this region are chosen to be a doubly infinite series of Legendre polynomials of the thickness and width coordinates (x_2 and x_3) of the overlay.

The side Regions III (+) and III (−) are somewhat more difficult to cope with analytically than the former two. Each region, if isolated, is a quarter-space so that concentration of waves at the corner would be expected. However, mathematically this seems to be the simplest configuration which cannot be solved by an exact approach or even by the approximate methods that are workable for rectangular bars. In order to treat these side regions, therefore, some simplified but reasonable procedure must be introduced. The main points of the treatment adopted here for these regions are the following : first, the same exponential decay factors for the depth coordinate (x_3) as employed in the central Region II are used in Region III, a necessary step in order to match the displacements exactly along the entire interfaces between Regions II and III when considering all regions together as a whole ; and second, to ensure that the distribution of the wave is confined laterally near the overlay, the amplitude is assumed to decay exponentially with x_2 measured away from Region II − Region III interfaces, and the form of the decay factor is adopted from a result of the so called "exponential-crested surface waves" given in Tiersten's analysis (1969). The particle displacement fields of these side-regions then consist of an infinite series of products of the two decay factors above.

In consideration of the propagation medium as a whole, the solutions in the four regions have the same propagation factor and are matched so that the displacements are continuous at each point on the interfaces between the regions. The traction-free conditions on the free surfaces of Region III are approximated implicitly through the use of the exponential-crested surface waves, but all of the other boundary conditions of stress - the traction-free conditions on the top and the two sides of the overlay and the continuity of stresses across all interfaces between regions - are introduced into the integral traction terms of two variational equations of motion, one for Region I and the other for Region II.

2. Description of Variational Theories

The basic methods used in this analysis are variational theories which have been successfully developed for isolated plates and rectangular bars. Historically the two-dimensional equations in a variational theory for plates were deduced from the three-dimensional equations of elasticity by a procedure, based on the series expansion method of Poisson (1829) and Cauchy (1828) and the integral theorem of Kirchhoff (1850). But the early authors were interested only in low frequencies and included just enough terms of order zero of the series for the purpose at hand. It was more than one hundred years later that Mindlin (1955) worked out the detailed exposition of a power series method and its application to approximations of orders zero and one. Mindlin and Medick (1959) revised the theory by introducing Legendre polynomials to take advantage of orthogonality, and later, Medick (1966) extended the concept and developed the one-dimensional equations for rectangular bars.

The main procedure of the two-dimensional theory for infinite plates consists of : (i) expanding the displacements in the plate in a series of Legendre polynomials of the thickness coordinate in a variational integral of motion that uses the ordinary differential equations of motion as the argument of the integral, (ii) changing the three-dimensional displacement fields to be varied into the two-dimensional polynomial fields, (iii) integrating across the thickness of the plate and thus converting the ordinary three-dimensional differential equations of motion into an infinite series of two-dimensional ones and (iv) applying appropriate truncation to produce approximate equations for practical application.

The same general procedure applies to the one-dimensional theory for rectangular bars, however since the displacements are expanded in a doubly infinite series of Legendre polynomials of both the thickness and the width coordinates of the bar, a doubly infinite series of one-dimensional equations is obtained.

A general review of variational methods for the above theories is given in Chapter III in order to elucidate the procedures, and as will be seen, these procedures are used in almost the same form in this analysis until the boundary conditions at the interfaces are introduced.

3. Major Procedures of Analysis

In the complete mathematical analysis presented in the next chapter, the algebra is rather lengthy and laborious. Thus, in order to provide a general outline of the whole mathematical structure, the procedures can be grouped into the blocks given by the flow-diagram of Figure 2 which indicates the major steps for the dispersion calculation. The various algebraic symbols on the chart are defined in Chapter III and the reader may find it helpful to refer back to this chart as the analysis is developed.

Somewhat as in the case of the conventional exact methods used for elastic waves in the half-space, the plate, or the layered problem, there are three major steps in this waveguide solution. First, appropriate trial forms of the displacement fields for all the three regions (Blocks 1, 4 and 10 in Figure 2) are assumed. Second, the relations between the phase velocity and the decay constants to be used with the depth coordinate of the substrate (the eigenvalues in the analysis) are found for a given width parameter from the two-dimensional equations of motion for the central Region II (Block 5), and then the corresponding eigenvectors (Block 6) are obtained from which the displacement solutions are constructed with unknown weighting factors introduced (Block 7). Note that a relation for the decay along the width coordinate for Region III is also needed (Block 2) and the boundary conditions at the interfaces between Regions II and III are introduced (Block 3). This whole second step corresponds to the eigen-problem step in the exact approach. Finally, the thickness parameters are solved from the one-dimensional equations of motion for the overlay Region I at each of the given sets of phase velocities and width parameters, which are systematically chosen to complete the dispersion curves (Blocks 11 and 12). Note that in this final third step, which yields the dispersion and thus resembles the boundary-condition step in the exact method, the main equations are the one-dimensional equations

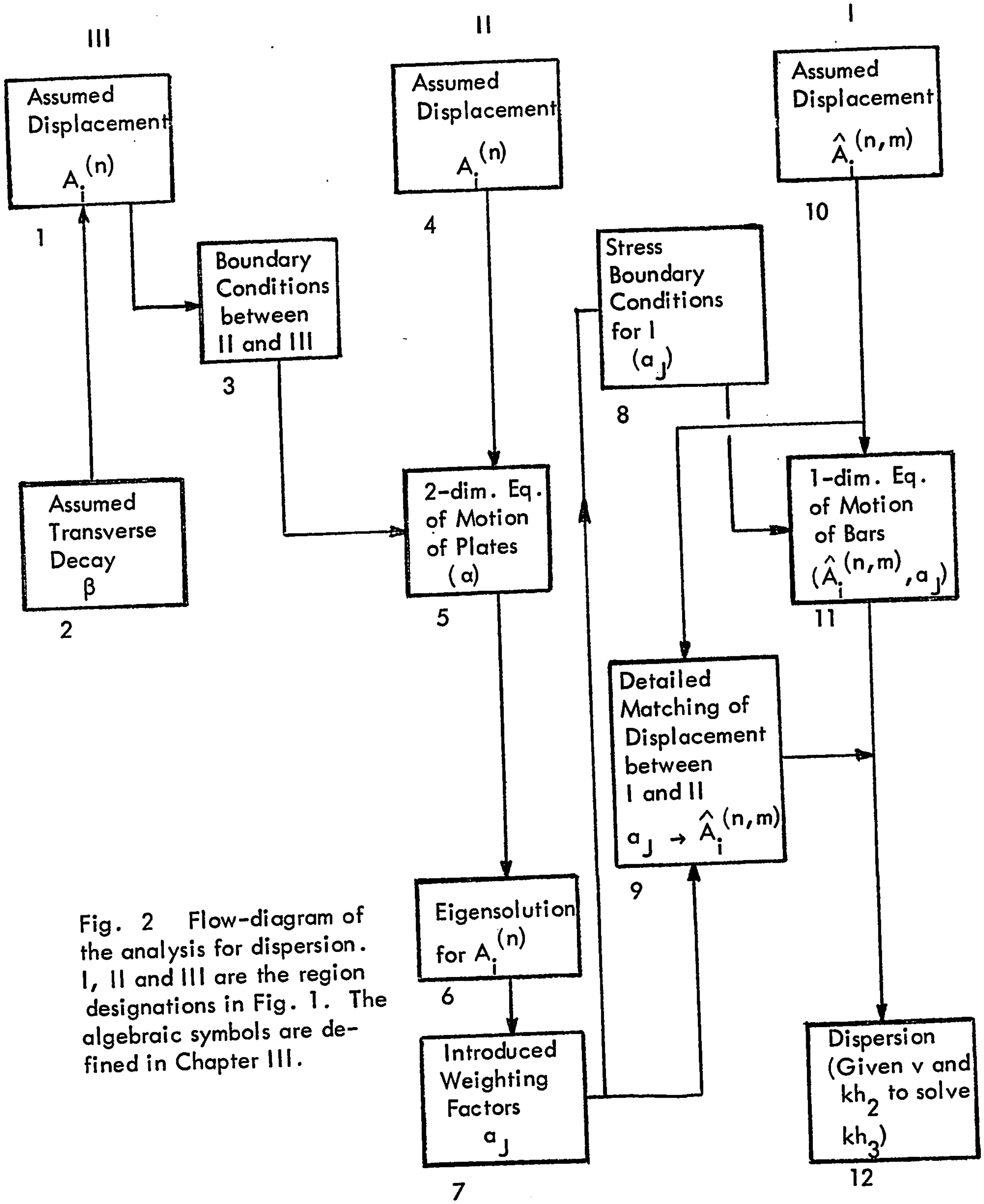

Fig. 2 Flow-diagram of the analysis for dispersion. I, II and III are the region designations in Fig. 1. The algebraic symbols are defined in Chapter III.

of motion forthe overlay Region I (Block 11). More specifically, the equations of motion and the boundary conditions are woven together in the solving procedures in the analysis as they are in the derivation of the one - and two-dimensional variational theories of rods and plates.

Now let us look at the flow-diagram in a different way. Blocks 4 to 7 are the procedures for Region II considered as an isolated plate, and Blocks 10 to 12 plus 8 for Region I treated as an isolated bar, however as might be expected, differences exist in the variational theories used here from those for isolated bars and plates. For an isolated plate, the assumed displacements in Block 4 would have no exponential dependence on the depth coordinate and all the traction boundaries in Block 3 would be free. Similarly all the boundaries in Block 8 for an isolated bar would be free. In other words, since the isolated cases are single-region problem with all boundaries free, while this overlay waveguide problem is one of a multi-connected region containing interfaces of discontinuity, it is obvious that the latter problem is more difficult to solve. Consequently the particular procedures in Blocks 8 and 9 which handle the difficulty of interfaces are of key importance in the analysis. These procedures constitute a novel step that may be applicable to other more general problem of multi-connected regions. As implied by Block 3, the same techniques are applied to the interfaces between Regions II and III, but here they are much simpler because the assumed displacements of Regions II and III are automatically matched at these interfaces.

To summarize, the important concepts that are central to the solution of this overlay waveguide problem are :

(i) modified plate modes are carefully assumed for the central region of the substrate and modified bar modes for the overlay,

(ii) exponential-crested surface waves are introduced as a simplified and reasonable assumption for the side-regions of the substrate,

(iii) a special procedure is provided to overcome the difficulty introduced by the various interfaces involved in the problem.

CHAPTER III

MATHEMATICAL ANALYSIS

In the previous chapter, the theories of plates, bars and exponentially crested surface waves with necessary modifications for the analysis of overlay wave-guide were briefly described and the major procedures of the analysis were outlined in Figure 2. This chapter develops successively the algebra for the assumed displacements (Blocks 1, 4 and 10 in Figure 2), the equations of motion with the boundary conditions of stress for Region II (Blocks 5, 6 and 7) and for Region I (Blocks 11 and 8), the important "detailed matching" step for the continuity of displacements at the bottom interface of the overlay (Block 9), and then the dispersion (Block 12). After that, the algebra for the displacements themselves is rather straight-forward and no block diagram has been shown.

The symbols used in the text are defined at their first occurrence and a list of them is summarized in the preface. Since all of the equations appear only in this chapter, their numbering is referred to the appropriate section, e.g., Equation (1.2) or simply (1.2) indicates the second equation in Section 1, Chapter III.

1. Assumed Displacements

For clarity, the designation of the subscripts and the superscripts is summarized as follows :

$i, j, k, l = 1, 2, 3$ and $a, b, c, d = 1$ and 3 only, are used as subscripts for various components measured along the coordinate axes.

$n, m, p, q = 0, 1, 2 \ldots$ are used as superscripts for the order of a term in a series.

$I, J, K, L = 1, 2, 3, 4, 5$ label the eigenvalues in Sections 3, 5, 6.

$N, M = 1, 2, \ldots \ldots 15$ label the homogeneous equations of Region I in Sections 4, 5, 6.

The trial forms of displacement for Regions I, II and III are assumed as :

$$\text{(I)} \quad \hat{u}_i = \sum_{n=0}^{\infty} \sum_{m=0}^{\infty} P_n Q_m \hat{u}_i^{(n,m)}, \qquad \hat{u}_i^{(n,m)} = \hat{A}_i^{(n,m)} X \qquad (1$$

$$\text{(II)} \quad u_i = \sum_{n=0}^{\infty} P_n u_i^{(n)}, \qquad u_i^{(n)} = A_i^{(n)} Z X \qquad (1$$

$$\text{(III)} \quad \bar{u}_{i\,(\pm)} = \sum_{n=0}^{\infty} (\pm 1)^n Y_{(\pm)} u_i^{(n)} \qquad (1$$

where common notations for Region I are "hatted" with a circumflex (^) and those of Region III with a bar (-). Whenever a double sign ($\pm$ or $\mp$) occurs in a formula or in subscripts, the upper sign refers to the right-side Region III (+) and the lower to the left III (−) . The function abbreviations and symbol notations involved are defined as follows.

$\hat{u}_i^{(n,m)}$ are the amplitudes of the product polynomial distributions of displacement in the plane of the bar cross-section or simply the polynomial (bar) displacements of order (n, m), which in turn have their own amplitudes $\hat{A}_i^{(n,m)}$. Similarly, $u_i^{(n)}$ are the amplitudes of the polynomial distributions of displacement across the plate thickness or simply the polynomial (plate) displacements of order n with their own amplitudes $A_i^{(n)}$. For the isolated bar and plate, the distribution of the displacement components can be expressed by the polynomials which are then used as the bases in the identification of bar and plate modes (Mindlin and Medick, 1959, Figure 1 ; Medick, 1968, Table 1). However, the mode identification for this overlay waveguide is more complicated and will be discussed later.

Some fundamental functions have been abbreviated for simplicity,

$$X = \exp [i k (x_1 - v t)] \qquad (1.4a)$$

$$Y_{(\pm)} = \exp [\mp \beta k (x_2 \mp h_2)] \qquad (1.4b)$$

$$Z = \exp (\alpha k x_3) \qquad (1.5a)$$

$$P_n = P_n (x_2 / h_2) \qquad (1.5b)$$

$$Q_n = Q_n (x_3 / h_3 - 1) \qquad (1.5c)$$

where

i	=	$\sqrt{-1}$,
k	=	real propagation constant,
v	=	propagating phase velocity,
h_2, h_3	=	semi-width and semi-thickness of the overlay (see Figure 1) ,
α, β	=	constants of attenuation along x_3 and x_2 respectively,
and P_n, Q_n	=	Legendre polynomials of order n .

The extra symbol Q_n for Legendre polynomials of the argument coordinate x_3 is introduced in addition to the conventional P_n , which is solely used for x_2 , in order to avoid confusion when their arguments are omitted for a clearer and neater formulation in the sequel. The Cartesian tensor notation and summation convention are adopted for all coordinate indices except those in parentheses. A comma followed by a coordinate subscript indicates the spatial derivative and a dot on top of a displacement symbol indicates the temporal derivative, i.e.,

$$u_{i,j} = \partial u_i / \partial x_j \quad \text{and} \quad \dot{u}_i = \partial u_i / \partial t \ .$$

The summation sign is retained for the indices other than those of the coordinates.

It is worth noting particularly that the form of the polynomial displacements $u_i^{(n)}$ for Regions II and III is the same in (1.2) and (1.3) . Under such an arrangement, since at the interfaces between Regions II and III, $x_2 = \pm h_2$, $P_n(\pm 1) = (\pm 1)^n$ and $Y_{(\pm)} = 1$, then

$$u_i = \bar{u}_{i(\pm)} \quad \text{at} \quad x_2 = \pm h_2 \tag{1.6}$$

which means that the boundary conditions of the continuity of displacement along the interfaces between Regions II and III have been automatically satisfied by the assumed forms of the displacements. To ensure that the continuity of displacement is satisfied at each point on the interface between Regions I and II, a rather strong "detailed matching" condition will be assumed later such that the corresponding terms for each order of Legendre polynomial P_n in the solutions for Regions I and II are equal at the interface.

2. Equations of Motion for Region II from a Variational Approach

In a conventional exact approach to solving an elastic propagation problem for a certain defined configuration with boundary conditions, it is common to start with the differential equations of motion,

$$E = T_{ij,i} - \rho \ddot{u}_j = 0 \tag{2.1}$$

where E is an abbreviation symbol, T_{ij} are the tensor stresses, ρ is the density of the medium and the u_i are the displacement fields. Equation (2.1) is just Newton's law stating that the divergence of stress is equal to the rate of change of momentum at each point within the defined region. This approach cannot be followed for the waveguide geometry here because Region II is part of a multi-connected region, a problem which cannot be solved exactly. Instead, we start with the integral,

$$\int_{x_1} \int_{-\infty}^{o} \int_{-h_2}^{h_2} E\, \delta u_i \, d x_2 \, d x_3 \, d x_1 = 0 \tag{2.2}$$

Here the E which vanishes identically within the defined boundaries is used as the argument of the integral. The integration is over the whole volume of Region II as shown from the limits of the triple integral. No definite limit is needed for x_1 which is the direction of propagation in the derivation but it is understood to be from $-\infty$ to ∞ as the medium is assumed to be very long in terms of the wavelength.

Now, substituting u_i from (1.2) into (2.2), changing the three-dimensional variation δu_i into a two-dimensional variation $\delta u_i^{(n)}$, integrating the term $T_{2i,2}$ by parts with respect to x_2 and using the orthogonal relation (Churchill, 1963)

$$(P_n , P_m) = \int_{-h_2}^{h_2} P_n P_m \, d x_2 = C_n h_2 \delta_{nm} , \quad C_n = 2/(2n+1) \tag{2.3}$$

where δ_{nm} is the Kronecker delta, (2.2) becomes

$$\int_{x_1} \int_{-\infty}^{o} [E^{(n)}] \, \delta u_i^{(n)} \, d x_3 \, d x_1 = 0 \tag{2.4}$$

With an arbitrary $\delta u_i^{(n)}$,

$$E^{(n)} = T_{aj,a}^{(n)} - T'^{(n)}_{2j} + F_{2j}^{(n)} - \rho C_n h_2 \ddot{u}_i^{(n)} = 0 \quad (2.5)$$

wherein

$$T_{ij}^{(n)} = \int_{-h_2}^{h_2} T_{ij} P_n \, d x_2 \quad (2.6)$$

$$T'^{(n)}_{2j} = \int_{-h_2}^{h_2} T_{2j} P_{n,2} \, d x_2 \quad (2.7)$$

$$F_{2j}^{(n)} = [T_{2j} P_n]_{x_2 = -h_2}^{x_2 = +h_2} \quad (2.8)$$

The differential of the Legendre polynomials in (2.7) can be expressed as

$$P_{n,2} = \sum_{p=1,3}^{n} (2 / C_{n-p} h_2) P_{n-p} \quad (2.9)$$

where the summation index p indicated covers odd integers only from 1 to the upper limi When the order of n becomes large, this term introduces complications, but fortunately a good approximation can be obtained for n = 0, 1, 2. Substituting (2.9) into (2.7) and then into (2.5), gives the stress equations of motion for Region II,

$$T_{aj,a}^{(n)} - \sum_{p=1,3}^{n} (2 / C_{n-p} h_2) T_{2j}^{(n-p)} + F_{2j}^{(n)} - \rho C_n h_2 \ddot{u}_j^{(n)} = 0 \quad (2.10)$$

These are the equations in a variational approach which replace the differential equations (2.1) of the conventional wave approach. More specifically, a set of three equations (2.1) of the actual displacements u_i and stresses T_{ij} are transformed into the infinite sets of equations of order n ($n = 0, 1, 2, \ldots \infty$), each containing three equations of the polynomial (plate) displacements $u_i^{(n)}$ and stresses $T_{ij}^{(n)}$. In the following, it is desirable to have every term of (2.10) expressed in terms of the polynomial displacements $u_i^{(n)}$.

Substituting u_i of (1.2) into the ordinary equations of strain,

$$S_{i,j} = \frac{1}{2}(u_{i,j} + u_{j,i}) \tag{2.11}$$

and defining

$$S_{ij} = \sum_{n=0}^{\infty} P_n S_{ij}^{(n)} \tag{2.12}$$

we get the polynomial strains,

$$S_{ij}^{(n)} = \frac{1}{2}\left[u_{i,a}^{(n)}\,\delta_{aj} + u_{j,a}^{(n)}\,\delta_{ai} + (2/C_n h_2)\sum_{p=1,3}^{\infty}(u_i^{(n+p)}\,\delta_{2j} + u_j^{(n+p)}\,\delta_{2i})\right. \tag{2.13}$$

Accordingly, the ordinary stresses can be expressed as

$$T_{ij} = c_{ijkl}\, S_{kl} = \sum_{p=0}^{\infty} P_p\, c_{ijkl}\, S_{kl}^{(p)} \tag{2.14}$$

where the c_{ijkl} are the elastic constants in tensor form. Substituting (2.14) into

(2.6) and using (2.3), gives the polynomial stresses,

$$T_{ij}^{(n)} = C_n h_2 c_{ijkl} S_{kl}^{(n)} \tag{2.15}$$

Up to this point, the derivation follows exactly that of Mindlin and Medick (1959) except that we are doing differential and integral operations with respect to x_2 or x_3 directly instead of their x_2/h_2 or x_3/h_3, because here exponential functions are also used together with the Legendre polynomials, thus some equations are slightly different in appearance from theirs.

It is now assumed that the stresses on the interfaces between Regions II and III represented by the traction terms $F_{2j}^{(n)}$ of (2.8) in (2.10) are given by the stresses in the side-region III, in other words that the boundary conditions of stress on the interfaces, $T_{2j} = \bar{T}_{2j}$ at $x_2 = \pm h_2$, can be introduced into $F_{2j}^{(n)}$; then from (2.8)

$$F_{2j}^{(n)} = [\bar{T}_{2j} \; P_n]_{x_2=-h_2}^{x_2=+h_2} \tag{2.16}$$

The stresses at $x_2 = \pm h_2$ calculated from (1.3) in Region III are,

$$\begin{aligned} \bar{T}_{2j}(\pm h_2) &= c_{2jkl} \bar{u}_{k,l}(\pm) \\ &= \sum_{n=0}^{\infty} (\pm 1)^n \left(c_{2jka} u_{k,a}^{(n)} \mp \beta k c_{2jk2} u_k^{(n)} \right) \end{aligned} \tag{2.17}$$

Substituting (2.17) into (2.16) the final tractions become

$$F_{2j}^{(n)} = \sum_{p=0}^{\infty} \{ [1 - (-1)^{n+p}] \, c_{2jka} \, u_{k,a}^{(p)} - [1 + (-1)^{n+p}] \, \beta \, k c_{2jk2} \, u_k^{(p)} \} \tag{2.18}$$

The boundary conditions on the displacements at $x_2 = \pm h_2$ are automatically satisfied from the trial forms of the displacement (1.2) and (1.3), therefore both boundary conditions on the displacement and on the stress are actually involved in the derivation of (2.18).

By using (2.15), (2.13) and (2.18), equations (2.10) become the displacement equations of motion (2.19) for Region II in contact with Region III,

$$\begin{aligned} & C_n h_2 (c_{ajkb} \, u_{k,ba}^{(n)} - \rho \, \ddot{u}_j^{(n)}) + 2 \, c_{ajk2} \sum_{q=1,3}^{\infty} u_{k,a}^{(n+q)} \\ & - 2 \sum_{p=1,3}^{n} [c_{2jkb} \, u_{k,b}^{(n-p)} + (2/C_{n-p} \, h_2) \, c_{2jk2} \sum_{q=1,3}^{\infty} u_k^{(n-p+q)}] \\ & + \sum_{p=0}^{\infty} \{ [1 - (-1)^{n+p}] \, c_{2jka} \, u_{k,a}^{(p)} - [1 + (-1)^{n+p}] \, \beta \, k \, c_{2jk2} \, u_k^{(p)} \} = 0 \end{aligned} \tag{2.19}$$

3. Truncated (2,2) - Approximation for the Substrate

With a series solution it is necessary to decide upon the number of terms to be carried. It is convenient here to label the order of the approximation by the highest

Legendre polynomial used for each direction of Region I. Thus a (1,1) - approximation allows linear variation of particle displacements in the x_2 and x_3 directions within the overlay Region I and in the x_2 direction within the central Region II, while the (2, 2) - approximation allows quadratic variation for all the above directions.

It has been found that for reasonable estimates of the dispersion curves, the (1,1) - approximation is adequate and for this truncation most of the algebraic steps can be carried out explicitly, thus allowing direct numerical evaluation of the solutions. However, for investigation of the form of displacements, especially for the higher modes, it is desirable to go to a higher approximation and then it is not possible to do very much of the algebra explicitly and numerical search techniques have to be introduced. A reasonable compromise between computation time and usefulness of the solutions is provided by the (2,2) - approximation. Because of the symmetry of the problem about the vertical, central plane of the guide for isotropic materials, the equations may be divided into symmetric and antisymmetric modes which can then be treated independently.

We will proceed first with the (2,2) - approximation. On expanding (2.19) in such a way that n is 0, 1, 2 successively and keeping in mind that for any value of n employed the $n+q$, $n-p+q$, $n+p$ and p are allowed only to be 0, 1 or 2, the following nine homogeneous equations are obtained

$$-\beta k c_{2jk2} u_k^{(0)} + h_2 (c_{ajkb} u_{k,ba}^{(0)} - \rho \ddot{u}_j^{(0)}) + (c_{ajk2} + c_{2jka}) u_{k,a}^{(1)}$$

$$- \beta k c_{2jk2} u_k^{(2)} = 0$$

$$-(\beta k + \frac{1}{h_2}) c_{2jk2} u_k^{(1)} + \frac{h_2}{3} (c_{ajkb} u_{k,ba}^{(1)} - \rho \ddot{u}_j^{(1)}) \qquad (3.1)$$

$$+ (c_{ajk2} + c_{2jka}) u_{k,a}^{(2)} = 0$$

$$-\beta k c_{2jk2} u_k^{(0)} - (\beta k + \frac{3}{h_2}) c_{2jk2} u_k^{(2)} + \frac{h_2}{5} (c_{ajkb} u_{k,ba}^{(2)} - \rho \ddot{u}_j^{(2)}) = 0$$

The elastic tensor for isotropic medium,

$$c_{ijkl} = \lambda \delta_{ij} \delta_{kl} + \mu (\delta_{ik} \delta_{jl} + \delta_{il} \delta_{jk})$$

where λ and μ are the Lamé constants, is substituted into (3.1) and the factor μk^2 is removed. In the coordinate system used, the nine equations of (3.1) are automatically separated into symmetric modes and antisymmetric modes according to the rules :

$$\text{for the } A_i^{(n)}, \; i + n = \left[\begin{array}{l} \text{odd for symmetric modes,} \\ \text{even for antisymmetric modes.} \end{array} \right]$$

The final outcome is as follows :

$$\begin{bmatrix} \alpha^2+\epsilon_{01} & i\alpha\zeta & i\zeta/H_2 & -\theta_0 & 0 \\ i\alpha\zeta & \delta\alpha^2+\epsilon_{03} & \alpha\zeta/H_2 & 0 & -\theta_0 \\ 0 & 0 & \alpha^2+\epsilon_{12} & 3i\zeta/H_2 & 3\alpha\zeta/H_2 \\ -5\theta_0 & 0 & 0 & \alpha^2+\epsilon_{21} & i\alpha\zeta \\ 0 & -5\theta_0 & 0 & i\alpha\zeta & \delta\alpha^2+\epsilon_{23} \end{bmatrix} \begin{bmatrix} A_1^{(0)} \\ A_3^{(0)} \\ A_2^{(1)} \\ A_1^{(2)} \\ A_3^{(2)} \end{bmatrix} \tag{3.2}$$

for the symmetric modes, and

$$\begin{bmatrix} \alpha^2+\epsilon_{02} & i\zeta/H_2 & \alpha\zeta/H_2 & -\theta_0\delta \\ 0 & \alpha^2+\epsilon_{11} & i\alpha\zeta & 3i\zeta/H_2 \\ 0 & i\alpha\zeta & \delta\alpha^2+\epsilon_{13} & 3\alpha\zeta/H_2 \\ -5\theta_0\delta & 0 & 0 & \alpha^2+\epsilon_{22} \end{bmatrix} \begin{bmatrix} A_2^{(0)} \\ A_1^{(1)} \\ A_3^{(1)} \\ A_2^{(2)} \end{bmatrix} = 0 \tag{3.3}$$

for the antisymmetric modes, where

$$H_2 = k h_2 \quad (\text{and } H_3 = kh_3 \text{ for later use}) \tag{3.4}$$

$$\delta = 2 + \lambda/\mu, \quad \zeta = \delta - 1 \tag{3.5}$$

$$\theta_0 = \beta/H_2, \quad \theta_1 = 3(1+\beta H_2)/H_2^2 \quad \text{and} \quad \theta_2 = 5(3+\beta H_2)/H_2^2 \tag{3.6}$$

$$\epsilon_{n1} = V_n^2 - \delta - \theta_n , \quad \epsilon_{n2} = V_n^2 - 1 - \delta\,\theta_n$$
$$\text{and} \quad \epsilon_{n3} = V_n^2 - 1 - \theta_n . \tag{3.7}$$

The normalized velocity V_n is

$$V_n = r_n\, v / v_t , \quad n = 0, 1, 2 \tag{3.8}$$

where r_n are adjustment factors of value near unity (to be explained later) and v_t is the shear velocity of the substrate.

The attenuation β in (3.6) is adopted from a result for the exponentially crested waves (Tiersten, 1969), i.e.,

$$\beta = (1 - v^2 / v_R^2)^{1/2} \tag{3.9}$$

where v_R is the Rayleigh velocity for a half-space of the substrate material. The representation of (3.9) for β, as mentioned in Section 1 of Chapter II, is a provision that simplifies the involvement of the side-region III and thus makes this waveguide problem somewhat more amenable to solution. In as much as the Rayleigh surface wave velocity in isotropic solids is independent of direction in the plane of the surface, as indicated by Tiersten (1969), equation (3.9) is the real expression for exponential or hyperbolic crested waves in a half-space. In the waveguide problem under consideration, the displacements along the plane $x_2 = h_2$ are not term-by-term those of a free-surface Rayleigh wave, for example, in the isotropic case the Rayleigh wave has two decay constants for depth whereas it will be seen that for the present approach to the waveguide problem the number of decay constants for depth depends on the order of the truncation. A rigorous condition for the choice of a value or a set of values for β in (3.1) has not been found. Several different forms for the dependence of β on problem parameters have been tried for both isotropic and anisotropic configurations and no justification has been found in terms of better satisfaction of boundary conditions, of consistency with limiting cases, or of simplification of computation, for using other than the single value of β defined by (3.9). In the discussion of truncation and of numerical results which follow, β will be assumed to be given by (3.9).

Now (3.2) for the symmetric case will be discussed as the example of normal manipulation. Since the mathematical procedures for (3.3) of the anti-symmetric case are entirely the same, only results of important steps are given for the latter case.

In order to have a non-trivial solution of (3.2), the determinant of the matrix must vanish. Setting this determinant equal to zero gives the secular equation. Normally the v^2 implicitly expressed in the ϵ_{ni} which appear in the diagonal terms of the matrix is the eigenvalue, in this case however, it should be remarked that the v^2 is also implied in all θ_n in virtue of β. Nevertheless, the relation between v and α can be fixed from the secular equation when the semi-width h_2 is given and the substrate material is chosen. It happens to be more convenient to solve for α in a bi-quintic equation of real coefficients for each given v. In the coordinate system for this symmetric case, only the five positive roots, designated by α_J ($J = 1, 2, 3, 4, 5$), have meaning for the necessary decaying of the wave amplitudes down into the depth of the substrate. The next step is similar to the procedure of finding a set of eigenvectors for each α_J. As mentioned before, explicit expression for α_J and their corresponding eigenvectors in this (2,2) - approximation is impossible and numerical computation has to be assumed. Changing notation for the individual eigenvectors,

$$(A_1^{(0)}, A_3^{(0)}, A_2^{(1)}, A_1^{(2)}, A_3^{(2)})_J = (A_{1J}, A_{2J}, A_{3J}, A_{4J}, A_{5J}) \tag{3.10}$$

the complete set of the calculated eigenvectors can be denoted by

A_{IJ} (I, J = 1, 2, 3, 4, 5) .

Note that the above eigenvalue solutions are for the polynomial displacements and they should be combined according to (1.2) to get the actual particle displacements of Region II . For this symmetric (2,2) - approximation, the displacements are :

$$\begin{aligned}
u_1 &= P_0 u_1^{(0)} + P_2 u_1^{(2)} = \sum_{J=1}^{5} (A_{1J} + P_2 A_{4J}) a_J Z_J \\
u_2 &= P_1 u_2^{(1)} = \sum_{J=1}^{5} P_1 A_{3J} a_J Z_J \\
u_3 &= P_0 u_3^{(0)} + P_2 u_3^{(2)} = \sum_{J=1}^{5} (A_{2J} + P_2 A_{5J}) a_J Z_J
\end{aligned} \tag{3.11}$$

where the a_J are the newly introduced weighting factors and $Z_J = \exp(\alpha_J k x_3)$ are the Z functions of (1.5) with α_J specified. The X function of (1.4), denoting propagation, is omitted in (3.11) and will be omitted in most of the following equations. Similarly, according to (1.3) the particle displacements of Region III are :

$$\bar{u}_{1\,(\pm)} = (u_1^{(0)} + u_1^{(2)})\, Y_{(\pm)} = \sum_{J=1}^{5} (A_{1J} + A_{4J})\, a_J\, Z_J\, Y_{(\pm)}$$

$$\bar{u}_{2\,(\pm)} = \pm\, u_2^{(1)}\, Y_{(\pm)} = \pm \sum_{J=1}^{5} A_{3J}\, a_J\, Z_J\, Y_{(\pm)} \qquad (3.1\text{:}$$

$$\bar{u}_{3\,(\pm)} = (u_3^{(0)} + u_3^{(2)})\, Y_{(\pm)} = \sum_{J=1}^{5} (A_{2J} + A_{5J})\, a_J\, Z_J\, Y_{(\pm)}$$

With the antisymmetric (2,2) – approximation we begin with (3.3) and the secular equation is a bi-quartic equation in α . Denoting the roots by α_J (J = 1, 2, 3, 4) and the eigenvectors by

$$(A_2^{(0)}\,,\, A_1^{(1)}\,,\, A_3^{(1)},\, A_2^{(2)})_J = (A_{1J}, A_{2J}\,, A_{3J}\,, A_{4J}) \qquad (3.1\text{:}$$

the particle displacements of Regions II and III become :

$$
\begin{aligned}
u_1 &= P_1\, u_1^{(1)} &&= P_1 \sum_{J=1}^{4} A_{2J}\, a_J\, Z_J \\
u_2 &= P_0\, u_2^{(0)} + P_2\, u_2^{(2)} &&= \sum_{J=1}^{4} (A_{1J} + P_2 A_{4J})\, a_J\, Z_J \\
u_3 &= P_1\, u_3^{(1)} &&= P_1 \sum_{J=1}^{4} A_{3J}\, a_J\, Z_J
\end{aligned}
\tag{3.14}
$$

$$
\begin{aligned}
\bar{u}_{1\,(\pm)} &= \pm\, u_1^{(1)}\, Y_{(\pm)} &&= \pm \sum_{J=1}^{4} A_{2J}\, a_J\, Z_J\, Y_{(\pm)} \\
\bar{u}_{2\,(\pm)} &= (u_2^{(0)} + u_2^{(2)})\, Y_{(\pm)} &&= \sum_{J=1}^{4} (A_{1J} + A_{4J})\, a_J\, Z_J\, Y_{(\pm)} \\
\bar{u}_{3\,(\pm)} &= \pm\, u_3^{(1)}\, Y_{(\pm)} &&= \pm \sum_{J=1}^{4} A_{3J}\, a_J\, Z_J\, Y_{(\pm)}
\end{aligned}
\tag{3.15}
$$

Note that the same notations, A_{IJ} , a_J and Z_J are used in the symmetric and the antisymmetric approximation , but obviously they are numerically different in the two cases.

4. General Equations of Motion for the Overlay from a Variational Approach

A detailed formulation of the one-dimensional theory of wave propagation in elastic bars of rectangular cross section has been given by Medick (1966 and 1968).

In the theory an algorithm was employed to generate the one-dimensional equations of motion, the strain-displacement relation, the stress-strain relation, and the associated boundary conditions by subjecting all of the displacement fields, strains and stresses to variation. However in this thesis, we proceed rather in a pattern analogous to that used to develop the two-dimensional theory for plates as shown in Section 2 and consider all other relations and conditions as undisturbed constraints.

Starting with (2.1) but using the "hatted" variables $\hat{T}_{ij}$, $\hat{\rho}$ and $\hat{u}_i$, substituting (1.1) and here performing the cross integration of $\hat{T}_{2i,2}$ and $\hat{T}_{3i,3}$ with respect to x_2 and x_3 respectively, we obtain

$$\hat{T}^{(n,m)}_{1i,1} - \sum_{p=1,3}^{n} (2/C_{n-p}\, h_2)\, \hat{T}^{(n-p,m)}_{2i} - \sum_{p=1,3}^{m} (2/C_{m-p}\, h_3)\, \hat{T}^{(n,m-p)}_{3i}$$

$$+ \hat{F}^{(n,m)}_{2i} + \hat{F}^{(n,m)}_{3i} - \hat{\rho}\, C_n C_m h_2 h_3 \ddot{\hat{u}}^{(n,m)}_i = 0 \tag{4.1}$$

where

$$\hat{T}^{(n,m)}_{ij} = \int_{-h_2}^{h_2} \int_{0}^{2h_3} \hat{T}_{ij} P_n Q_m \, d x_3 \, d x_2 \tag{4.2}$$

$$\hat{F}^{(n,m)}_{2i} = \int_{0}^{2h_3} [\hat{T}_{2i} P_n]_{x_2 = -h_2}^{x_2 = +h_2} Q_m \, d x_3 \tag{4.3}$$

$$\hat{F}^{(n,m)}_{3i} = \int_{-h_2}^{h_2} [\hat{T}_{3i} Q_m]_{x_3 = 0}^{x_3 = 2h_3} P_n \, d x_2 , \tag{4.4}$$

and the following relations for the Q_m have been used

$$(Q_s, Q_m) = C_m h_3 \delta_{sm} \tag{4.5}$$

$$Q_{m,3} = \sum_{p=1,3}^{m} (2/C_{m-p} h_3)\, Q_{m-p} \tag{4.6}$$

Equations (4.1), which replace (2.1) comprise doubly infinite sets of equations of order (n,m) with $n, m = 0, 1, \ldots \infty$, each of which contains three equations of the polynomial (bar) displacements $\hat{u}_i^{(n,m)}$ and stresses $\hat{T}_{ij}^{(n,m)}$.

Parallel to the derivation for Region II, the polynomial strains and stresses of Region I can be expressed in the form

$$\begin{aligned}\hat{S}_{ij}^{(n,m)} = \frac{1}{2} [\, & \hat{u}_{i,1}^{(n,m)} \delta_{1j} + \hat{u}_{j,1}^{(n,m)} \delta_{1i} \\ & + (2/C_n h_2) \sum_{p=1,3}^{\infty} (\hat{u}_i^{(n+p,m)} \delta_{2j} + \hat{u}_j^{(n+p,m)} \delta_{2i} \\ & + (2/C_n h_3) \sum_{p=1,3}^{\infty} (\hat{u}_i^{(n,m+p)} \delta_{3j} + \hat{u}_j^{(n,m+p)} \delta_{3i})\,]\end{aligned} \tag{4.7}$$

$$\hat{T}_{ij}^{(n,m)} = C_n C_m h_2 h_3 \hat{c}_{ijkl} \hat{S}_{kl}^{(n,m)} \tag{4.8}$$

Since

$$\hat{T}_{2i} = 0 \quad \text{at} \quad x_2 = \pm h_2$$

$$\hat{T}_{3i} = 0 \quad \text{at} \quad x_3 = 2\,h_3 \tag{4.9}$$

and

$$\hat{T}_{3i} = T_{3i} \quad \text{at} \quad x_3 = 0\,, \tag{4.10}$$

and supposing that T_{3i} at $x_3 = 0$ can be determined later as the series,

$$T_{3i}\,(x_3 = 0) = \sum_{p=0}^{\infty} P_p\, G_{3i}^{(p)}\,, \tag{4.11}$$

then (4.3) and (4.4) become,

$$\hat{F}_{2i}^{(n,m)} = 0 \tag{4.12}$$

and

$$\hat{F}_{3i}^{(n,m)} = -(-1)^m\, C_n\, h_2\, G_{3i}^{(n)}\,. \tag{4.13}$$

Equations (4.13) are obtained under the same assumptions used for (2.16) and will drastically alter the equations of motion (4.1) of the overlay from those of Medick's isolated bar due to the mechanical contact of the bottom side of the overlay with the substrate.

Substituting (4.7) into (4.8) and the result, together with (4.12) and (4.13), into (4.1), the polynomial <u>displacement</u> equations of motion for the rectangular overlay are obtained,

$$(\rho v^2 \delta_{jk} - \hat{c}_{1jk1})\, \hat{u}_k^{(n,m)} + (2\,i/C_n H_2) \sum_{q=1,3}^{\infty} \hat{c}_{1jk2}\, \hat{u}_k^{(n+q,m)}$$

$$+ (2\,i/C_m H_3) \sum_{q=1,3}^{\infty} \hat{c}_{1jk3}\, \hat{u}_k^{(n,m+q)}$$

$$- (2/C_n H_2) \sum_{p=1,3}^{n} [\, i\, \hat{c}_{2jk1}\, \hat{u}_k^{(n-p,m)} + (2/C_{n-p} H_2) \sum_{q=1,3}^{\infty} \hat{c}_{2jk2}\, \hat{u}_k^{(n-p+q,m)}$$

$$+ (2/C_m H_3) \sum_{q=1,3}^{\infty} \hat{c}_{2jk3}\, \hat{u}_k^{(n-p,m+q)} \,]$$

$$- (2/C_m H_3) \sum_{p=1,3}^{m} [\, i\, \hat{c}_{3jk1}\, \hat{u}_k^{(n,m-p)} + (2/C_n H_2) \sum_{q=1,3}^{\infty} \hat{c}_{3jk2}\, \hat{u}_k^{(n+q,m-p)}$$

$$+ (2/C_{m-p} H_3) \sum_{q=1,3}^{\infty} \hat{c}_{3jk3}\, \hat{u}_k^{(n,m-p+q)} \,]$$

$$- (-1)^m (C_m H_3 k)^{-1}\, G_{3j}^{(n)} = 0 \qquad (4.14)$$

where H_2 and H_3 are defined in (3.4) .

As mentioned before, (4.14) corresponds to the boundary-condition step of the conventional exact approach and contains two kinds of unknowns : the weighting factors a_J of Region II in the terms of $G_{3j}^{(n)}$ and the polynomial amplitudes $\hat{A}_k^{(n,m)}$ of Region I in all of the other terms. In order to make (4.14) solvable, one has to transform a_i into $\hat{A}_k^{(n,m)}$ and for this purpose the "detailed matching" of displacements on the interface between Regions I and II, mentioned at the end of Section 1 and represented by Block 9 on the flow-chart in Figure 2, can be introduced at this stage. By such a manipulation all the boundary conditions at the interface are taken into consideration on the one hand, and on the other hand (4.14) is transformed into a suitable set of homogeneous equations in which the number of equations is equal to the number of unknowns so that the vanishing of the coefficient determinant leads directly to the solution of this waveguide problem. However to avoid unnecessarily complicated expressions, the analysis here will first introduce the (2,2) truncation within the overlay in the next section and then apply the detailed matching in Section 6.

5. Truncated (2,2) - Approximation for the Overlay

On expanding (4.14) with $n,m = 0, 1, 2,$ a total of 27 equations, three ($j = 1, 2, 3$) for every combination of n and m, is obtained for the (2, 2) - approximation and is given in full in Appendix A. After substituting the Lamé constants $\hat{\mu}$ and $\hat{\lambda}$ for the $\hat{c}_{ijkl}$ of Region I, the 27 equations separate into two independent sets, one for the symmetric modes with $(i + n)$ odd in $\hat{A}_i^{(n,m)}$ and $G_{3i}^{(n)}$, and one for the antisymmetric modes, with $(i + n)$ even according to the same rules as stated in Section 3. Since the only mirror plane of symmetry is the plane $x_2 = 0$ in the configuration shown in Figure 1, the superscript n in $\hat{A}_i^{(n,m)}$

and $G_{3i}^{(n)}$ associated with the Legendre polynomial P_n displays the symmetry above ; but since the symmetry plane of the overlay itself $x_3 = h_3$ is not a symmetry plane of the complete problem, because of the presence of the substrate, the superscript m in $\hat{A}_i^{(n,m)}$ associated with the Legendre polynomials Q_m is arbitrary in both the symmetric and the antisymmetric modes.

It is convenient to relabel the coefficients $\hat{A}_i^{(n,m)}$ into two column vectors, one for the fifteen elements associated with symmetric modes

$$(\hat{S}_1, \hat{S}_2 \dots \hat{S}_{15}) = [\hat{A}_1^{(0,0)}, \hat{A}_3^{(0,0)}, \hat{A}_1^{(0,1)}, \hat{A}_3^{(0,1)}, \hat{A}_1^{(0,2)}, \hat{A}_3^{(0,2)},$$
$$\hat{A}_2^{(1,0)}, \hat{A}_2^{(1,1)}, \hat{A}_2^{(1,2)}, \hat{A}_1^{(2,0)}, \hat{A}_3^{(2,0)}, \hat{A}_1^{(2,1)}, \hat{A}_3^{(2,1)}, \hat{A}_1^{(2,2)}, \hat{A}_3^{(2,2)} \tag{5.1}$$

and one for the twelve elements of the antisymmetric modes

$$(\hat{A}_1, \hat{A}_2 \dots \hat{A}_{12}) = [\hat{A}_2^{(0,0)}, \hat{A}_2^{(0,1)}, \hat{A}_2^{(0,2)}, \hat{A}_1^{(1,0)}, \hat{A}_3^{(1,0)},$$
$$\hat{A}_1^{(1,1)}, \hat{A}_3^{(1,1)}, \hat{A}_1^{(1,2)}, \hat{A}_3^{(1,2)}, \hat{A}_2^{(2,0)}, \hat{A}_2^{(2,1)}, \hat{A}_2^{(2,2)}] \tag{5.2}$$

If the terms in $G_{3j}^{(n)}$ can be expressed in terms of the elements $\hat{S}_M$ for the symmetric case in such a manner that g_{NM} is the corresponding part of the coefficient of $\hat{S}_M$ in the N th equation and if F_{NM} represents the part of the coefficient of $\hat{S}_M$ not associated with $G_{3j}^{(n)}$ in this same equation, the g_{NM} and the f_{NM} can be grouped into matrices so that, after dividing the equations through by $\hat{\mu}$, the set of equations :

$$\sum_{M} [(f_S)_{NM} + (g_S)_{NM}] \hat{S}_M = 0 \qquad N,M = 1, 2, .. 15 \quad (5.3)$$

can be written for the symmetric case ; and similarly for the antisymmetric case

$$\sum_{M} [(f_A)_{NM} + (g_A)_{NM}] \hat{A}_M = 0 \qquad N,M = 1,2, .. 12 \quad (5.4)$$

Here subscripts "S" and "A" stand for "Symmetric" and "Antisymmetric" and the individual elements of f_S and f_A are written out in Appendix B .

It will be recalled that the quantity $G_{3j}^{(n)}$ defined by (4.11) is the coefficient of the Legendre polynomial of order n in the substrate stress T_{3j} when the latter is evaluated at $x_3 = 0$ from the displacements in Region II. Substituting from (3.11) into the ordinary expressions of stress,

$$\begin{aligned} T_{31} &= \mu (u_{3,1} + u_{1,3}) \\ T_{32} &= \mu (u_{3,2} + u_{2,3}) \\ T_{33} &= (\lambda + 2 \mu) u_{3,3} + \lambda (u_{1,1} + u_{2,2}) , \end{aligned}$$

and then letting $x_3 = 0$, the form of (4.11) for the symmetric (2,2) - approximation is obtained,

$$\begin{aligned} T_{31} &= G_1 + P_2 G_4 \\ T_{32} &= P_1 G_3 \\ T_{33} &= G_2 + P_2 G_5 \end{aligned} \qquad (5.5)$$

where the notation

$$(G_1 , G_2 , G_3 , G_4 , G_5) = (G_{31}^{(0)}, G_{33}^{(0)}, G_{32}^{(1)}, G_{31}^{(2)}, G_{33}^{(2)}) \tag{5.6}$$

has been used. The components are given by

$$G_I = \mu k \sum_{J=1}^{5} G_{IJ} \alpha_J \qquad I, J = 1, 2, 3, 4, 5 \tag{5.7}$$

where

$$\begin{aligned} G_{1J} &= A_{1J} \alpha_J + i A_{2J} \\ G_{2J} &= \delta A_{2J} \alpha_J + (A_{3J} / H_2 + i A_{1J}) \lambda / \mu \\ G_{3J} &= A_{3J} \alpha_J + 3 A_{5J} / H_2 \\ G_{4J} &= A_{4J} \alpha_J + i A_{5J} \\ G_{5J} &= \delta A_{5J} \alpha_J + i A_{4J} \lambda / \mu \end{aligned} \tag{5.8}$$

Similarly, for the antisymmetric modes, introducing the notation

$$(G_1 , G_2 , G_3 , G_4) = (G_{32}^{(0)} , G_{31}^{(1)} , G_{33}^{(1)} , G_{32}^{(2)}) \tag{5.9}$$

gives the following expressions for the stresses at the interface under the overlay from (3.14)

$$T_{31} = P_1\, G_{31}^{(1)}$$

$$T_{32} = G_{32}^{(0)} + P_2\, G_{32}^{(2)} \qquad (5.10)$$

$$T_{33} = P_1\, G_{33}^{(1)}$$

so that

$$G_I = \mu k \sum G_{IJ}\, a_J \qquad I, J = 1, 2, 3, 4 \qquad (5.11)$$

where

$$G_{1J} = A_{1J}\, a_J + A_{3J} / H_2$$

$$G_{2J} = A_{2J}\, a_J + i\, A_{3J}$$

$$G_{3J} = \delta\, A_{3J}\, a_J + (3\, A_{4J} / H_2 + i\, A_{2J})\, \lambda / \mu \qquad (5.12)$$

$$G_{4J} = A_{4J}\, a_J$$

Note that G_I of (5.11) are the terms for the elements of g_A in (5.4). Although the same notation is used for G_I, G_{IJ}, a_J, A_{IJ} and a_J in the symmetric and antisymmetric case, the symbols represent different values and different numbers in each case.

6. "Detailed Matching" of Displacements and the Search for Solutions

In this section an important procedure, "detailed matching" of displacements for the interface between Regions I and II, that is the step of Block 9 in

Figure 2, is introduced and the last part of the analysis is developed. If the conditions of continuity of displacement across the interface between Regions I and II are now imposed, considering the form of the substrate and overlay displacements from (1.1) and (1.2) and recalling that the substrate displacements are a linear combination of the terms in (3.11), the general form of the statement of continuity of displacement at $x_3 = 0$ will be

$$\sum_n P_n \sum_J a_J A_{iJ}^{(n)} = \sum_n P_n \sum_m (-1)^m \hat{A}_i^{(n,m)} \tag{6.1}$$

It is assumed here that there is "detailed matching" in the latter equation in that coefficients of corresponding Legendre polynomials on opposite sides of the equation are equal, i.e., for each combination of i and n,

$$\sum_J a_J A_{iJ}^{(n)} = \sum_m (-1)^m \hat{A}_i^{(n,m)} \tag{6.2}$$

Note that in the above two equations, the factor $(-1)^m$ comes from the Legendre polynomial Q_m at $x_3 = 0$ and the symmetry rules mentioned before are valid.

Again by taking the symmetric (2,2) - approximation as an illustration of the analysis, from (3.11) and (1.1) for the five combinations of i and n, (6.2) may be expressed in a compact form,

$$\sum_J A_{IJ} a_J = \hat{b}_I \qquad I, J = 1, 2, \ldots 5 \tag{6.3}$$

where $\hat{b}_I$ stands for grouped representations of $\hat{A}_i^{(n,m)}$ according to the right-hand side of (6.2) as follows, in terms of the element of the column vector $\hat{S}_M$,

$$
\begin{aligned}
\hat{b}_1 &= \hat{S}_1 - \hat{S}_3 + \hat{S}_5 \\
\hat{b}_2 &= \hat{S}_2 - \hat{S}_4 + \hat{S}_6 \\
\hat{b}_3 &= \hat{S}_7 - \hat{S}_8 + \hat{S}_9 \\
\hat{b}_4 &= \hat{S}_{10} - \hat{S}_{12} + \hat{S}_{14} \\
\hat{b}_5 &= \hat{S}_{11} - \hat{S}_{13} + \hat{S}_{15}
\end{aligned}
\tag{6.4}
$$

Solving for a_J from (6.3) and substituting into (5.7), gives

$$
G_I = \mu k \sum_K \sum_J G_{IJ} (A^{-1})_{JK} \, b_K , \qquad I, J, K = 1, 2, .. 5 \tag{6.5}
$$

where $(A^{-1})_{JK}$ is the reduced cofactor of A_{KJ}. Now it is seen in (6.5) that the G_I, which originally contained the weighting factors a_J as unknowns in (5.7), are thus transformed into expressions with the polynomial amplitudes $\hat{S}_M$, via $\hat{b}_K$, so that g_S can be added to f_S in (5.3). But care must be taken in so doing, converting G_I of (6.5) back into $G_{3i}^{(n)}$ according to (5.6), dividing by $\hat{\mu}$, multiplying by the corresponding factors associated with $G_{3i}^{(n)}$ in (A.1) in Appendix A, changing $\hat{b}_I$ of (6.4) back into $\hat{S}_M$ and then identifying the resultant terms as the $(g_S)_{NM}$.

At this stage the only unknown quantity in (5.3), for specified phase velocity $V = v/v_t$ and semi-width $H_2 = k h_2$, is relative semi-thickness

$H_3 = k\,h_3$ and the determinant of this homogeneous set of equations must vanish for non-trivial solutions.

Iterative search techniques, such as the golden-section method can be used to determine a numerical value of H_3 which causes the determinant to vanish, thus establishing one point on the dispersion curves for the symmetric modes. Families of dispersion curves are produced by repeating the procedure for the same value of H_2 but successive assumed values of V. Once the value of H_3 which causes the coefficient determinant in (5.3) to vanish has been found, the relative values of the components of $\hat{S}_M$, that is the appropriate $\hat{A}_i^{(m,n)}$, can be determined by say Gaussian reduction of (5.3). These components give the particle displacements in the overlay by means of (1.1). The weighting factors a_J are found by inverting (6.3) and these in turn determine the particle displacements in the substrate through (3.11) and (3.12).

In summary, for the symmetric modes, the eigenvalues and eigenvectors for the substrate solutions are determined from (3.2) thus establishing the form of the substrate displacements, (3.11), except for the weighting factors. Using this form of substrate displacement, detailed matching of the displacements across the interface between Regions I and II allows these weighting factors to be replaced in the traction integral terms of the overlay equations by the overlay coefficients $\hat{A}_i^{(n,m)}$; compare (5.7) and (6.5). The latter interchange produces the homogeneous set, (5.3), which has only one parameter, H_3, for assumed values of V and H_2, and a search is made for a value of H_3 which allows a non-trivial solution, and for this value of H_3 the various displacements can be determined explicitly.

As exactly parallel procedure is used for the antisymmetric modes, if the following regrouping is used instead of (6.4),

$$
\begin{aligned}
\hat{b}_1 &= \hat{A}_1 - \hat{A}_2 + \hat{A}_3 \\
\hat{b}_2 &= \hat{A}_4 - \hat{A}_6 + \hat{A}_8 \\
\hat{b}_3 &= \hat{A}_5 - \hat{A}_7 + \hat{A}_9 \\
\hat{b}_4 &= \hat{A}_{10} - \hat{A}_{11} + \hat{A}_{12}
\end{aligned}
\tag{6.6}
$$

Letting I, J, K = 1, 2, 3, 4 (not including 5), the formulation above is valid for the antisymmetric modes with appropriate reduction in the number of equations. The corresponding set of equations for the symmetric and antisymmetric modes are summarized in the following table.

Symmetric		Antisymmetric	
Quantities	Equation	Equation	Quantities
$A_i^{(n)}$	(3.2)	(3.3)	$A_i^{(n)}$
A_{IJ}	(3.10)	(3.13)	A_{IJ}
u_i	(3.11)	(3.14)	u_i
$\bar{u}_i$	(3.12)	(3.15)	$\bar{u}_i$
$\hat{S}_M$	(5.1)	(5.2)	$\hat{A}_M$
f_S , g_S	(5.3)	(5.4)	f_A , g_A

Symmetric		Antisymmetric	
Quantities	Equation	Equation	Quantities
G_I	(5.5)	(5.10)	G_I
G_I	(5.6)	(5.9)	G_I
G_I	(5.7)	(5.11)	G_I
G_{IJ}	(5.8)	(5.12)	G_{IJ}
$\hat{b}_I$	(6.3)	(6.3)	$\hat{b}_I$
$\hat{b}_I$	(6.4)	(6.6)	$\hat{b}_I$
G_I	(6.5)	(6.5)	G_I
$i + n$ =	odd	$i + n$ =	even
I, J =	1, 2, 3, 4, 5	I, J =	1, 2, 3, 4
M =	1, 2, ..., 15	M =	1, 2, ..., 12 .

7. Truncated (1,1) - Approximation

In this section the truncated (1, 1) - approximation is presented in some detail though the general procedure is the same as that given in Sections 1 to 6 for the (2,2) - approximation. Here the polynomial indices (n, m, etc) are 0 and 1 only, and if all the terms containing a polynomial index of 2 are omitted, the (1,1) - approximation is obtained from the (2,2) equations without modifying the computing techniques. However in the light of the lower order involved in the (1,1) - approximation the search technique is not needed, instead, an explicit formulation can be provided wherein not only is direct numerical evaluation possible but also the structure of the theory is more clearly illustrated. Moreover, in order to display the theory in more unison, here the symmetric and antisymmetric modes can be kept together to the last moment at which the equations of the dispersion curves are obtained.

Taking the first two equations in (3.1) with the terms containing $u_k^{(2)}$ omitted and replacing the isotropic tensor by Lamé constants, six equations for the (1,1) - approximation are obtained :

$$\begin{aligned} M_{jk}^{(0)} A_k^{(0)} + M'_{jk} A_k^{(1)} &= 0 \\ M_{jk}^{(1)} A_k^{(1)} &= 0 \end{aligned} \qquad (7.1)$$

Here the 6×6 coefficient matrix can be decomposed into four 3×3 submatrices denoted in (7.1) by $M_{jk}^{(0)}$, $M_{jk}^{(1)}$, M'_{jk} and a null one at the lower off-diagonal corner. The forms of the three former submatrices are as follows :

$$[M_{jk}^{(n)}] = \begin{bmatrix} \alpha^2 + \epsilon_{n1} & & i\alpha\zeta \\ & \alpha^2 + \epsilon_{n2} & \\ i\alpha\zeta & & \alpha^2 + \epsilon_{n3} \end{bmatrix} , \quad n = 0, 1 \qquad (7.2)$$

$$[M'_{jk}] = \frac{\zeta}{H_2}\begin{bmatrix} & i & \\ i & & \alpha \\ & \alpha & \end{bmatrix} \tag{7.3}$$

where all notations are the same as shown in (3.4) to (3.7). Note that the two diagonal submatrices $M^{(0)}_{jk}$ and $M^{(1)}_{jk}$ have non-vanishing elements only at $j+k$ = even and the M'_{jk} only at $j+k$ = odd. This pattern ensures the separability of the symmetric modes from the antisymmetric. Obviously if now separated, the same expressions are obtained as those in (3.2) and (3.3) with the terms of $A^{(2)}_i$ omitted. Both the symmetric (1,1) - and the antisymmetric (1,1) - approximations have three homogeneous equations for the secular equation. According to the same rules of symmetry, $[A^{(0)}_1, A^{(0)}_3, A^{(1)}_2]$ belong to the symmetric modes while $[A^{(0)}_2, A^{(1)}_1, A^{(1)}_3]$ belong to the antisymmetric. For the reasons mentioned above, the possibility of separation is ignored here and (7.1) is treated as a whole in this (1,1) - approximation.

The secular equation for (7.1) becomes

$$| M^{(0)}_{jk} | \cdot | M^{(1)}_{jk} | = 0 \tag{7.4}$$

Solving for six α's

$$\begin{aligned} \alpha_{n1} &= [1 + (\theta_n - V_n^2)/\delta]^{1/2} \\ \alpha_{n2} &= (1 + \delta\theta_n - V_n^2)^{1/2}, \qquad n = 0, 1 \\ \alpha_{n3} &= (1 + \theta_n - V_n^2)^{1/2} \end{aligned} \tag{7.5}$$

It is very interesting to point out that when H_2 ($= k\,h_2$) approaches infinity, i.e., a case of very wide Region II, only the diagonal submatrices $M_{jk}^{(n)}$, $n = 1, 2,$ survive. The elements of these submatrices reduce exactly to those of the layered problem (Farnell and Adler 1972, Equation 15) and accordingly so do the α's of (7.5) because $\theta_n = 0$ when $H_2 \to \infty$. Actually this feature occurs also in the (2,2) - approximation, but it cannot be seen so clearly because of the many implicit expressions involved.

Now solving for the eigenvectors corresponding the α's and denoting them by,

$$\left[\begin{array}{c|c} m_{ij}^{(0)} & m'_{ij} \\ \hline & m_{ij}^{(1)} \end{array}\right] = \left[\begin{array}{ccc|ccc} 1 & & i\,\alpha_{03} & & i\,\gamma_{12} & \\ & 1 & & i\,\gamma_{11} & & 0 \\ -i\,\alpha_{01} & & 1 & & \alpha_{12}\,\gamma_{12} & \\ \hline & & & 1 & & i\,\alpha_{13} \\ & & & & 1 & \\ & & & -i\,\alpha_{11} & & 1 \end{array}\right] \tag{7.6}$$

where

$$\gamma_{11} = \frac{1}{H_2} \cdot \frac{\alpha^2_{11} - 1}{1 - \alpha^2_{01} - \theta_0 - (\alpha^2_{01} - \alpha^2_{11}) / \zeta}$$

$$\gamma_{12} = \frac{1}{H_2} \quad \frac{1}{1 - \alpha^2_{12} - \theta_0 + (\alpha^2_{02} - \alpha^2_{12}) / \zeta} \tag{7.7}$$

then the polynomial displacements can be formed as follows

$$u_i^{(0)} = m_{ij}^{(0)} \; a_j^{(0)} \; Z_{0\,(j)} + m'_{ij} \, a_j^{(1)} \, Z_{1\,(j)}$$

$$u_i^{(1)} = m_{ij}^{(1)} \, a_j^{(1)} \, Z_{1\,(j)} \tag{7.8}$$

where $a_j^{(0)}$ and $a_j^{(1)}$ are the added weighting factors and

$$Z_{n\,(j)} = \exp\,[\,\alpha_{nj}\, k\, x_3\,]\,, \qquad n = 0,\,1 \text{ and } j = 1,\,2,\,3 \tag{7.9}$$

are the Z-functions of Equation (1.5) with the specified α_{nj} of Equation (7.5).

Here it should be mentioned once again that in this analysis as compared with the exact approach, the decay constant α along the depth coordinate x_3 has been used as the eigenvalue and the eigenvectors obtained are for the polynomial displacements and not for the actual displacements. The latter have to be compiled from the former according to (1.2).

Consequently the real displacements of the (1,1) – approximation are

$$u_i = u_i^{(0)} + P_1 u_i^{(1)}$$

$$= m_{ij}^{(0)} a_j^{(0)} Z_{0\,(j)} + (m'_{ij} + P_1 m_{ij}^{(1)}) a_j^{(1)} Z_{1\,(j)} \qquad (7.10)$$

and

$$\bar{u}_i\,(\pm) = (u_i^{(0)} \pm u_i^{(1)})\, Y_{(\pm)}$$

$$= [\, m_{ij}^{(0)} a_j^{(0)} Z_{0\,(j)} + (m'_{ij} \pm m_{ij}^{(1)}) a_j^{(1)} Z_{1\,(j)} \,]\, Y_{(\pm)} \qquad (7.11)$$

Here both u_i and $u_{i\,(\pm)}$ are general, containing symmetric and antisymmetric components together.

For later use, the stresses T_{3j} at the interface between Regions I and II can be expressed by substituting the general form of the displacements (7.10) into the ordinary expression for the stress,

$$T_{3j} = G_{3j}^{(0)} + P_1 G_{3j}^{(1)}, \qquad \text{at } x_3 = 0 \qquad (7.12)$$

where

$$G_{3j}^{(0)} = \mu k\, (t_{jk}^{(0)} a_k^{(0)} + t'_{jk} a_k^{(1)})$$

$$G_{3j}^{(1)} = \mu k\, (0 + t_{jk}^{(1)} a_k^{(1)}) \qquad (7.13)$$

and

$$t_{jk}^{(n)} = \begin{bmatrix} 2\alpha_{n1} & & 1+\alpha_{n3}^2 \\ & \alpha_{n2} & \\ \delta(1-\alpha_{n1}^2)-2 & & 2\alpha_{n3} \end{bmatrix}, \quad n = 0,1 \tag{7.14}$$

$$t'_{jk} = \begin{bmatrix} & 2\alpha_{12}\gamma_{12} & \\ \alpha_{11}(\gamma_{11}-\frac{1}{H_2}) & & \frac{1}{H_2} \\ & \frac{\delta-2}{H_2} - \gamma_{12}[\delta(1-\alpha_{12}^2)-2] & \end{bmatrix} \tag{7.15}$$

Heretofore in this section only Region II has been considered. Before turning to Region I for its equations of motion, it is convenient to have the polynomial components of stress, $G_{3j}^{(0)}$ and $G_{3j}^{(1)}$ ready to transform into expressions in the polynomial amplitudes $\hat{A}_i^{(n,m)}$. The same procedure used to obtain (6.5) in the (2,2) - approximation is employed here except that an explicit expression with the symmetric and antisymmetric modes combined together now results from the manipulation.

In this (1,1) - approximation, the "detailed matching" equation (6.2) shows

$$\begin{aligned} m_{ij}^{(0)} a_j^{(0)} + m'_{ij} a_j^{(1)} &= \hat{A}_i^{(0,0)} - \hat{A}_i^{(0,1)} \\ m_{ij}^{(1)} a_j^{(1)} &= \hat{A}_i^{(1,0)} - \hat{A}_i^{(1,1)} \end{aligned} \tag{7.16}$$

Solving for $a_i^{(0)}$ and $a_i^{(1)}$ and substituting into (7.13), gives

$$G_{3j}^{(0)} = \mu k [\tau_{jk}^{(0)} (\hat{A}_k^{(0,0)} - \hat{A}_k^{(0,1)}) + \tau'_{jk} (\hat{A}_k^{(1,0)} - \hat{A}_k^{(1,1)})]$$

$$G_{3j}^{(1)} = \mu k [\quad 0 \quad + \tau_{jk}^{(1)} (\hat{A}_k^{(1,0)} - \hat{A}_k^{(1,1)})] \tag{7.17}$$

where the non-vanishing terms are, for $n = 0$ and 1,

$$\tau_{11}^{(n)} = \alpha_{n1} (1 - \alpha_{n3}^2) / \varphi_n , \quad \varphi_n = 1 - \alpha_{n1} \alpha_{n3}$$

$$\tau_{13}^{(n)} = [1 + \alpha_{n3} (\alpha_{n3} - 2 \alpha_{n1})] / \varphi_n$$

$$\tau_{22}^{(n)} = \alpha_{n2} \tag{7.18}$$

$$\tau_{31}^{(n)} = \delta (1 - \alpha_{n1}^2) / \varphi_n - 2$$

$$\tau_{33}^{(n)} = \delta \alpha_{n3} (1 - \alpha_{n1}^2) / \varphi_n$$

$$\tau'_{12} = \gamma_{12} (\alpha_{12} - \alpha_{01}) (1 - \alpha_{03}^2) / \varphi_0$$

$$\tau'_{21} = \gamma_{11} (\alpha_{11} - \alpha_{02}) / \varphi_1$$

$$\tau'_{23} = \alpha_{13} \tau'_{21} + 1 / H_2$$

$$\tau'_{32} = \delta \gamma_{12} (\alpha_{01} - \alpha_{12}) [(\alpha_{03} - \alpha_{01}) / \varphi_0 - \alpha_{12}] + (\zeta - 1) / H_2$$

Now the equations of motion for Region I in which every term is explicitly expressed can be obtained in the (1,1) - approximation by (i) taking the first, second, fourth and fifth equations only from (A.1) ; (ii) omitting all terms of the polynomial displacements in which either or both of n and m are equal to 2 ; (iii) replacing the $\hat{c}_{ijkl}$ by the Lamé constants $\hat{\lambda}$ and $\hat{\mu}$; (iv) replacing the stress terms by (7.17) and (7.18), and (v) dividing by $\hat{\mu}$. The result is 12 homogeneous equations with variables $(A_k^{(0,0)}, A_k^{(0,1)}, A_k^{(1,0)})$, k = 1, 2, 3 completely split into the symmetric and antisymmetric modes, six equations each according to the same rules of symmetry mentioned before.

To illustrate better what is contained in each element, both the symmetric and antisymmetric mode equations in the (1,1) - approximation are shown in full in matrix form below.* In (7.19) and (7.20), all stress terms are expressed directly through the notations

$$J_{ij}^{(n)} = \mu\,\tau_{ij}^{(n)} / 2\,\hat{\mu}\,H_3 \quad \text{and} \quad J'_{ij} = \mu\,\tau'_{ij} / 2\,\hat{\mu}\,H_3 \tag{7.21}$$

Equations (7.19) and (7.20) in the (1,1) - approximation correspond to (5.3) and (5.4) respectively in the (2,2) - approximation. Here it is easy to see in (7.19) and (7.20) the distribution of the f_{NM} terms and the g_{NM} terms, the latter ones are represented by $J_{ij}^{(n)}$ and J'_{ij} and contribute the major effects in the mode structure of the waveguide problem, since if they are omitted, the equations would become those

---

* Equation (7.19) for the symmetric mode is given on page 56 and (7.20) for the antisymmetric mode on page 57.

For the symmetric modes

$$
\left[\begin{array}{cccc|cc}
f_{11} - J_{11}^{(0)} & -i\,J_{13}^{(0)} & J_{11}^{(0)} & f_{14} + i\,J_{13}^{(0)} & f_{17} - i\,J'_{12} & i\,J'_{12} \\
-i\,J_{31}^{(0)} & f_{22} - J_{33}^{(0)} & f_{23} + i\,J_{31}^{(0)} & J_{33}^{(0)} & -J'_{32} & J'_{32} \\
3\,J_{11}^{(0)} & f_{32} + 3\,i\,J_{13}^{(0)} & f_{33} - 3\,J_{11}^{(0)} & -3\,i\,J_{13}^{(0)} & 3\,i\,J'_{12} & f_{38} - 3\,i\,J'_{12} \\
f_{41} + 3i\,J_{31}^{(0)} & 3\,J_{33}^{(0)} & -3\,i\,J_{31}^{(0)} & f_{44} - 3\,J_{33}^{(0)} & f_{47} + 3\,J'_{32} & -3\,J'_{32} \\
\hline
f_{71} & 0 & 0 & f_{74} & f_{77} - J_{22}^{(1)} & J_{22}^{(1)} \\
0 & 0 & f_{83} & 0 & 3\,J_{22}^{(1)} & f_{88} - 3\,J_{22}^{(1)}
\end{array}\right]
\left[\begin{array}{c}
\hat{A}_1\,(0,0) \\
\hat{A}_3\,(0,0) \\
\hat{A}_1\,(0,1) \\
\hat{A}_1\,(0,1) \\
\hline
\hat{A}_2\,(1,0) \\
\hat{A}_2\,(1,1)
\end{array}\right] = 0
\tag{7.19}
$$

where the f_{NM} acquire the same expressions as in (B.1) and (B.2).

For the antisymmetric modes

$$
\left[\begin{array}{cc|cccc}
f_{11} - J_{22}^{(0)} & J_{22}^{(0)} & f_{14} - i\,J'_{21} & -J'_{23} & i\,J'_{21} & J'_{23} \\
3\,J_{22}^{(0)} & f_{22} - 3\,J_{22}^{(0)} & 3\,i\,J'_{21} & f_{25} + 3\,J'_{23} & f_{26} - 3\,i\,J'_{21} & -3\,J'_{23} \\
\hline
f_{41} & 0 & f_{44} - J_{11}^{(1)} & -i\,J_{13}^{(1)} & J_{11}^{(1)} & f_{47} + i\,J_{13}^{(1)} \\
0 & f_{52} & -i\,J_{31}^{(1)} & f_{55} - J_{33}^{(1)} & f_{56} + i\,J_{31}^{(1)} & J_{33}^{(1)} \\
0 & f_{62} & 3\,J_{11}^{(1)} & f_{65} + 3i\,J_{13}^{(1)} & f_{66} - 3\,J_{11}^{(1)} & -3\,i\,J_{13}^{(1)} \\
0 & 0 & f_{74} + 3\,i\,J_{31}^{(1)} & 3\,J_{33}^{(1)} & -3\,i\,J_{31}^{(1)} & f_{77} - 3\,J_{33}^{(1)}
\end{array}\right]
\left[\begin{array}{c}
\hat{A}_2\,(0,0) \\
\hat{A}_2\,(0,1) \\
\hline
\hat{A}_1\,(1,0) \\
\hat{A}_3\,(1,0) \\
\hat{A}_1\,(1,1) \\
\hat{A}_3\,(1,1)
\end{array}\right] = 0
\tag{7.20}
$$

where the F_{NM} acquire the same expressions in (B.3) and (B.4) .

of an isolated rectangular rod. Here again the only parameter in each matrix is the value of H_3 for chosen V and H_2 and thus the determinant of the matrix is treated as a polynomial in $1/H_3$, the real roots of which are determined by a root-solving routine, instead of the time-consuming search technique in the (2,2) - approximation, to give the appropriate values of H_3 of the dispersion curves for all possible modes in the (1,1) - approximation at once.

CHAPTER IV

NUMERICAL CALCULATION AND MODE CLASSIFICATION

1. General Description of Numerical Calculation

The derivation of the equations for the (1,1) - and (2,2) - approximations has been presented in the previous chapter. For a reasonable estimate of the dispersion curves, the (1,1) - approximation is adequate especially for the fundamental modes at low values of the parameter $k h_3$, and since the algebraic steps of this approximation have been carried out explicitly, a direct numerical evaluation of the solutions can be used. However, for the investigation of the quadratic variations of displacements within Region I, it is necessary to go to the (2,2) - approximation. For the latter it is not possible to do the algebra explicitly and some numerical search techniques have to be introduced. The ranks of the matrices (i.e., the numbers of the homogeneous equations) for the symmetric and antisymmetric modes in various approximations and the average computing times needed to obtain a set of dispersion curves (50 points) by an IBM 360/75 central processor are tabulated with remarks as follows :

Approximation	Number of 2-d. Eqs.		Number of 1-d. Eqs.		Computing Time IBM 360/75	Remarks
	SYM	ANTI	SYM	ANTI		
(0,0) -	2	1	2	1	<5 secs	Gives Rayleigh n only for SYM, L modes only for A
(1,1) -	3	3	6	6	20 secs	Dispersion reason $\hat{u}_i$ linear, algel explicit, direct r merical computat used.
(2,2) -	5	4	15	12	500 secs	Dispersion more c curate, $\hat{u}_i$ quadr algebra not expli search computati needed.
(3,3) -	6	6	24	24		Algebra has not b done.

Note that even the simplest (0,0) - approximation gives interesting solutions, whose symmetric equivalent equations for a plate were obtained by Poisson (1829) and Cauchy (1828) and are commonly called the equations of the classical theory of extensional vibrations of thin plates (Love, 1959, p. 497) .

From the ranks of the matrices and the computing times listed above, it can be seen that the extension to higher-order truncations more than the (2,2) would involve a tremendous increase in algebraic complexity and also of computing time without much anticipated increase in absolute accuracy, therefore, the dispersion curves and displacement patterns reported below are normally taken from the (2,2) - approximation. The numerical search technique developed by Lim and Farnell (1968) is used for the evaluation of the step corresponding to the procedure of Block 12 in Figure 2, Chapter II, and it has been found that double precision arithmetic must be used for the calculation of the polynomial eigenvectors, Block 6 in Figure 2. In the searching, a search range of the thickness parameter $k_t h_3$ is estimated at the given values of the phase velocity v / v_t and of the width parameter $k_t h_2$, and the real root of $k_t h_3$ in the estimated range is located by finding the corresponding minimum absolute value of the determinant of (5.3) for symmetric modes and of (5.4) for antisymmetric modes. Note that in the presentation of dispersion curves, the propagating real phase constant k in the width and thickness parameters is replaced by $k_t = \omega / v_t = 2\pi / \lambda_t$, the wave number with respect to the bulk shear velocity v_t of the substrate. Search feasibility depends upon how well the range interval is chosen at the start of the search, for example it is desirable that for each search there be one and only one value of $k_t h_3$ in the range. A dependable procedure has been to use the results of the (1,1) - approximation as a guide for the choice of search range bearing in mind that some modes may exist in the (2,2) - approximation which do not appear in the (1,1) - approximation.

2. Mode Classification vs Truncation

The dispersion curves determined in this analysis give the normalized phase velocity v / v_t as a function of the width parameter $k_t h_3$ for fixed values of the parameter $k_t h_2$. When $k_t h_2$ approaches infinity, the dispersion curves corresponding to the layered problem are obtained and on this basis the modes are classified as follows :

> The nth Rayleigh-like (or Love-like) mode is a mode that degenerates to the nth Rayleigh (or Love) mode of the layered problem when $k_t h_2 \rightarrow \infty$.

The suffix "-like" attached to the modes-names "Rayleigh" and "Love" is used because any mode in this overlay waveguide has three components of displacement (two sagittal and one transverse) at any point in the guided region except that the sagittal-plane components of an antisymmetric mode or the transverse component of a symmetric mode reduce to zero on the plane $x_2 = 0$ due to symmetry. Strictly speaking therefore, no mode in this overlay waveguide is a real Rayleigh mode or a real Love mode although it approaches one or the other when $k_t h_2 \rightarrow \infty$; and it is by this asymptotic behaviour the name Rayleigh-like or Love-like is used for the modes, though the suffix may be omitted sometimes in the sequel.

It has been found that some additional modes emerge when working on the truncated approximations with increasing orders from zero to two. Designating " R " and " L " as the Rayleigh-like and Love-like modes with prefix "s" and "a" for "symmetric" and "antisymmetric" and a following subscript n for the order of the mode, the mode classification for the (0,0) -, (1,1) - and (2,2) - approximations can be listed as

Approximation	Symmetric Modes	Antisymmetric Modes
(0,0)	$s\,R_n$	$a\,L_n$
(1,1)	$s\,R_n$, $s\,L_n$	$a\,L_n$, $a\,R_n$
(2,2)	$s\,R_n$, $s\,L_n$, $s\,R'_n$	$a\,L_n$, $a\,R_n$, $a\,L'_n$

When $k_t h_2 \to \infty$, modes $s\,R_1$, $s\,R'_1$ and $a\,R_1$ degenerate into the first Rayleigh mode of the layered problem ; modes $s\,R_2$, $s\,R'_2$ and $a\,R_2$ into the second Rayleigh mode ; and modes $s\,L_1$, $a\,L_1$ and $a\,L'_1$ into the first Love mode. From the scheme of increasing modes for higher order truncation in the above list, it is anticipated that modes $s\,L'_n$ and $a\,R'_n$ would appear in the (3,3) - approximation because of the introduction of cubic variation of displacements in x_2 - direction.

3. Adjustment Parameters

As noted in Sections 3 and 5, Chapter III, adjustment parameters are introduced into truncated approximations in order to compensate for some of the errors due to the omission of the polynomials of higher degrees. In principle, such parameters are used to reconcile the results of the approximate theory with some reference data from the three-dimensional theory ; for example, the data in the neighbourhood of cutoff frequency in an exact infinite plate were used for such purpose in the approximate two-dimensional theory of extensional vibrations of elastic plates (Mindlin, 1955 ; Mindlin and Medick, 1959). Unfortunately, such data are not always available for other problems and then a limiting case of the problem is usually used for the purpose. In the one-dimensional theory of wave propagation in elastic bars of rectangular cross section (Medick, 1966 and 1968) where the exact cutoff frequencies are not known, the bar of degenerate cross section, namely the infinite plate, was used as a means of finding the parameters.

For the configuration in this analysis, the layered problem, which has been investigated so extensively (Farnell and Adler, 1972), serves well as a limiting case for reference to find the adjustment parameters. It is readily seen that the configuration approaches a layered substrate when the width parameter $k_t h_2$ becomes very large due to the very wide relative width of the overlay. The minimum value of $k_t h_2$ required to represent the layered problem satisfactorily is not very critical. It has been found that when $k_t h_2$ is greater than 10, dispersion data obtained for the s R and a L modes have reached the limiting case and there is effectively no deviation from curve to curve for different higher values of $k_t h_2$. The deviation between curves for values of $k_t h_2$ near 10 is relatively larger for the s L and a R modes. The value of $k_t h_2 = 320$ ($h_2 = 43\ \lambda_t$) is taken in this analysis to be sufficient to make the ratio of h_2 / h_3 large enough to give the layered-problem dispersion curves for all modes and for the whole range of $k_t h_3$

concerned, and the adjustment parameters are chosen to give the best fit of this $k_t h_2 = 320$ dispersion curve to those of the corresponding layered-problem.

The distribution and use of adjustment parameters is somewhat arbitrary ; two methods have been suggested in the variational theory for plates (Mindlin, 1955), using them to affect the correct either the strain or the kinetic energy densities. The latter is simpler to apply and has been found satisfactory for this problem. The adjustment parameters, designated by r_n , are associated with the shear velocities in (3.7) and (B.1) so that the simple velocity ratios in these equations are replaced by

$$V_n = r_n v / v_t , \qquad n = 0, 1, 2 \text{ for Region II,}$$

$$V_{nm} = (r_n r_m)^{1/2} v / \hat{v}_t, \qquad n,m = 0, 1, 2 \text{ for Region I,}$$

where v_t and $\hat{v}_t$ are the bulk shear velocities of the substrate and overlay respectively.

The appropriate values of r_0 and r_1 are obtained rather easily by a computer-based trial and error method in the (1,1) - approximation realizing that values close to unity must be anticipated if the truncation is valid. For example in the guide consisting of a gold overlay on a fused-quartz substrate to be considered below, a couple of trials with interpolation reached the following values of r_n which matched the dispersion curves for $k_t h_2 = 320$ in the (1,1) - approximation to the corresponding Rayleigh and Love curves of the exact layered-problem : $r_0 = 1.005$, $r_1 = 1.010$ for symmetric modes and 1.015 for antisymmetric modes. It was found that in going to the (2,2) - approximation for the same problem, r_0 and r_1 need not be changed, and the satisfactory value of r_2 was the unadjusted value of unity and that all of these r_n are not very sensitive to the material combinations as verified in calculations with the (1,1) - approximation for dural on dural, zinc oxide on silicon etc. The same values of the parameters are used for a range of material combinations in the next chapter though it is not difficult to re-evaluate them for different combinations. Moreover, it has been found that r_0 is more sensitive to the s R and a L modes while r_1 to the s L and a R modes and the sensitivities of both depend somewhat upon the phase velocities of the waves. As an illustration, let I_0 be the increment of $k_t h_3$ for a 1 % increase of r_0 at constant r_1 and I_1 that of r_1 at constant r_0. The values of I_0 and I_1 for the first modes of a gold-on-fused-quartz guide at the normalized velocities V = .8 and .6 for h_2 / h_3 = 640 are as follows :

			$s\,R_1$	$s\,L_1$	$a\,R_1$	$a\,L_1$
V = .8	I_0	=	-.0025	-.0006	-.0003	-.0024
	I_1	=	-.0000	-.0017	-.0020	-.0000
V = .6	I_0	=	-.0055	-.0020	-.0017	-.0048
	I_1	=	-.0000	-.0027	-.0031	-.0000

CHAPTER V

RESULTS

In this chapter examples of the dispersion curves and displacement distributions as calculated with the methods of Chapter III are presented. In order to see the effects of guide thickness, attention is centered on the first Rayleigh-like and Love-like modes from the (2,2) - approximation on a single pair of materials, a gold overlay on a fused quartz substrate, and some of the second modes that are adjacent to the first are considered (Tu and Farnell, 1972b, 1971a and 1971b). The pair of materials chosen was selected in order to facilatate comparison of the thin-film limiting results with earlier calculations and with experimental measurements (Tiersten, 1969; Adkins and Hughes, 1969). No complete verification exists for the thicker film results to be shown except for consistency of successive approximations, degeneracy into known layer-on-half-space results when the guide width becomes large in terms of the wavelength, and degeneracy into rod solutions when the substrate stiffness and density vanish. The results obtained with the (2,2) - approximation in another limiting case, that of the topographic guide (Mason et al., 1971; Tu and Farnell, 1972a), which obtains its guiding action from a topographic deformation of the half-space substrate or in the language here a relatively thick overlaid ridge of the same material as the substrate, agree well with experimental measurements and provide an essential verification to the analysis of this thesis. Chapter VI is concerned specifically with topographic guides and with brief remark on the rigid substrate guide (Waldron, 1971 and 1972).

The dispersion curves from the (1,1) - approximation for overlays of platinum, polystyrene, nickel and an artificial gold on a common substrate of fused quartz are presented in the latter part of this chapter in order to illustrate both the application of the analysis to various material combinations and the general behaviour of the overlay guides.

1. Dispersion from the (2,2) - Approximation

The dispersion curves as calculated with the (2,2) - approximation for a gold overlay on a fused-quartz substrate (for material constants see Section 4) are shown in Fig. 3 to 8. The displacement distributions will be considered in the next section. As noted previously, the natural form of a dispersion curve for calculations using the methods above expresses the normalized velocity v/v_t as a function of $k_t h_3$ for a fixed value of $k_t h_2$, and these are the parameters used in Fig. 3 to 6. The more common form in which the aspect ratio (h_2/h_3) of the overlay is the fixed parameter on each curve can be interpolated from the former curves and is used in Fig. 7 and 8. In all of the figures, therefore, the abscissa on the curves is the layer thickness, $2h_3$, expressed in terms of $k_t h_3$ and the ordinate the mode phase velocity v relative to the shear velocity v_t with parameters $k_t h_2$ in Fig. 3 to 6 and with parameters h_2/h_3 in Fig. 7 and 8. Since the symmetric and antisymmetric modes can be separated as shown in the analysis, the dispersion curves in the figures are divided according to modes of the symmetric Rayleigh-like (sR, sR'), the antisymmetric Rayleigh-like (aR), the symmetric Love-like (sL) and the antisymmetric Love-like (aL, aL') as will be seen below.

It will be recalled that for an infinite isotropic layer on an isotropic half-space substrate, there are two independent sets of solutions. The modes which involve sagittal-plane displacements only are usually called the Rayleigh modes (Farnell and Adler, 1972) and the dispersion curves for the first two of these modes for an infinite gold layer on a half-space of fused quartz are marked "first Rayleigh" and "second Rayleigh" on Fig. 3 and 4. Similarly, the modes of the other set, the Love modes, for the infinitely wide layer have only the displacement component which is normal to the sagittal plane, and the dispersion curve for the first of these modes is marked "first Love" on Fig. 5 and 6. The curve for the second Love mode lies entirely above the range of $k_t h_3$ plotted here.

The dispersion curves for the symmetric modes sR_1 and sR_2 are shown for a wide range of $k_t h_2$ values in Fig. 3. The phase velocities of the sR_1 modes all approach the Rayleigh velocity of a free quartz surface ($v_R / v_t = 0.9058$) with zero slope for decreasing values of layer thickness (Tiersten, 1969). On the other hand, the curves for the sR_2 modes approach the substrate Rayleigh velocity v_R with a finite slope much as does the limiting second Rayleigh curve itself. However, for the waveguide modes, if the phase velocity exceeds v_R then the waveguide mode will radiate a simple Rayleigh wave onto the substrate free surface at an angle to the guide axis appropriate for phase matching. Since in this analysis $k_t h_2$ is given a positive real value to find a positive real $k_t h_3$ as a root for a valid solution, implying that k_t must be positive real, it is impracticable to use this analysis to find a solution in the "leaky-wave" region of velocities above $v = v_R$.

Two unanticipated symmetrical sets of modes, sR_1' and sR_2', which also evolve from the first and second Rayleigh layer modes are shown by the two groups of broken curves on Fig. 3. It is seen by the $k_t h_2$ values on the latter curves that the dispersion of these modes is a much more sensitive function of guide width than for the sR_1 set.

The other modes which evolve from the Rayleigh layer modes as the guide width is decreased are the antisymmetric aR_1 and aR_2 shown by the solid and broken curves respectively in Fig. 4. Here the dispersion curves for the aR_1 modes do not come to a common point at $k_t h_3 \to 0$ as do the sR_1 modes but rather appear to have a cut-off (Tiersten, 1969) in the sense that below a given value of $k_t h_3$ the calculated velocity would exceed the substrate Rayleigh velocity v_R and the mode would radiate a free-surface Rayleigh wave. For a given decrease in guide width, an aR_1 curve is displaced much more to the right than the corresponding curve for an sR_1 mode.

If the sets of modes which evolve from the first Love mode of the infinitely wide layer geometry are now considered, the dispersion curves develop as indicated in Fig. 5 and6. It is seen that the symmetrical set sL_1 of Fig. 5 enter the leaky wave region $v > v_R$ at finite slopes. While these modes have only transverse displacement components u_2 for very large values of $k_t h_2$, all three components are present for finite widths. Figure 6 shows the dispersion associated with the two antisymmetric modes aL_1 and aL_1'. The former set is different from all of the modes formerly noted in that the velocity for large $k_t h_3$ of a finite width guide is less than the velocity for an infinitely wide layer of the same thickness. It is this mode which, in the limit where the properties of the overlay and of the substrate materials are identical, becomes the first flexural mode for topographic waveguides (Ash et al., 1969; Mason et al., 1971; Tu and Farnell, 1972a). Note that in the latter limit, $\hat{v}_t$ approaches v_t and thus the dispersion curves of all of the modes considered other than aL_1 and aL_1' are forced into the leaky-wave regime.

Figures 7 and 8 show the dispersion information of Fig. 3 and 6, respectively, plotted in more conventional form where the aspect ratio h_2 / h_3 is the constant parameter on each curve. The solid curves and the curves with short dashes of Fig. 7 reproduce the corresponding sR_1 and sR_1' data as interpolated from Fig. 3. Also shown in Fig. 7 by long dashes are the dispersion curves calculated by Tiersten (1969) for thin film overlays, and the agreement between the present results and those for the thin approximation is seen to be good in the region where the latter approximation applies. Figure 8 gives the dispersion curves for the first antisymmetric Love modes aL_1 and aL_1' as interpolated from the data of Fig. 6. Again as the thickness of the overlay becomes comparable to its width, the phase velocity of the aL_1 mode falls below that of the infinitely wide layer for values of frequency and thickness large enough that $k_t h_3$ is beyond the cross-over region. For gold on fused quartz, the cross-over values are in the region of $k_t h_3 = 0.14$.

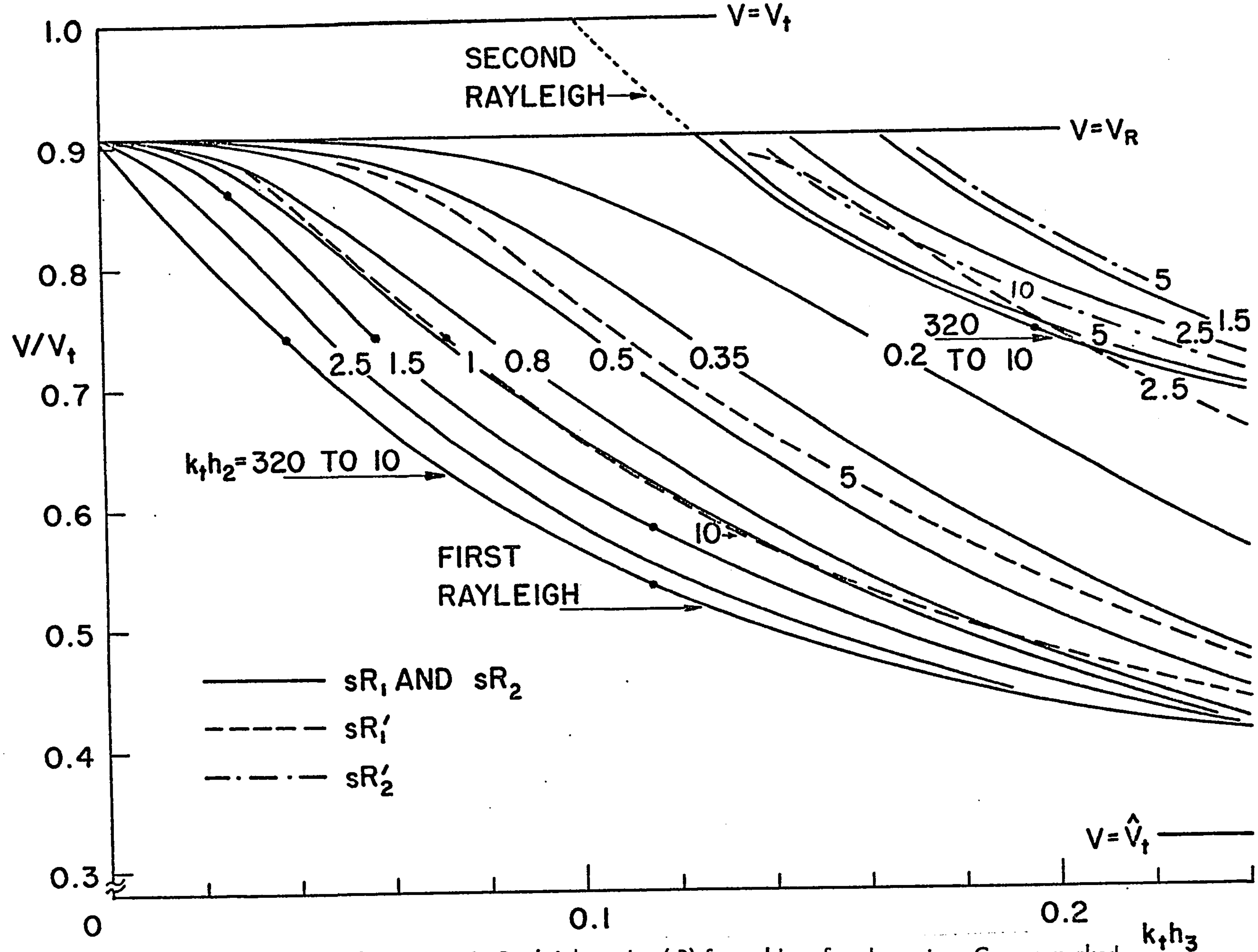

Fig. 3. Dispersion curves for symmetric Rayleigh modes (sR) for gold on fused quartz. Curves marked "first Rayleigh" and "second Rayleigh" are for layer modes. Displacements of the sR_1, sR_1' and sR_2 modes for points marked with solid dots are shown in Fig. 9, 17 and 19 respectively.

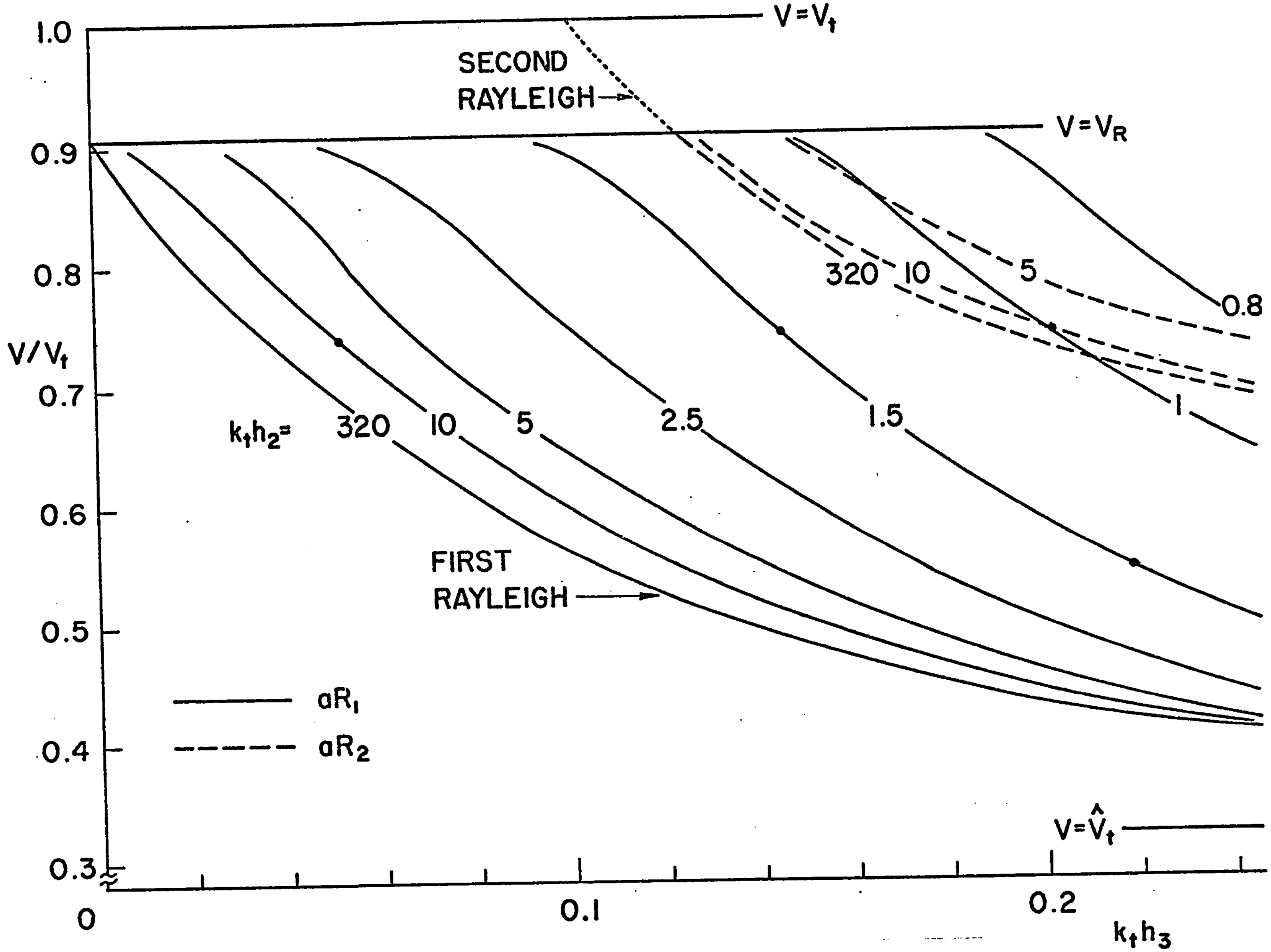

Fig. 4. Dispersion curves for antisymmetric Rayleigh modes (aR) for gold on fused quartz. Displacements of the aR_1 and aR_2 modes for points marked with solid dots are shown in Fig. 13 and 20.

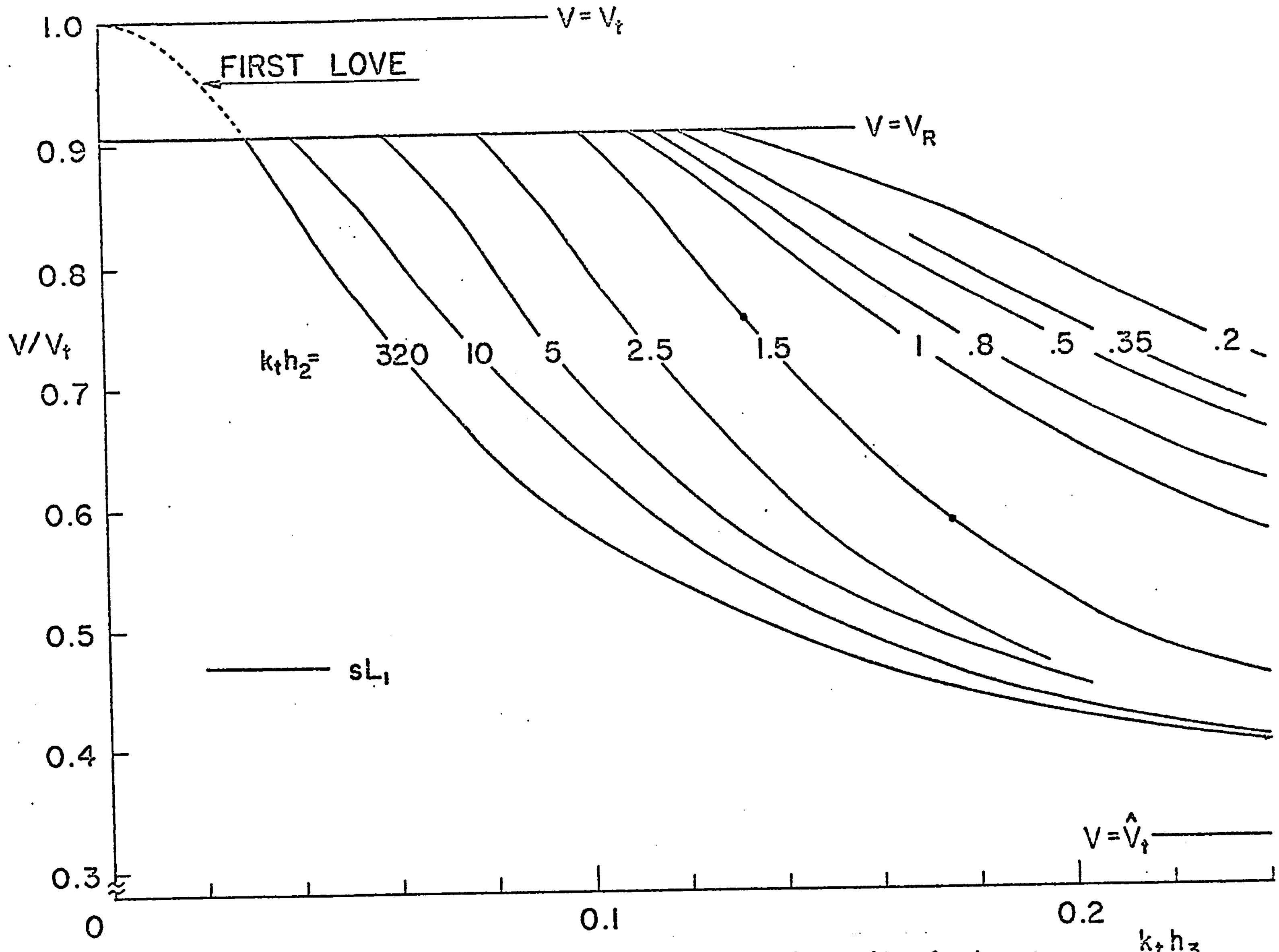

Fig. 5. Dispersion curves for first symmetric Love modes (sL_1) for gold on fused quartz. Displacements for points marked with solid dots are shown in Fig. 11.

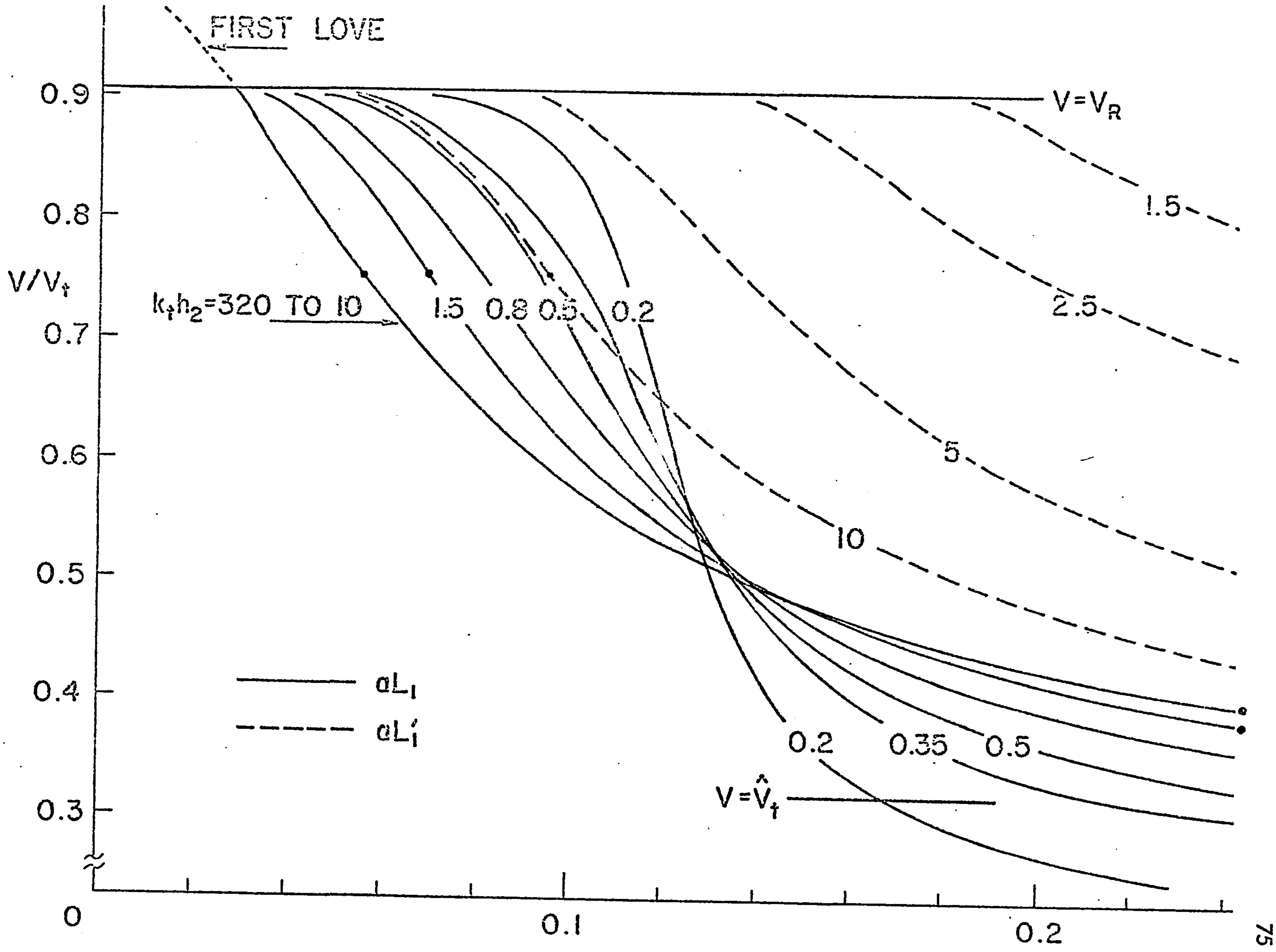

Fig. 6. Dispersion curves for antisymmetric Love modes (aL) for gold on fused quartz. Displacements of the aL_1 and aL_1' modes for points marked with solid dots are shown in Fig. 15 and 18.

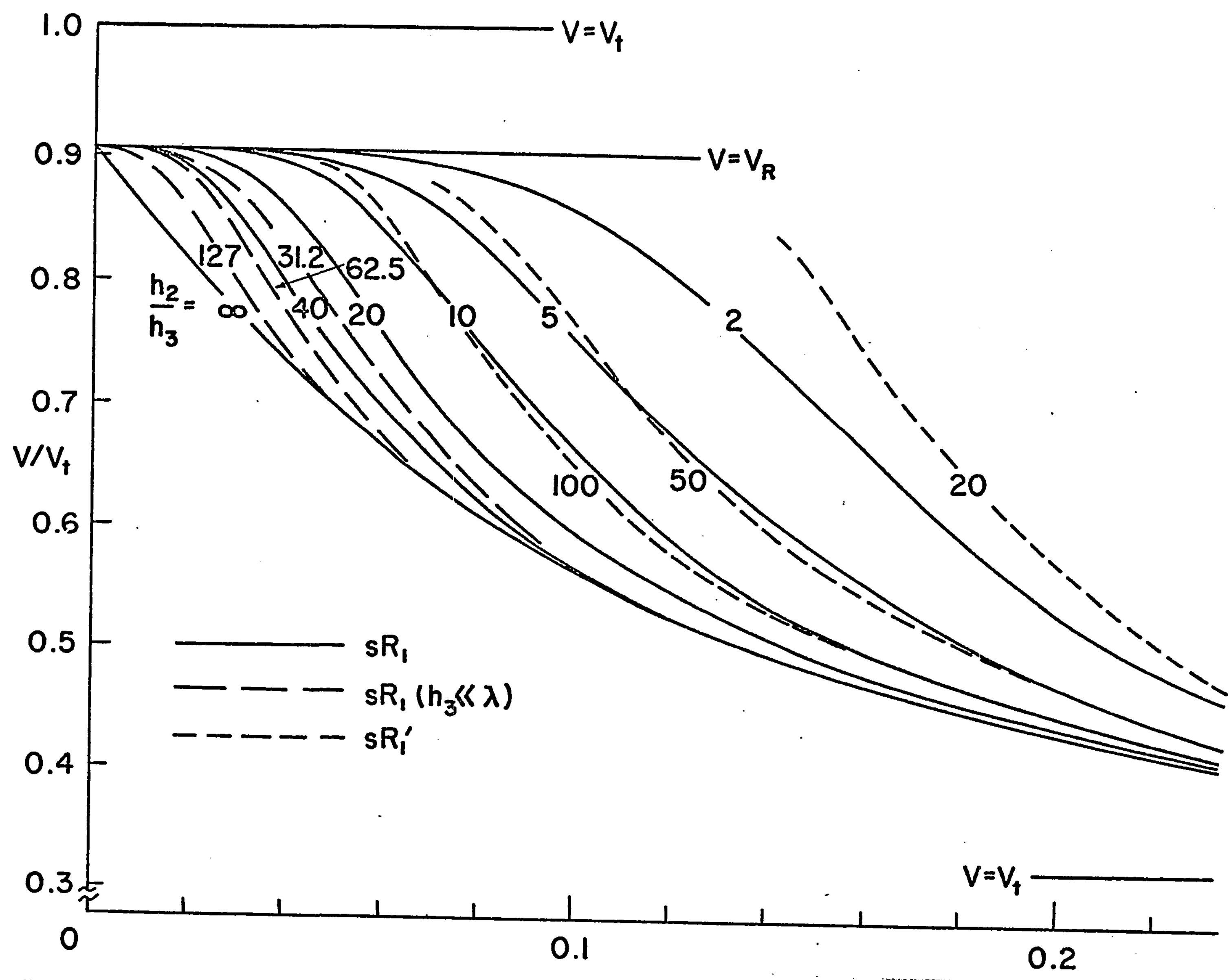

Fig. 7. Dispersion curves for symmetric Rayleigh modes (sR) of Fig. 3 here plotted for fixed aspect ratios of the overlay. Curves with long dashes ($h_3 << \lambda$) are from Tiersten (1969).

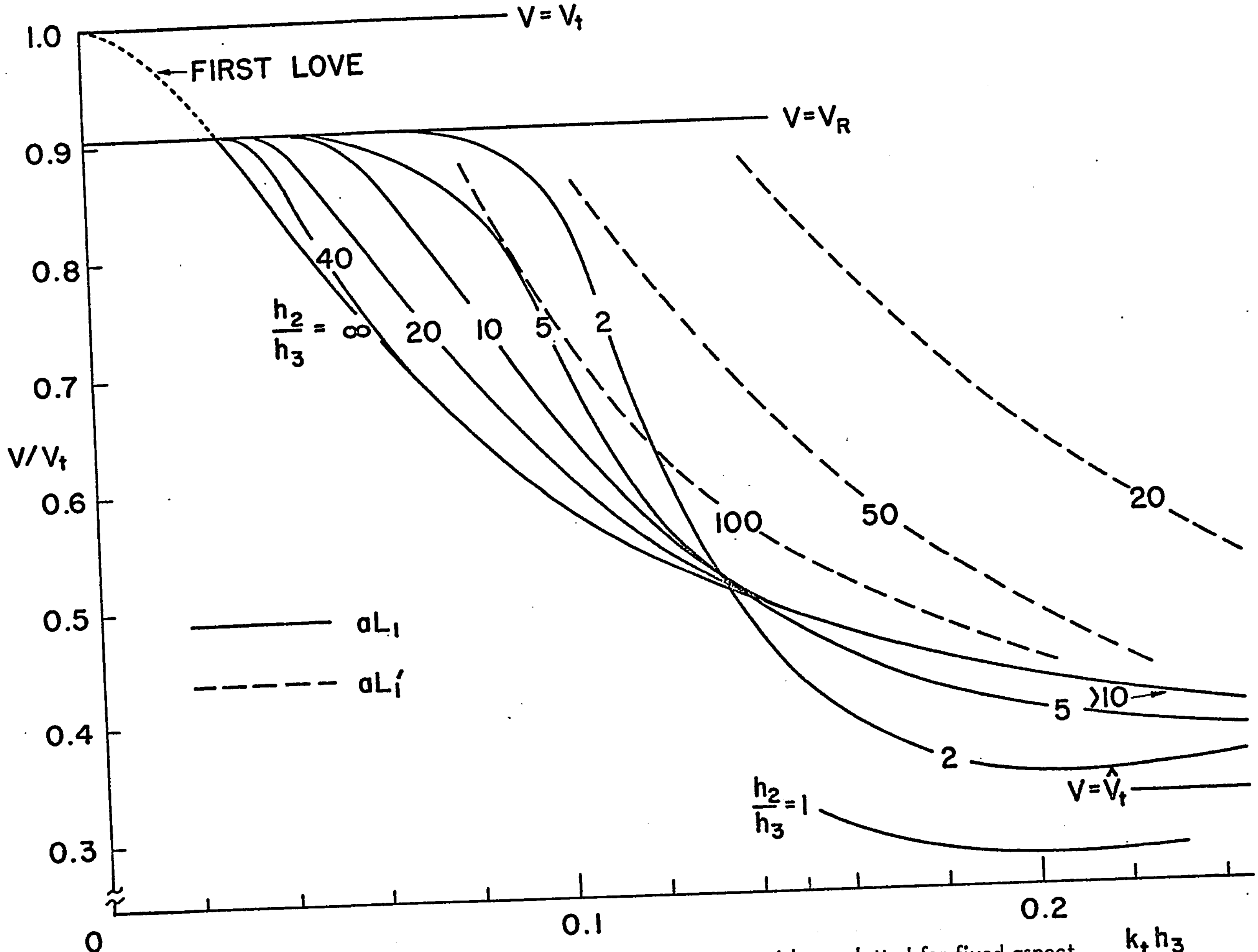

Fig. 8. Dispersion curves for antisymmetric Love modes (aL) of Fig. 6 here plotted for fixed aspect ratios of the overlay.

2. Displacements from the (2,2) - Approximation

As mentioned in the mode classification, Section 2, Chapter IV, each component of displacement is present to some degree at each general point of the guide region, and thus the displacement patterns for the various modes tend to be complicated in nature ; however, some of the salient features of the lower order modes will be illustrated here. Due to the symmetry with respect to the mirror plane $x_2 = 0$ for all modes, the sagittal components of displacement (the longitudinal u_1 and vertical u_3) of a symmetric mode and the transverse component (u_2) of an antisymmetric mode must be an even function of x_2 (P_0 and P_2) and thus are quadratic in Regions I and II and exponentially decaying in Region III in the (2,2) - approximation. On the contrary, the transverse component of a symmetric mode and the sagittal components of an antisymmetric mode are only allowed to be odd function of x_2 (P_1) in the (2,2) - approximation and thus are linear in Regions I and II, implying that they are zero at $x_2 = 0$ and increase linearly in magnitude to the edges of overlay, and again decay exponentially in Region III. To permit convenient comparisons, the displacements corresponding to several points on the dispersion curves of the former section are shown here. There are in general two figures for each point: one shows the distribution of displacement on the symmetry plane $x_2 = 0$ and expresses the behaviour in the centre of the overlay and the exponential decay down to the depth of the substrate ; while the other shows the distribution of displacement along the positive half-surface $x_3 = 0$ and expresses the symmetry characteristics of waves in the (2,2) - approximation. In all of the figures shown below, the abscissa is either $k_t x_3$ or $k_t x_2$ as required and the ordinate is the amplitude of the components of displacement normalized with respect to u_3 for R-modes and u_2 for L-modes at the origin (0, 0), or at the right corner of the overlay (h_2, 0) when the magnitude of the component to be normalized is zero at the origin.

Attention is focused first on a gold-on-fused-quartz guide of fixed overlay width $k_t h_2 = 1.5$ ($h_2 = 0.207\ \lambda_t = 0.187\ \lambda_R$). Figures 9a and 9b show the relative magnitude and phase of the different components for the sR_1 mode at three different velocities which are indicated by solid dots on Fig. 3. Along the vertical centre line $x_2 = 0$ of any cross section the transverse component vanishes because of symmetry and the two sagittal components are in phase quadrature giving the retrograde elliptical particle motion on the free surface which is characteristic of the first Rayleigh mode for layer geometry. The decay with depth of these components is close to that associated with the first Rayleigh mode at the corresponding layer thickness. As reference curves, the lines marked "layer" on Fig. 9a give the displacement components of the Rayleigh mode for an infinite layer (Farnell and Adler, 1972) of the same thickness as that used for the $v/v_t = 0.58$ curve, that is for the point marked by a solid dot on the dispersion curve for the first Rayleigh mode in Fig. 3. Of course for the (2,2) - approximation to the waveguide situation, the displacements are the "best" compromise, in the sense of Chapter III, to the true displacements which is obtainable with quadratic variation in the overlay cross-section, multiple exponential decay with depth into the substrate and the simple exponential decay transverse to the guide direction within the substrate.

The relative displacements of Fig. 9b are shown as a function of distance along the x_2-axis, for the same conditions and normalization as used in Fig. 9a. The abscissa value $k_t h_2 = 1.5$ corresponds to the right bottom corner of the overlay region, and for larger values of $k_t x_2$ the decay of each component is exponential with the decay factor β depending on the velocity in the manner of (3.9). While the transverse component of displacement is zero on the central symmetry plane, this component which is in phase ~~quadrature~~ with the vertical component grows to appreciable amplitude at the edge of the overlay region when the overlay is thick.

The representation of Fig. 10 shows the distortion of rectangular grids on successive planes spaced at intervals of $\lambda / 32$ in the direction of propagation. The broken lines indicate the outline of the undistorted guide and the quarter-wavelength planes. This sketch corresponds to the sR_1 mode at $v/v_t = 0.74$ on Fig. 9a and it is seen again that the particle motion is dominantly the sagittal-plane elliptical motion associated with the first Rayleigh mode but here the amplitude decreases in both directions away from the central plane.

The displacement distributions associated with the sL_1 mode for $k_t h_2 = 1.5$ are shown as a function of $k_t x_3$ on the central plane in Fig. 11a and as a function of $k_t x_2$ along the interface in Fig. 11b. Again because of symmetry, there is no transverse component of displacement on the central plane but this component grows with x_2 and reaches a maximum at the top free corner of the overlay. The displacements have been normalized here to the value of this component on the interface at the edge of the overlay. On the central plane the motion is Rayleigh-like but with the shape of the displacement curves reminiscent of the second or Sezawa mode rather than the first Rayleigh layer mode (Farnell and Adler, 1972), for example the surface particle displacement is progressive rather then retrogressive. At the edges of the guide the displacement is predominantly transverse so that the general motion could be described as transverse bulging accompanied by transverse buckling as illustrated by the grid displacements of Fig. 12.

For the antisymmetric modes, the sagittal-plane displacements are zero on the central plane as illustrated in Fig. 13 and 15 where the curves are again drawn for $k_t h_2 = 1.5$. For the aR_1 mode of Fig. 13a and b it is seen that these sagittal -plane displacements grow with x_2 on the interface and reach a maximum at the guide edge. At the guide edge the relative phase and shape with depth of the u_1 and u_3 components are those associated with the first Rayleigh layer mode. Thus the dominant motion is Rayleigh motion of the region near the sides of the guide with opposite phase on opposite sides giving the tilting Rayleigh motion of Fig. 14 accompanied by a relatively small transverse motion represented by the u_2 component.

The transverse component is the dominant one at each point for the aL_1 mode as shown by Fig. 15a and b. The central plane displacements are similar to those of the first Love mode of the layer geometry. The solid curve of Fig. 15a gives the displacement as a function of depth for this first pure Love mode propagating in a layer of the same thickness as that involved in the $v/v_t = 0.38$ waveguide curve. In the steeper region of the waveguide dispersion curves, that is below the cross-over region of Fig. 6, the general motion is predominantly a side-to-side motion of the layer as a whole in the manner illustrated by Fig. 16. However above the cross-over region the displacements are more concentrated in the layer and the pattern approaches that of the first flexural mode of a long plate cantilevered from a rigid substrate.

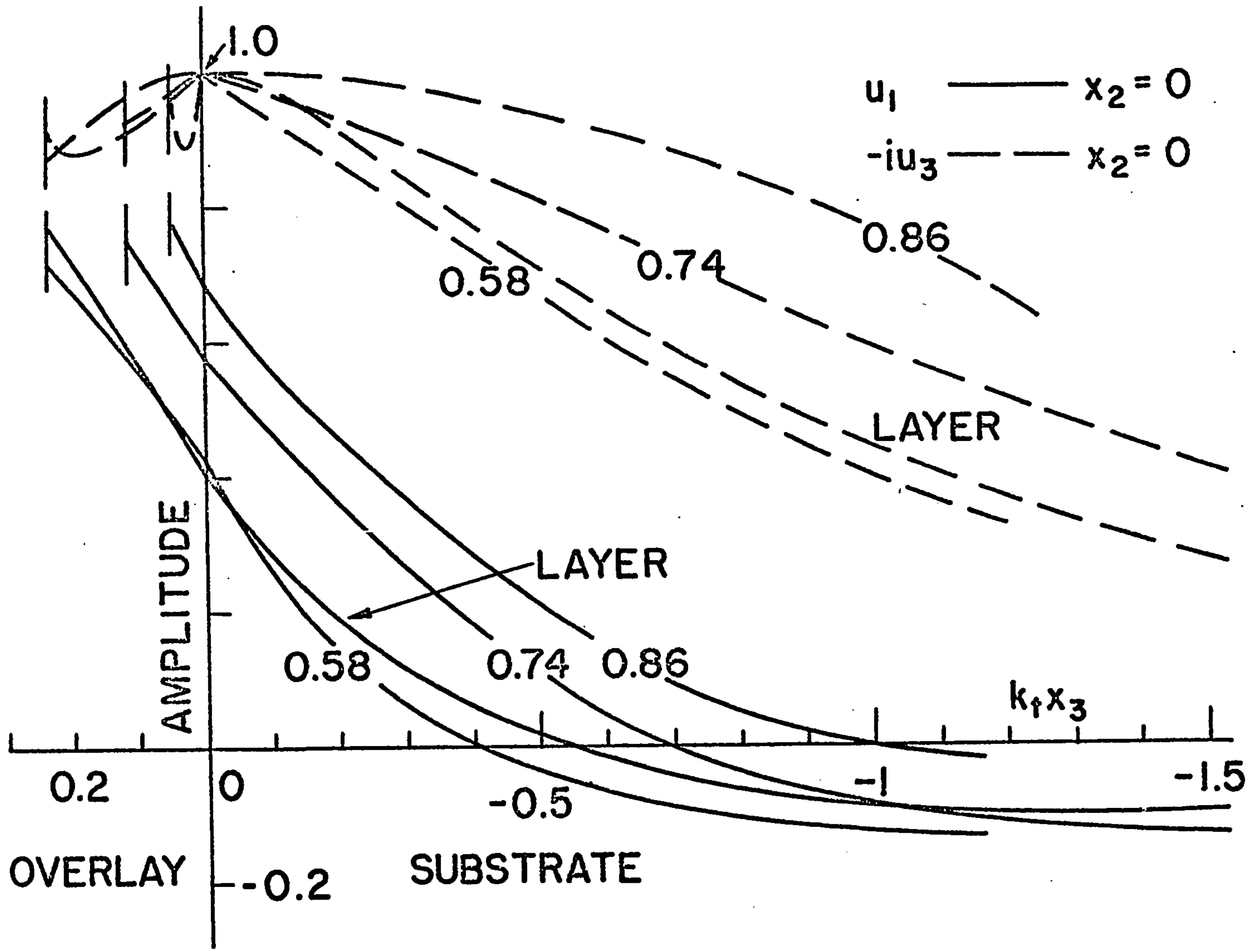

Fig. 9a. Displacement components on vertical centre line ($x_2 = 0$) for symmetric Rayleigh mode (sR_1) for points marked on dispersion curves, Fig. 3. $k_t h_2 = 1.5$ and velocity ratios are marked on curves. Curves marked "layer" are for infinite layer on thickness $k_t h_3 = 0.117$ on Fig. 3.

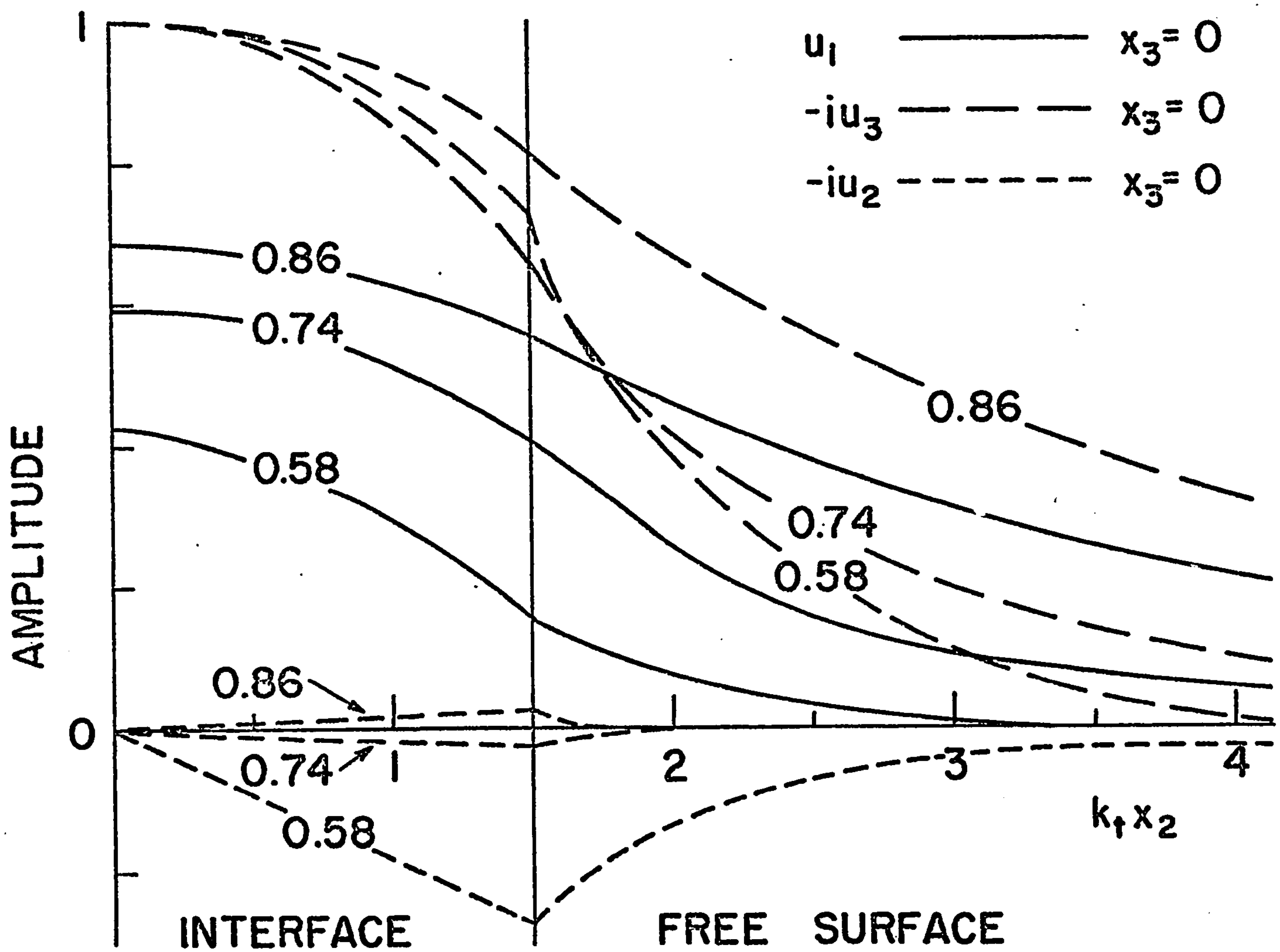

Fig. 9b. Displacement components on interface ($x_3 = 0$) for symmetric Rayleigh mode (sR_1) for points marked on dispersion curves, Fig. 3. $k_t h_2 = 1.5$ and velocity ratios are marked on curves.

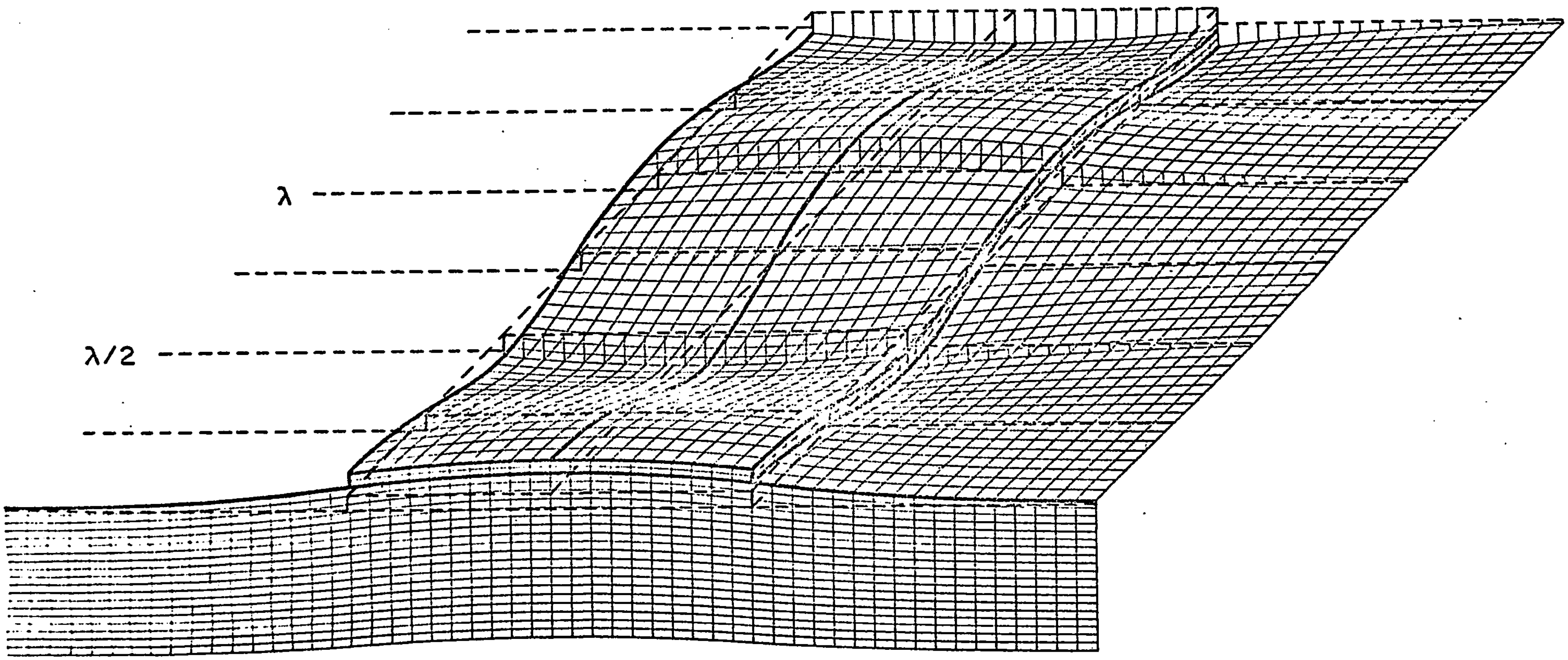

Fig. 10. Distortion of a rectangular grid due to symmetric Rayleigh mode (sR_1). $k_t h_2 = 1.5$ and $v/v_t = 0.74$ on Fig. 9. Broken lines are undistorted outlines of guide and quarter-wavelength planes.

GOLD/FUSED QUARTZ, (V/VT)=0.74,KTH2=1.5,KTH3=0.0570, SYMMETRIC RAYLEIGH MODE

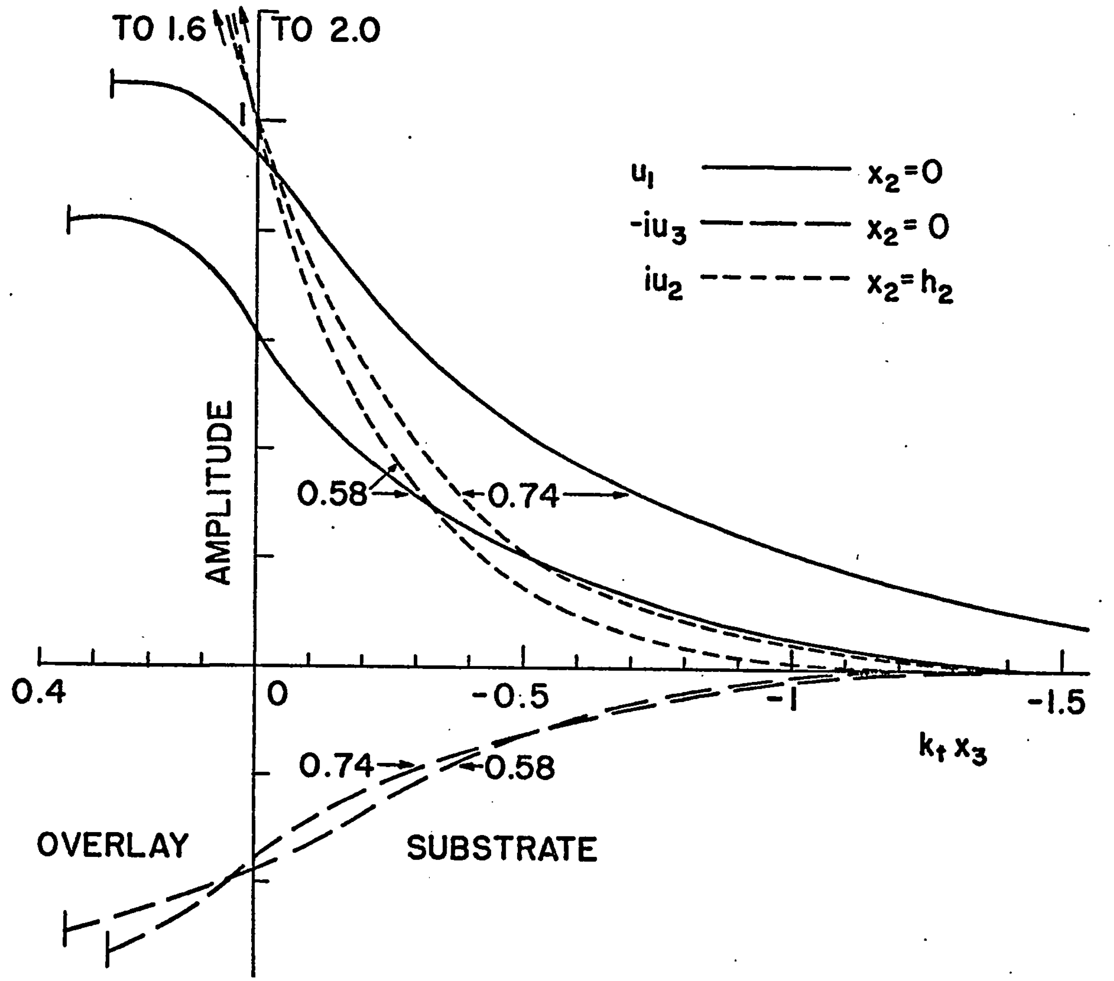

Fig. 11a. Displacement components on vertical centre line ($x_2 = 0$) for symmetric Love mode (sL_1) for points marked on dispersion curves, Fig. 5. $k_t h_2 = 1.5$ and velocity ratios are marked on curves.

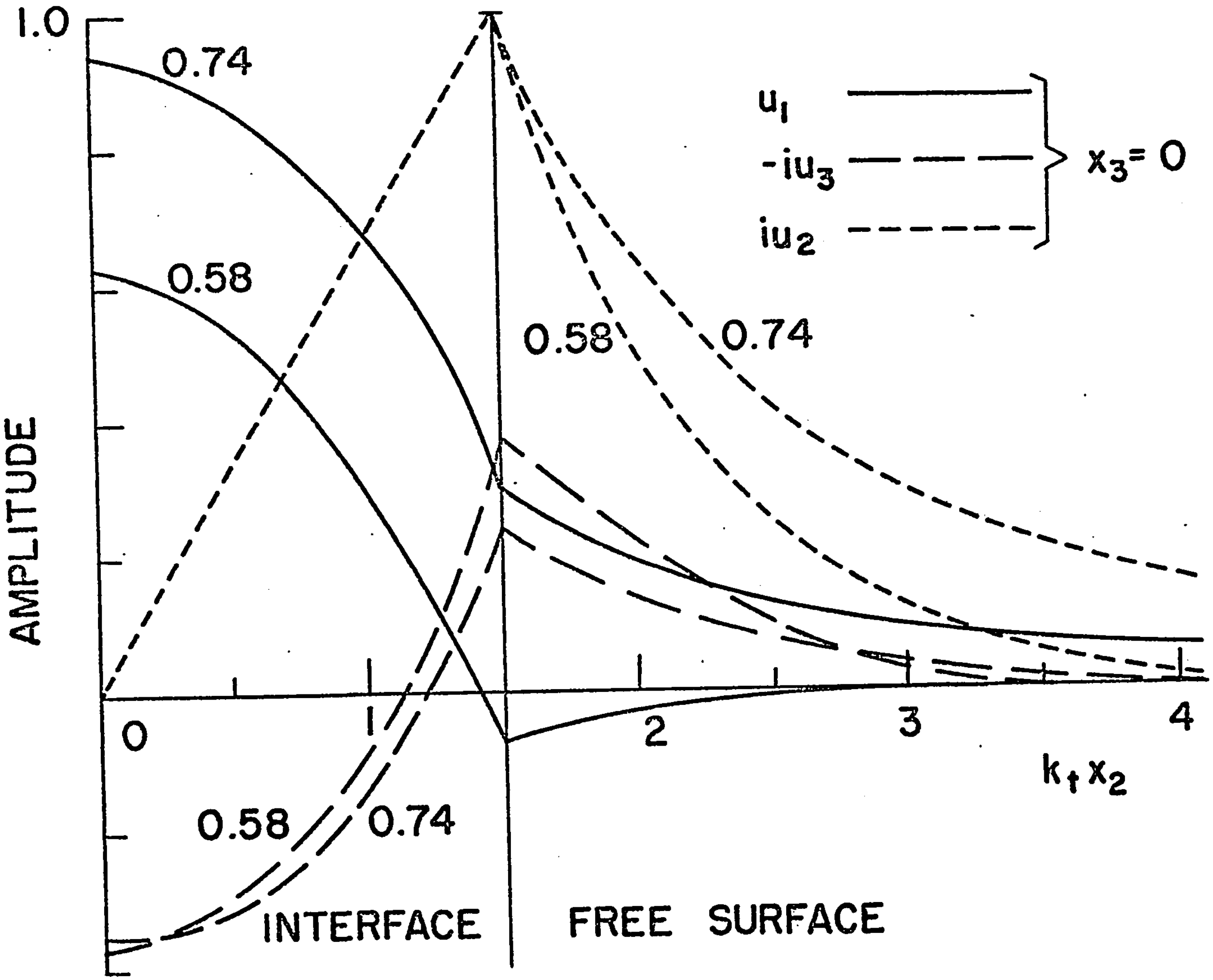

Fig. 11b. Displacement components on interface ($x_3 = 0$) for symmetric Love mode (sL_1) for points marked on dispersion curves, Fig. 5. $k_t h_2 = 1.5$ and velocity ratios are marked on curves.

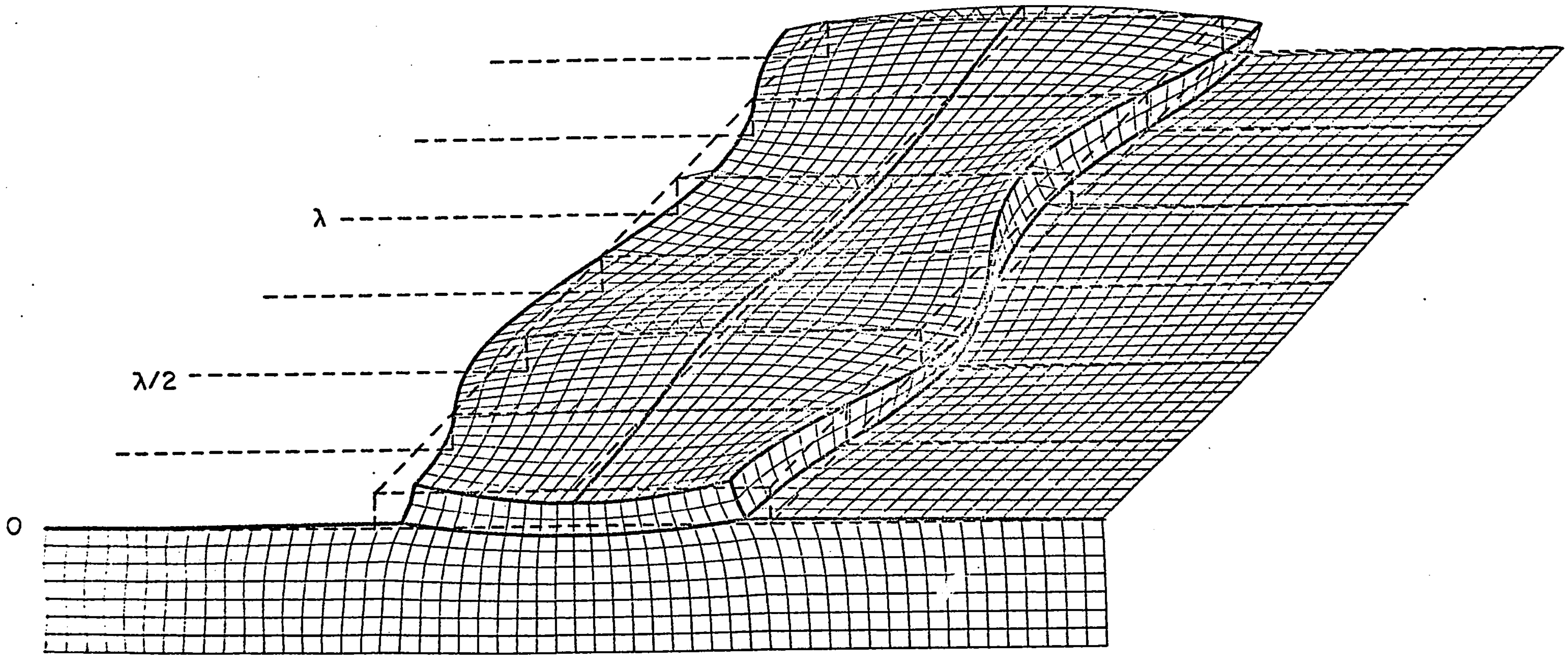

Fig. 12. Distortion of a rectangular grid due to symmetric Love mode (sL_1). $k_t h_2 = 1.5$ and $v/v_t = 0.74$ on Fig. 11.

GOLD/FUSED QUARTZ, (V/VT)=0.74, KTH2=1.5, KTH3=0.1354, SYMMETRIC LOVE MODE

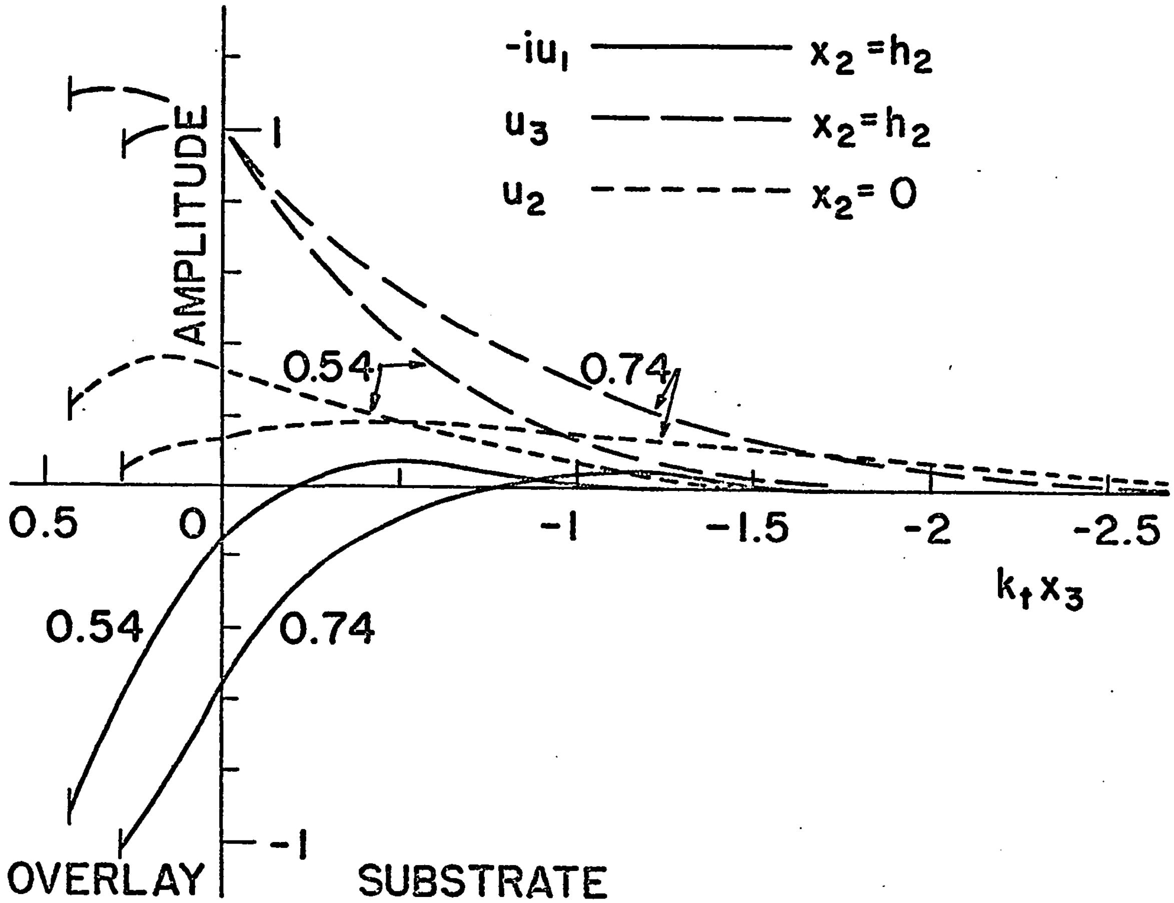

Fig. 13a. Displacement components on vertical centre line ($x_2 = 0$) for antisymmetric Rayleigh mode (aR_1) for points marked on dispersion curves, Fig. 4. $k_t h_2 = 1.5$ and velocity ratios are marked on curves.

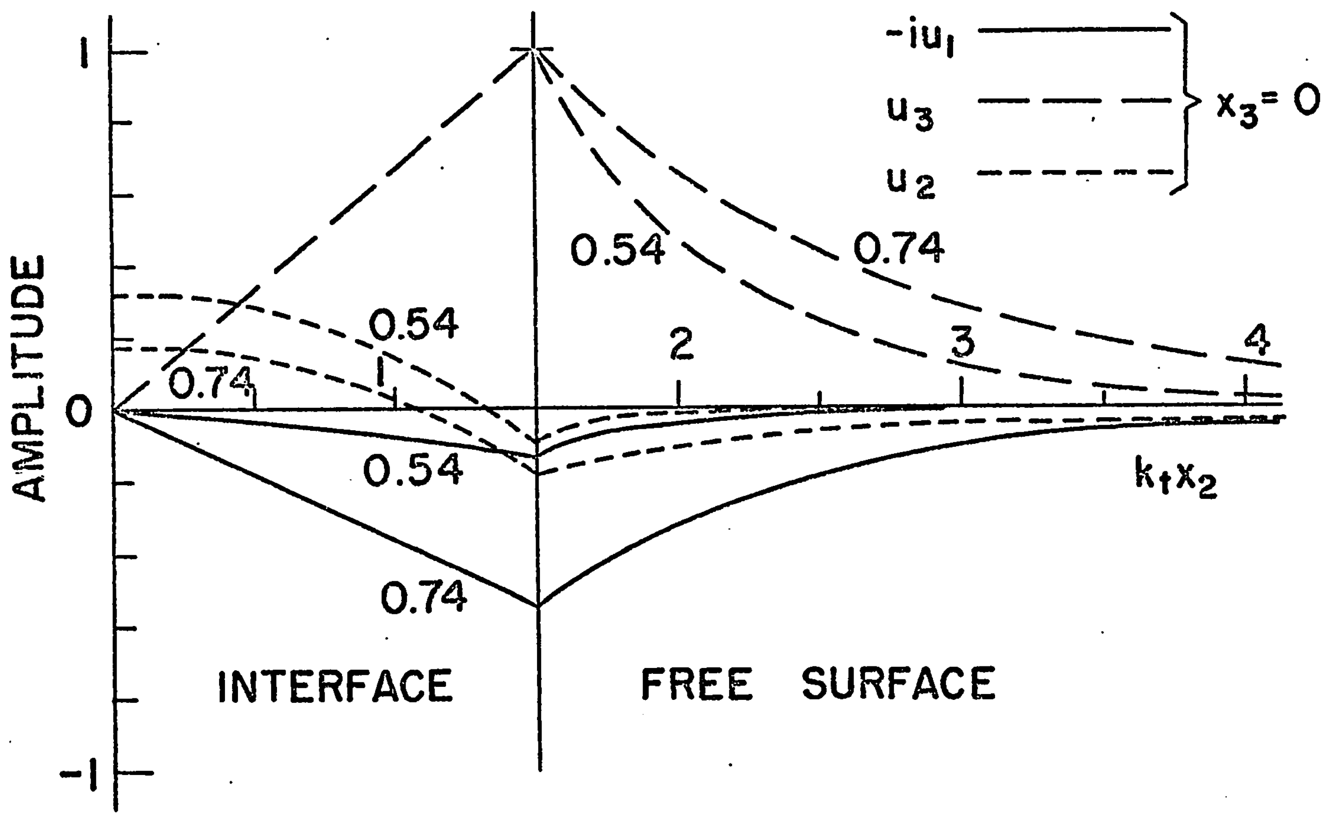

Fig. 13b. Displacement components on interface ($x_3 = 0$) for antisymmetric Rayleigh mode (aR_1) for points marked on dispersion curves, Fig. 4. $k_t h_2 = 1.5$ and velocity ratios are marked on curves.

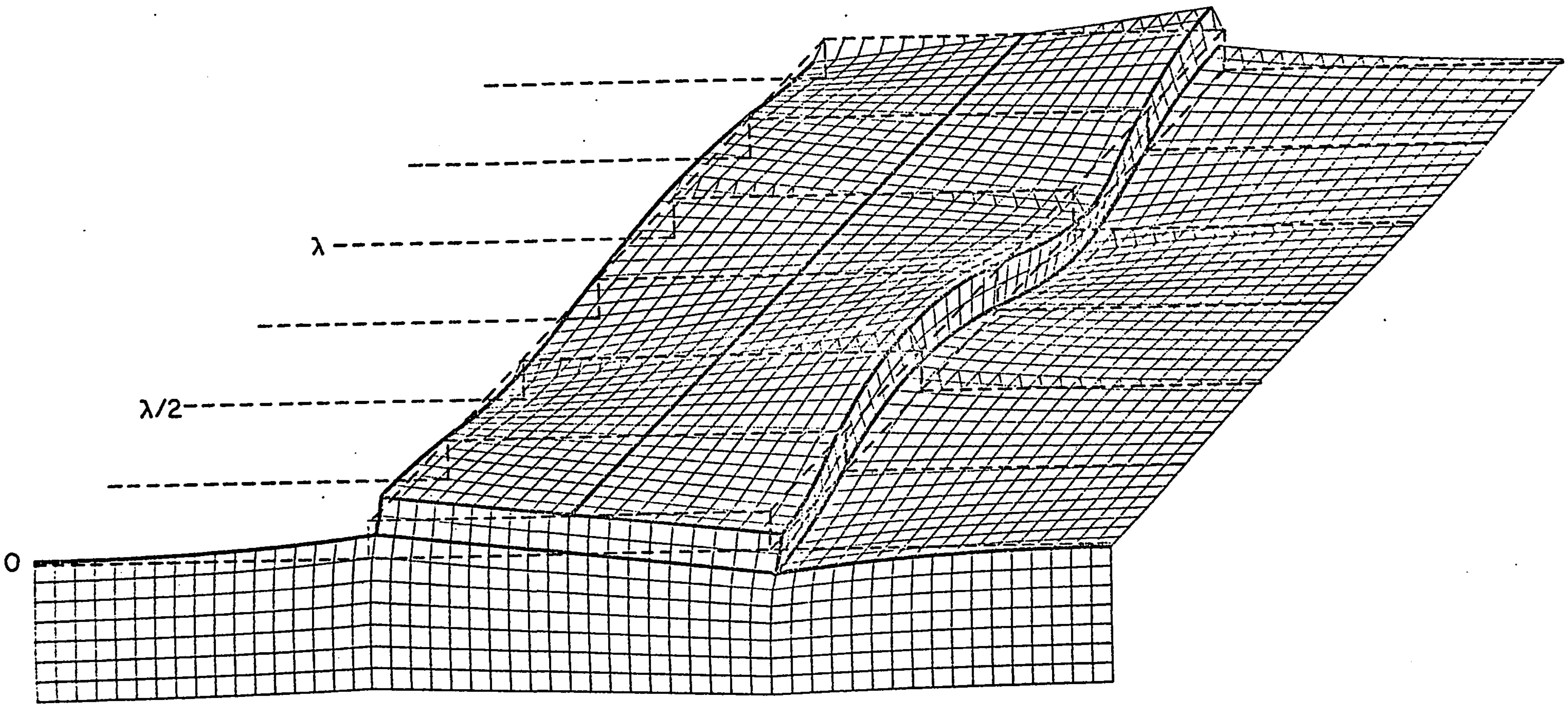

Fig. 14. Distortion of rectangular grid due to antisymmetric Rayleigh mode (aR_1). $k_t h_2 = 1.5$ and $v/v_t = 0.74$ on Fig. 13.

GOLD/FUSED QUARTZ, (V/VT)=0.74,KTH2=1.5,KTH3=0.1449, ANTISYMMETRIC RAYLEIGH MODE

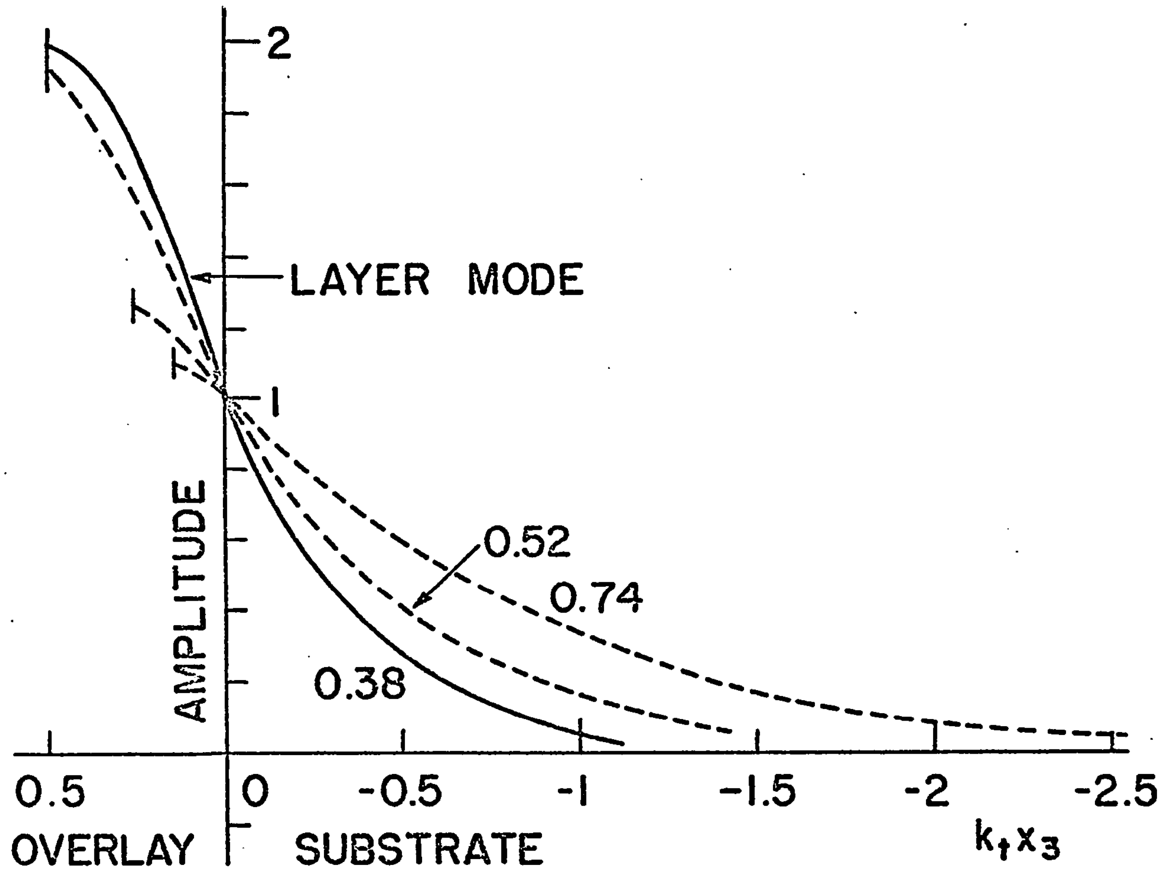

Fig. 15a. Displacement components on vertical centre line ($x_2 = 0$) for antisymmetric Love mode (aL_1) for points marked on dispersion curves, Fig. 6. $k_t h_2 = 1.5$ and velocity ratios are marked on curves. Solid curve is u_2 displacement for the first Love mode of an infinite layer with $k_t h_3 = 0.245$ as marked on Fig. 6.

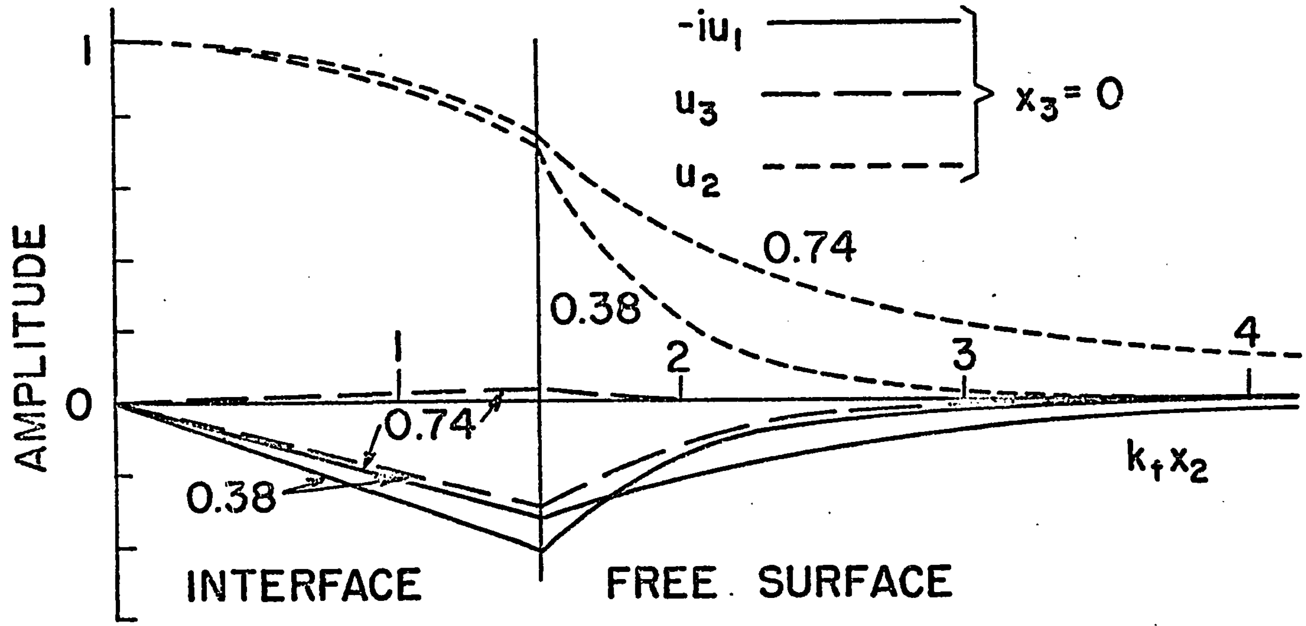

Fig. 15b. Displacement components on interface ($x_3 = 0$) for antisymmetric Love mode (aL_1) for points marked on dispersion curves, Fig. 6. $k_t h_2 = 1.5$ and velocity ratios are marked on curves.

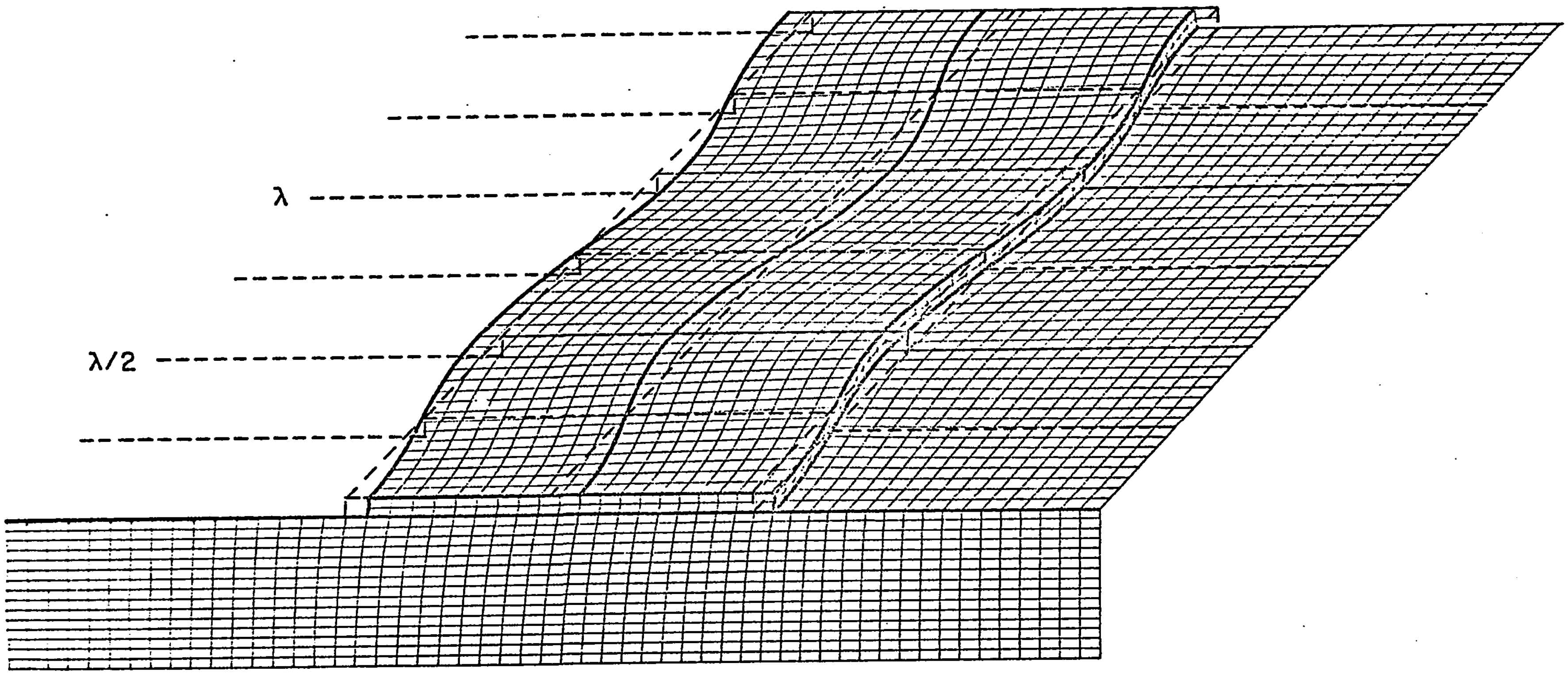

Fig. 16. Distortion of rectangular grid due to antisymmetric Love mode (aL_1). $k_th_2 = 1.5$ and $v/v_t = 0.74$ on Fig. 15.

GOLD/FUSED QUARTZ, (V/VT)=0.74,KTH2=1.5,KTH3=0.0719, ANTISYMMETRIC LOVE MODE

The displacement curves shown in Figures 9 to 16 above are for the modes that approach the first Rayleigh and Love modes of layered problem and would appear if calculated with the (1,1) - approximation. Now the modes sR_1' and aL_1', which approach the first modes of layered problem but would not appear in the (1,1) - approximation, and the modes sR_2 and aR_2, which would appear in the (1,1) - approximation but approach the second Rayleigh modes of layered problem will be considered. These modes have more structure in the displacement patterns and the sample points chosen are for points ($k_t h_2 = 10$ and $v/v_t = 0.74$) marked with solid dots on the dispersion curves for a gold-on-fused-quartz guide in Section 1. The previous scheme is used again to show the displacement patterns for each sample point with two figures giving the central plane and interface components. Figure 17a shows the relative amplitudes of the sR_1' mode (solid lines) as a function of depth along the central plane $x_2 = 0$ with the sR_1 mode (dash lines) of the same phase-velocity and width parameter plotted for comparison, and it is seen that there is not much difference between them along this line. However, from Fig. 17b in which the relative amplitudes of the two modes as a function of x_2 on the surface $x_3 = 0$ are plotted, interesting differences between them appear in that first the sagittal components of sR_1 mode have large amplitudes at the centre of the overlay and decrease slightly toward the edge, while those of the sR_1' mode have large amplitudes at the edge of the overlay and decrease through zero and then grow negatively as the centre is approached so that there are planes at $x_2 \simeq \pm h_2 / 2$ on which the vertical or the longitudinal displacement is zero. Moreover, the sR_1' mode has a rather unusual distribution of the transverse component, which is zero at the centre of the overlay and builds up linearly to a very large value, making this Rayleigh-like mode have some of the characteristics of a Love-like, compare Fig. 17b and Fig. 11b. This special distribution of transverse component is not a general behaviour of the sR_1' mode, since the same sR_1' mode at a different value of $k_t h_2$ does not contain such a prominent transverse component; such an appearance for the mode sR_1' of $k_t h_2 = 10$ and $v/v_t = 0.74$ is due to a result of mode coupling with the mode sL_1 of the same parameters as will be shown in Fig. 22 of the next section.

The transverse component of the aL_1' mode in Fig. 18 assumes a pattern similar to that of the vertical component of the sR_1' mode. Along the plane $x_2 = 0$, not much difference is found between the aL_1' and the aL_1 modes. Figure 18b shows the relative amplitudes of these modes along the surface $x_3 = 0$ and here it is interesting to note that the relation of the pattern of the transverse component for the aL_1' mode to that of the sL_1 mode in Fig. 18b is almost identical to the relation of the vertical component of the sR_1' mode to that of the sR_1 mode seen previously in Fig. 17b. The displacements of the aL_1' and aL_1 modes are essentially confined to the horizontal plane and the guide-wall motion is side-to-side with opposite sides moving in phase for both modes in Fig. 18b; but for the aL_1' mode the central region moves transversely in antiphase to the side walls and there are planes at $x_2 \simeq \pm h_2 / 2$ on which the transverse displacement is zero.

The displacements associated with the second modes sR_2 and aR_2 are shown in Fig. 19 and 20 with the first modes sR_1 and aR_1 plotted with dotted lines for comparison. It can be seen that in the overlay and the adjacent substrate region, the projection of the total displacement onto the sagittal-plane is a progressive ellipse in the sR_2 and aR_2 modes in contract to the retrogressive motions of the sR_1 and aR_1 modes. In addition, the shape of the u_1 curve for the second mode in both cases is similar to that of u_3 for the first mode

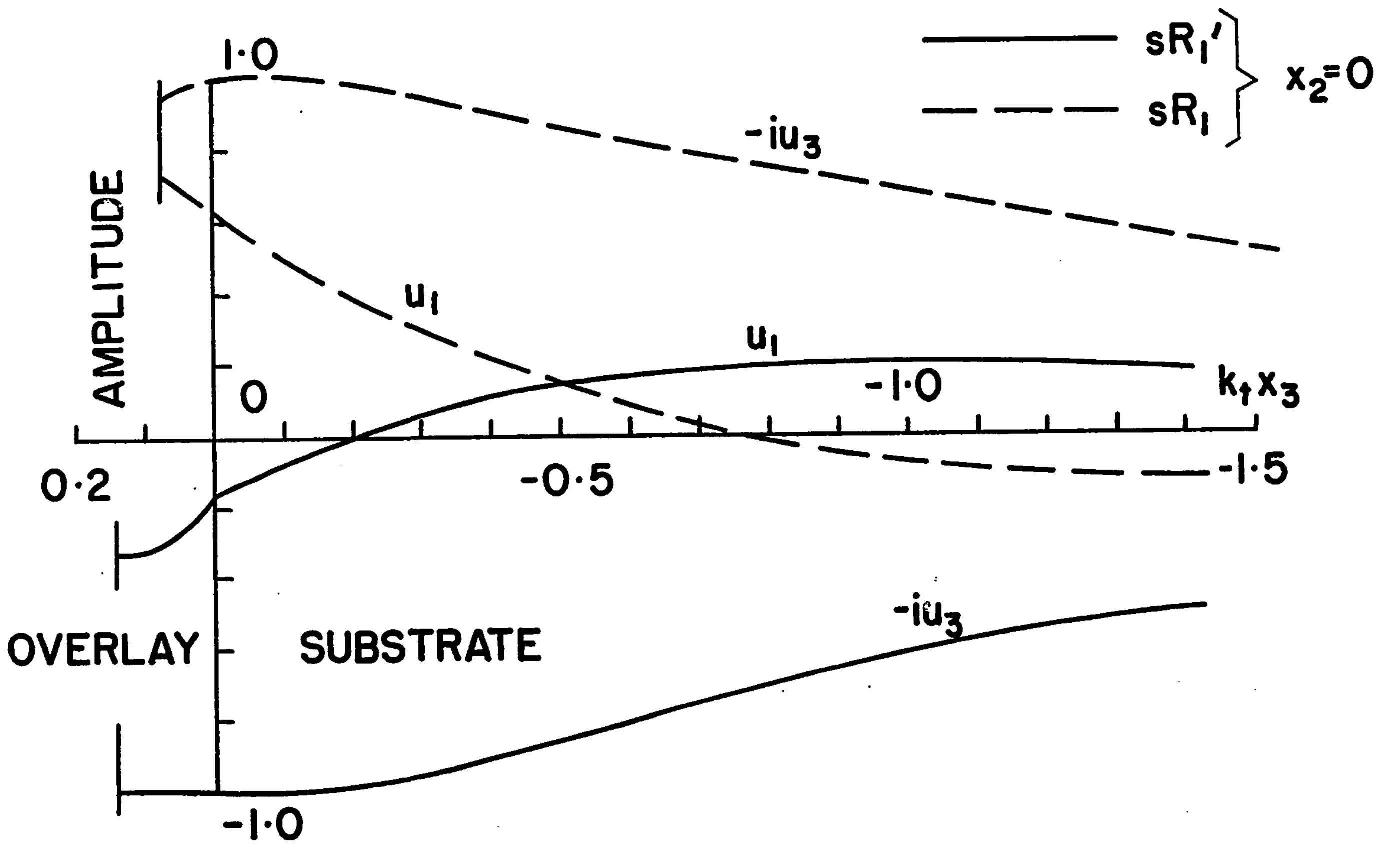

Fig. 17a. Displacement components on vertical centre line ($x_2 = 0$) for symmetric Rayleigh mode (sR_1') for point marked on dispersion curves, Fig. 3. $k_t h_2 = 10$ and $v/v_t = 0.74$ with the corresponding sR_1 mode plotted for comparison.

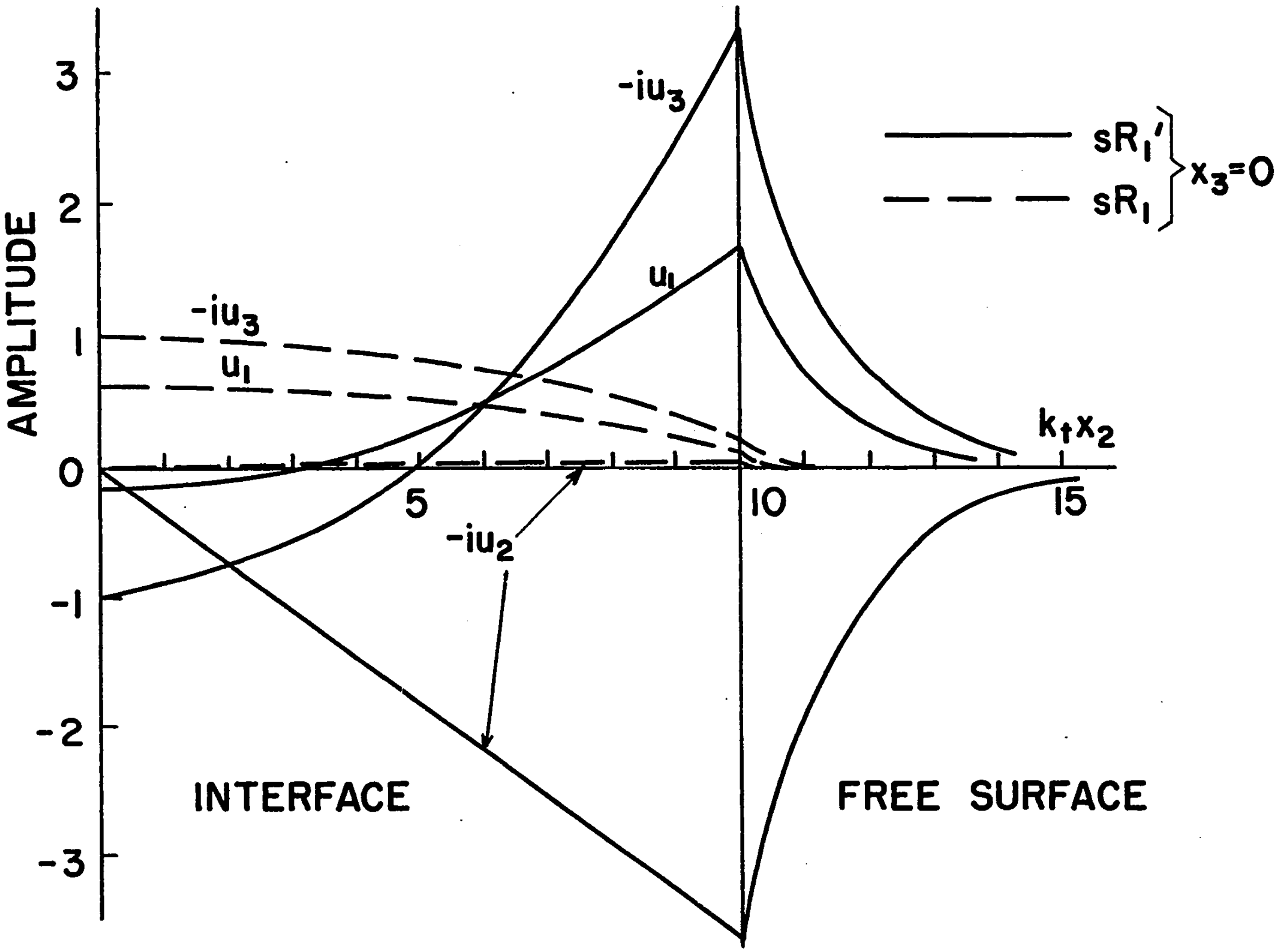

Fig. 17b. Displacement components on interface ($x_3 = 0$) for symmetric Rayleigh mode (sR_1') for point marked on dispersion curves, Fig. 3. $k_t h_2 = 10$ and v/v_f=0.74 with the corresponding sR_1 mode plotted for comparison.

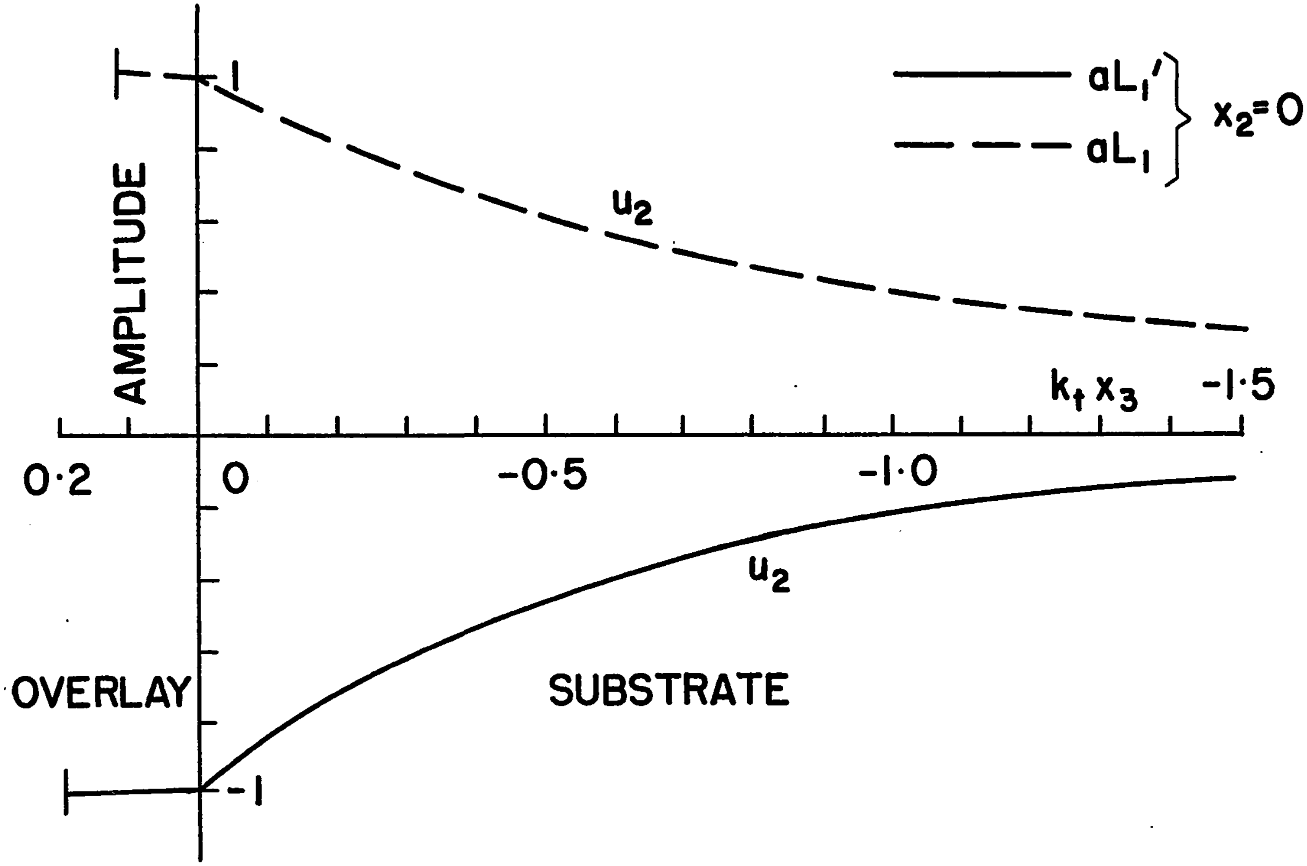

Fig. 18a. Displacement components on vertical centre line ($x_2 = 0$) for antisymmetric Love mode (aL_1') for point marked on dispersion curves, Fig. 6. $k_t h_2 = 10$ and $v/v_t = 0.74$ with the corresponding aL_1 mode plotted for comparison.

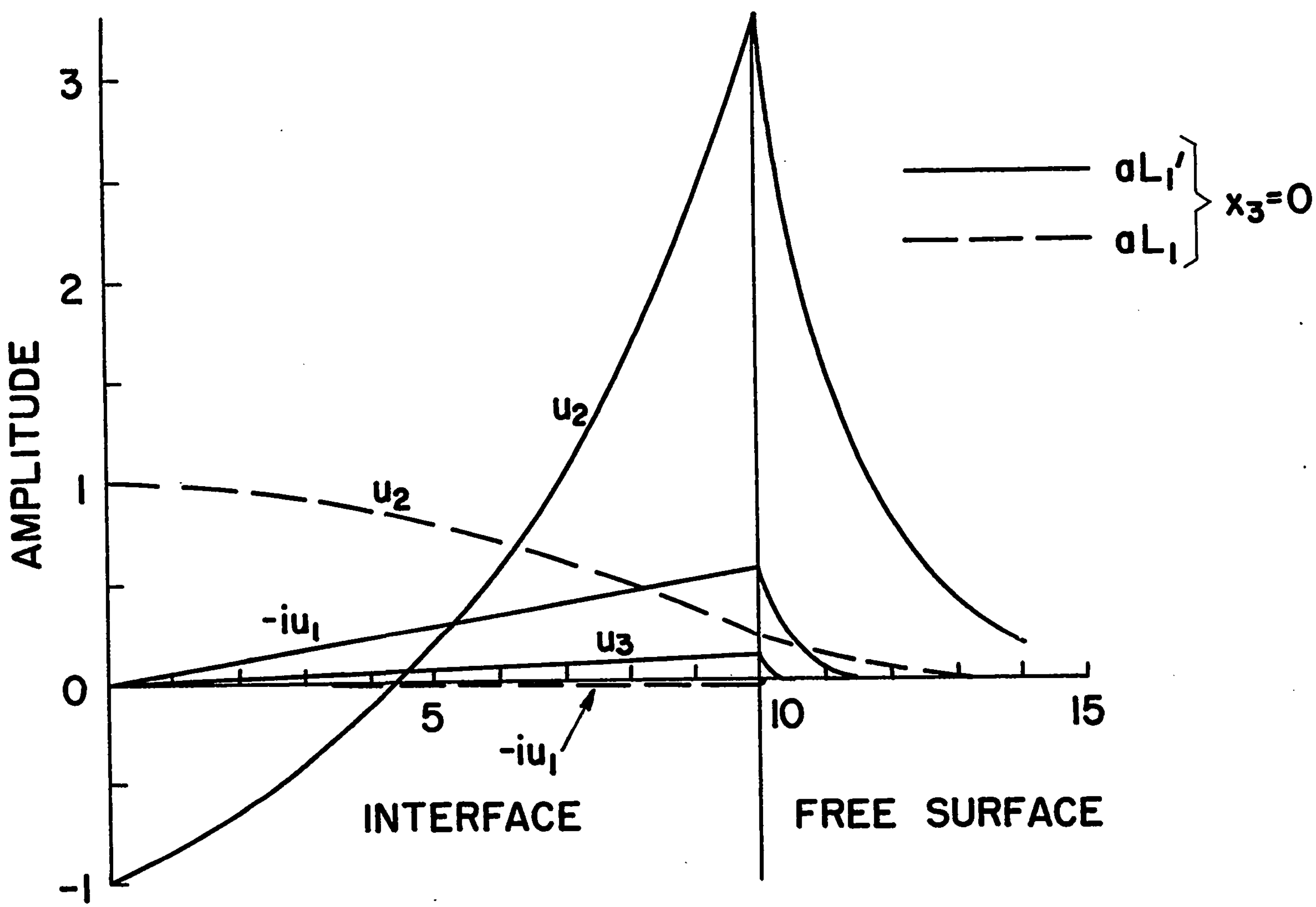

Fig. 18b. Displacement components on interface ($x_3 = 0$) for antisymmetric Love mode (aL_1') for point marked on dispersion curves, Fig. 6. $k_t h_2 = 10$ and $v/v_t = 0.74$ with the corresponding aL_1 mode plotted for comparison.

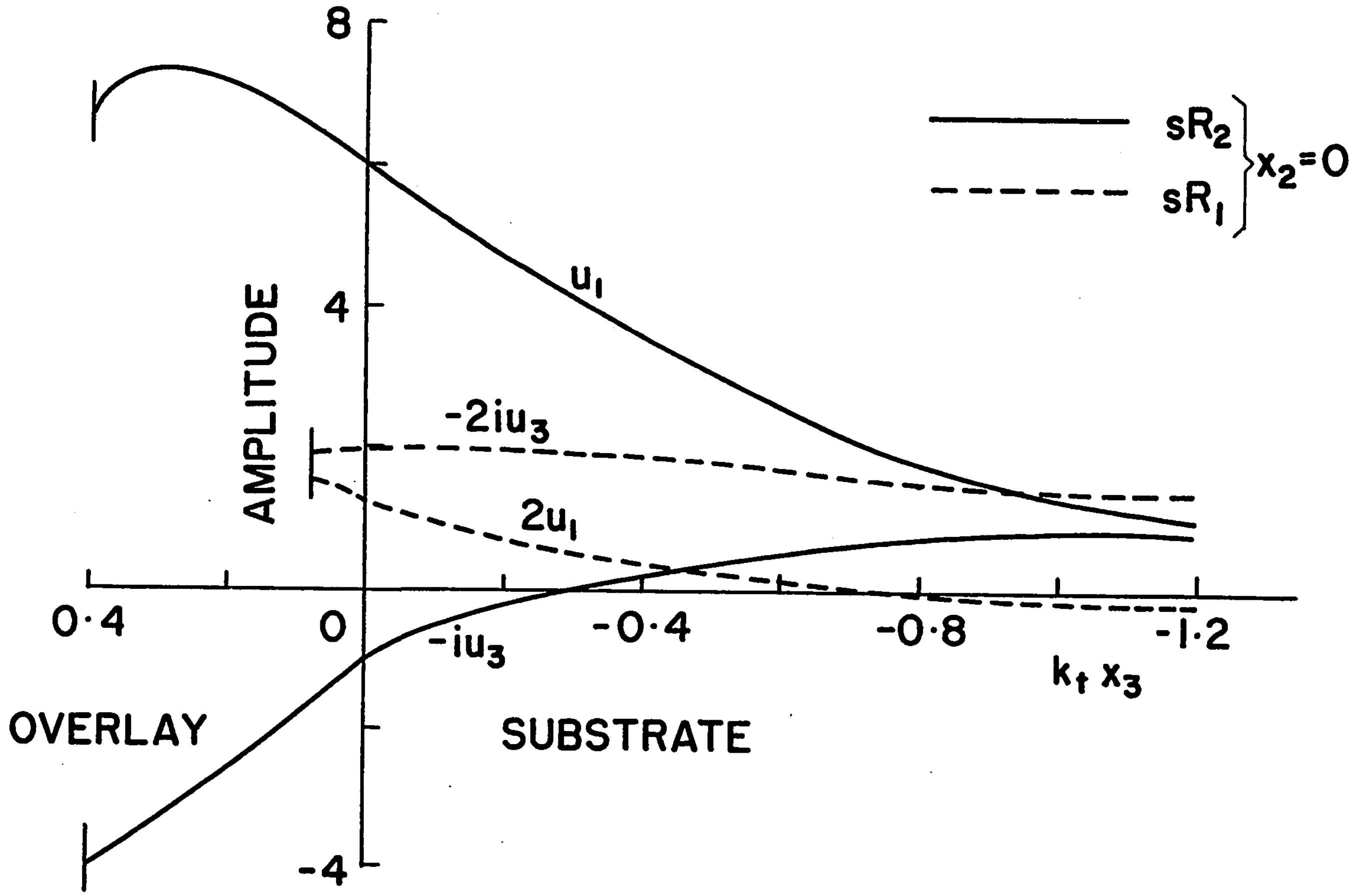

Fig. 19a. Displacement components on vertical centre line ($x_2 = 0$) for symmetric Rayleigh mode (sR_2) for point marked on dispersion curves, Fig. 3. $k_t h_2 = 10$ and $v/v_t = 0.74$ with the corresponding sR_1 mode plotted for comparison.

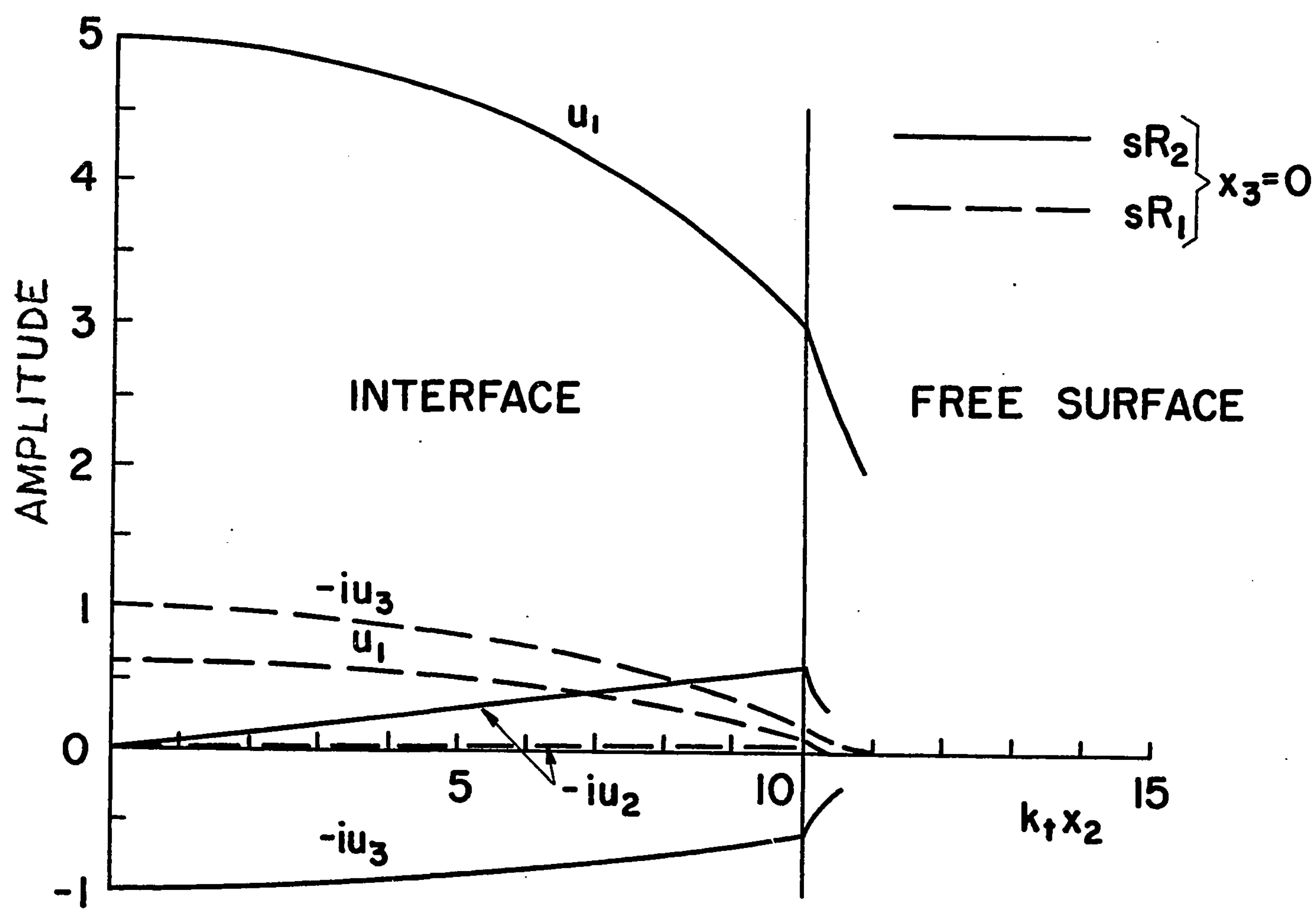

Fig. 19b. Displacement components on interface ($x_3 = 0$) for symmetric Rayleigh mode (sR_2) for point marked on dispersion curves, Fig. 3. $k_t h_2 = 10$ and $v/v_t = 0.74$ with the corresponding sR_1 mode plotted for comparison.

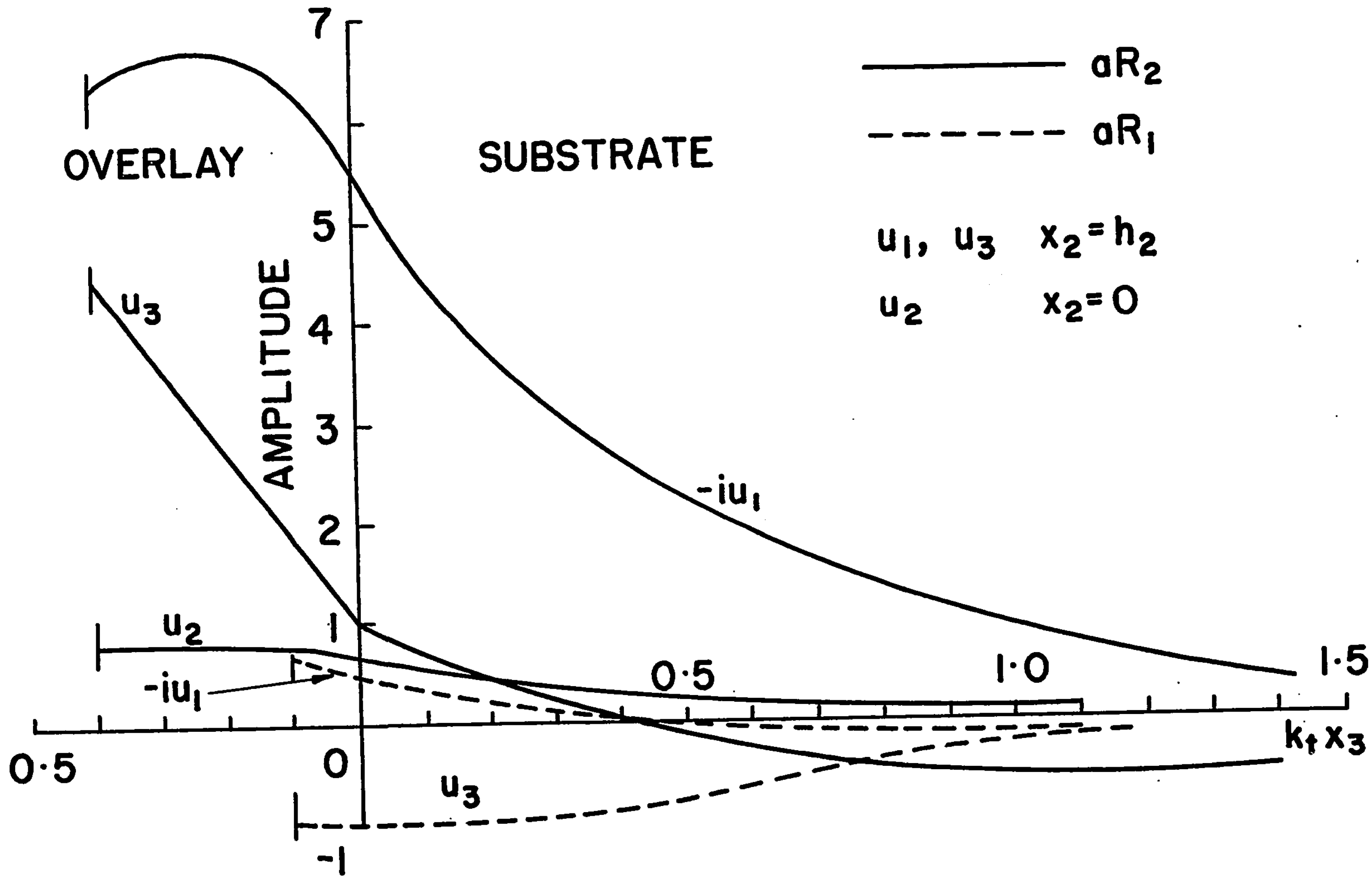

Fig. 20a. Displacement components on vertical centre line ($x_2 = 0$) for antisymmetric Rayleigh mode (aR_2) for point marked on dispersion curves, Fig. 4. $k_t h_2 = 10$ and $v/v_t = 0.74$ with the corresponding aR_1 mode plotted for comparison.

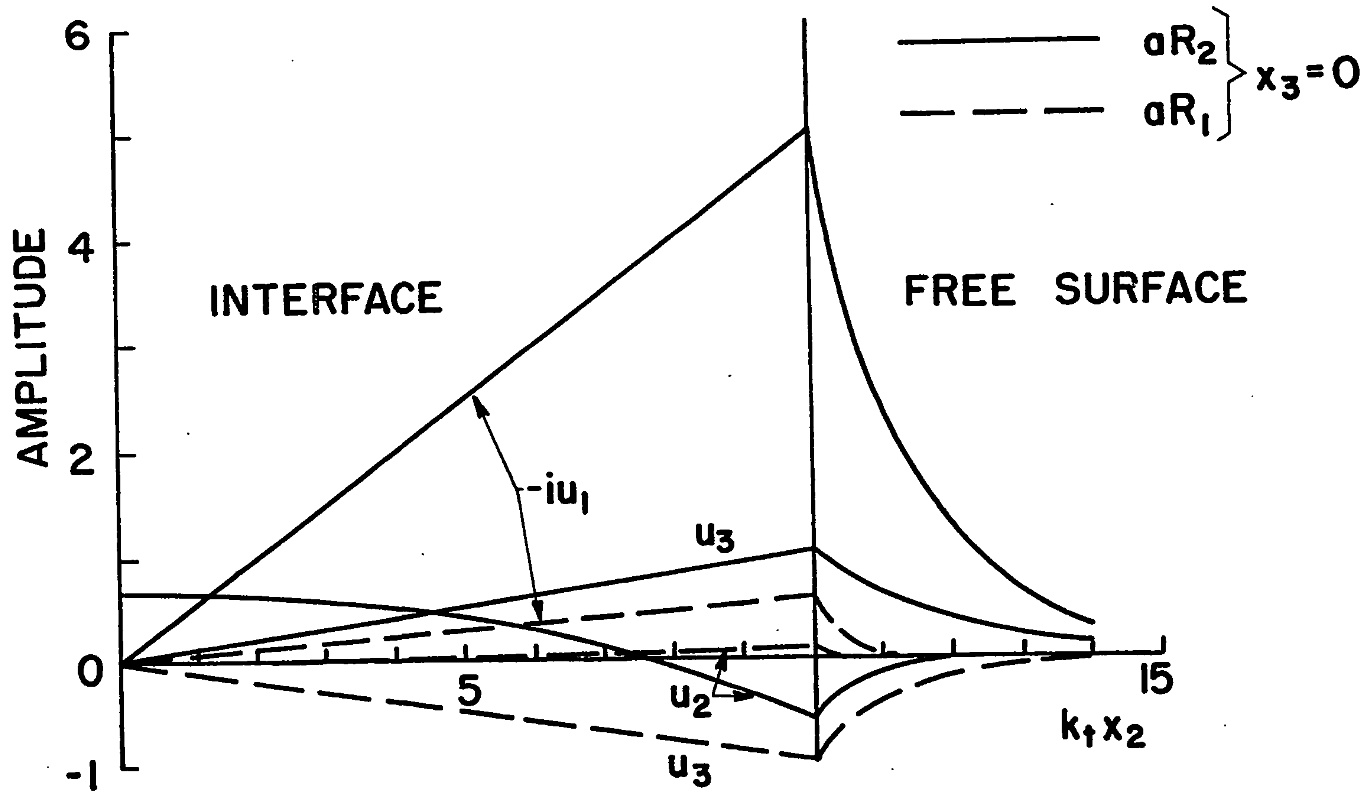

Fig. 20b. Displacement components on interface ($x_3 = 0$) for antisymmetric Rayleigh mode (aR_2) for point marked on dispersion curves, Fig. 4. $k_t h_2 = 10$ and $v/v_t = 0.74$ with the corresponding aR_1 mode plotted for comparison.

and the shape of u_3 for the second resembles u_1 of the first. This general behaviour is characteristic of the first and second Rayleigh modes of layered problem (Farnell and Adler, 1972).

3. Remarks on Stresses and on Mode Couplings

It will be recalled that the displacement continuity conditions are fulfilled at each point on all of the interfaces in the mathematical analysis of Chapter III, while the traction-free conditions on the surface of Region III is approximated and all of the other conditions of stress are introduced into the traction terms of the two dimension-reduced equations of motion (2.10) and (4.1). Thus the values of stress which appear as a result of this analysis can be expected to deviate from the exact values. Since the stress on a free surface and the difference of stress at an interface calculated from the regions on each side should be zero in the physical situation, the residual magnitudes of the stress on the free-surfaces and interfaces in this guide problem have been computed to serve as an aid to understanding the implicit approximations in the so-called (2,2) - approximation.

It has been found that in general the normal components of stress computed from this analysis deviate far more from continuity at the free-surfaces and interfaces than do the two associated shear components which should also be continuous. Taking an sR_1 point ($k_t h_2 = 1.5$ and $v/v_t = 0.74$) as a typical example, for which the displacement curves have been shown in Fig. 9, Fig. 21 sketches the residual magnitudes of the normal stress components, T_{22} and T_{33} on all of the free surfaces of the guide compared with that of T_{11} in the direction of propagation at boundries around the overlay. Due to the symmetry with respect to the mirror plane $x_2 = 0$, stresses are shown only on one side in the figure for clarity. Normalized with respect to the value of T_{11} which is almost constant along the centre line of the overlay $x_2 = 0$, the maximum absolute residues of stress, which should be zero exactly, are as follows: $T_{22} = 0.385$ and $T_{33} = 0.238$ at the lower corners and $T_{33} = 0.02$ at the upper corners of the overlay, all less than unity. The difference of stress calculated at the interfaces around Region II, which also should be zero exactly, are all less than 0.03 and omitted in the figure.

As seen in the above sections, the (2,2) - approximation gives very good dispersion relations and quite meaningful displacement patterns, while the (1,1) - approximation provides reasonable dispersion but rather poor approximations to the displacements in the overlay, for example, all of the curves within the region marked "INTERFACE" in Fig. 9b, 11b, 13b and 15b would become straight lines in a (1,1) - approximation because no quadratic polynomials are involved. Since the stress is calculated from a differentiation of the displacements, the stress results are always much less accurate in polynomial approximations than are the dispersion curves or the displacement distributions. The solutions from the (2,2) - approximation above still contain some residual normal stresses but only on the free surface of the substrate and on the side surfaces of the overlay and these residual stresses are appreciably smaller than the dominant ones. However if the stress is calculated with the (1,1) - approximation, residual values of the calculated stresses on the top surface of the overlay are about twice as large as in Fig. 21

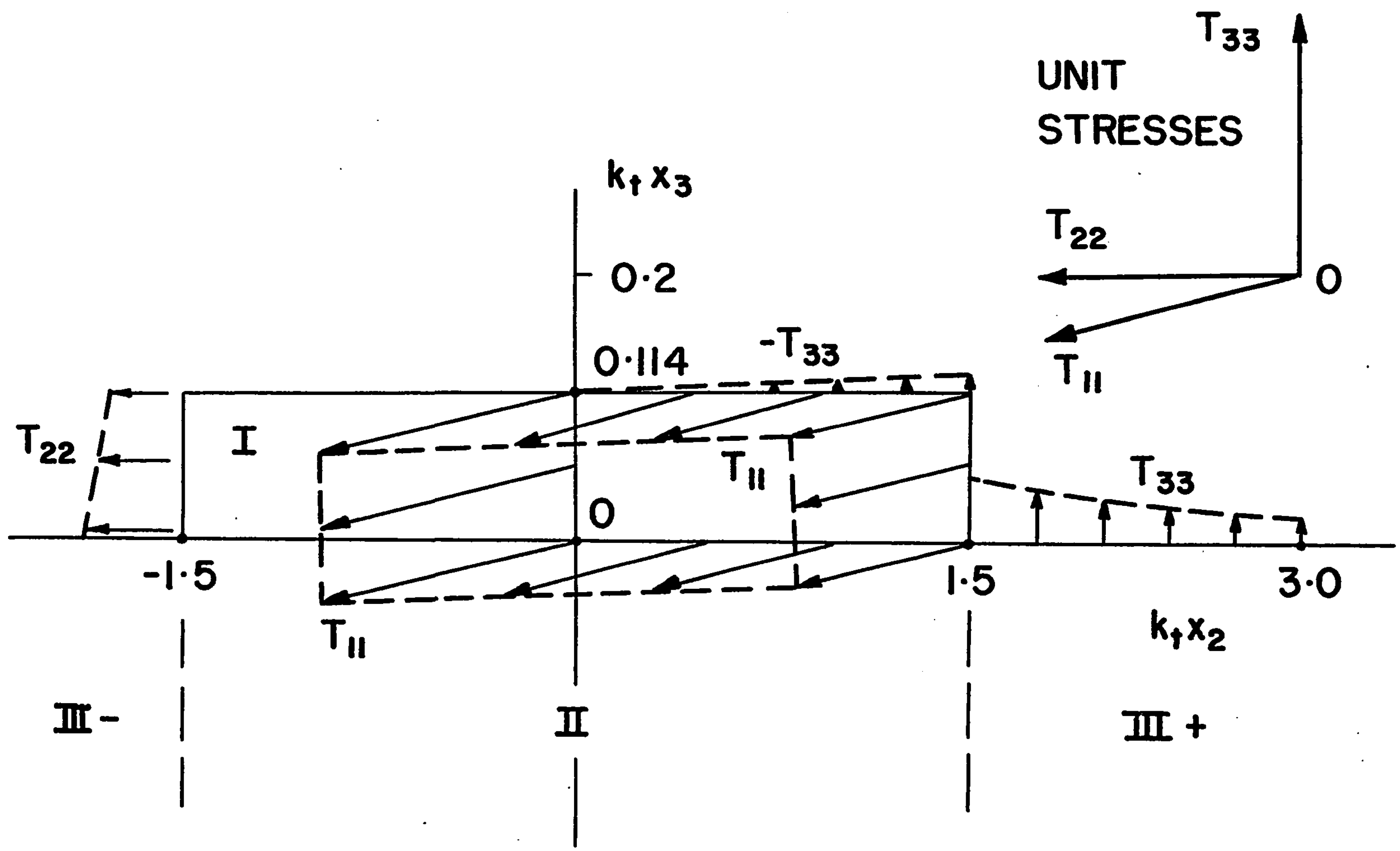

Fig. 21. Residual magnitudes of normal stress components, T_{22} or T_{33}, on free surfaces compared with the stress T_{11} in the direction of propagation for sR_1 mode, $k_t h_2 = 1.5$ and $v/v_t = 0.74$.

and the residual stresses on all the interfaces around Region II, which are approximately zero in the (2,2) - approximation, acquire appreciable non-zero values.

There are isolated points on the dispersion curves at which on a gross scale degeneracies appear to occur between two modes. If the region of one of these "degeneracies" is examined more closely, "coupled mode" behaviour is encountered. For example, if for the gold on fused quartz combination, the symmetric mode curves of Fig. 3 and 5 are overlaid it is seen that the curves for $k_t h_2 = 10$ of the sR_1' and the sL_1 modes appear to intersect in the vicinity of $k_t h_3 = 0.08$; similarly the $k_t h_2 = 10$ curves for the aR_1 and aL_1 modes of Fig. 4 and 6 appear to intersect near $k_t h_3 = 0.09$. However when these regions are examined in detail as shown in Fig. 22, it is found that no solutions exist with real propagation constant in the neighbourhood of the virtual crossings for either the (1,1) or the (2,2) - approximations. The displacement distribution for either mode near the crossover region is a mixture of the displacement pattern characteristic of the individual modes when examined further from the crossover region. While this mixing is characteristic of coupled mode propagation near a degeneracy, the shape of the dispersion curves is unusual for a passive system. Whether the behaviour shown is a physical reality or an artifact of some approximation in the analysis has not been determined.

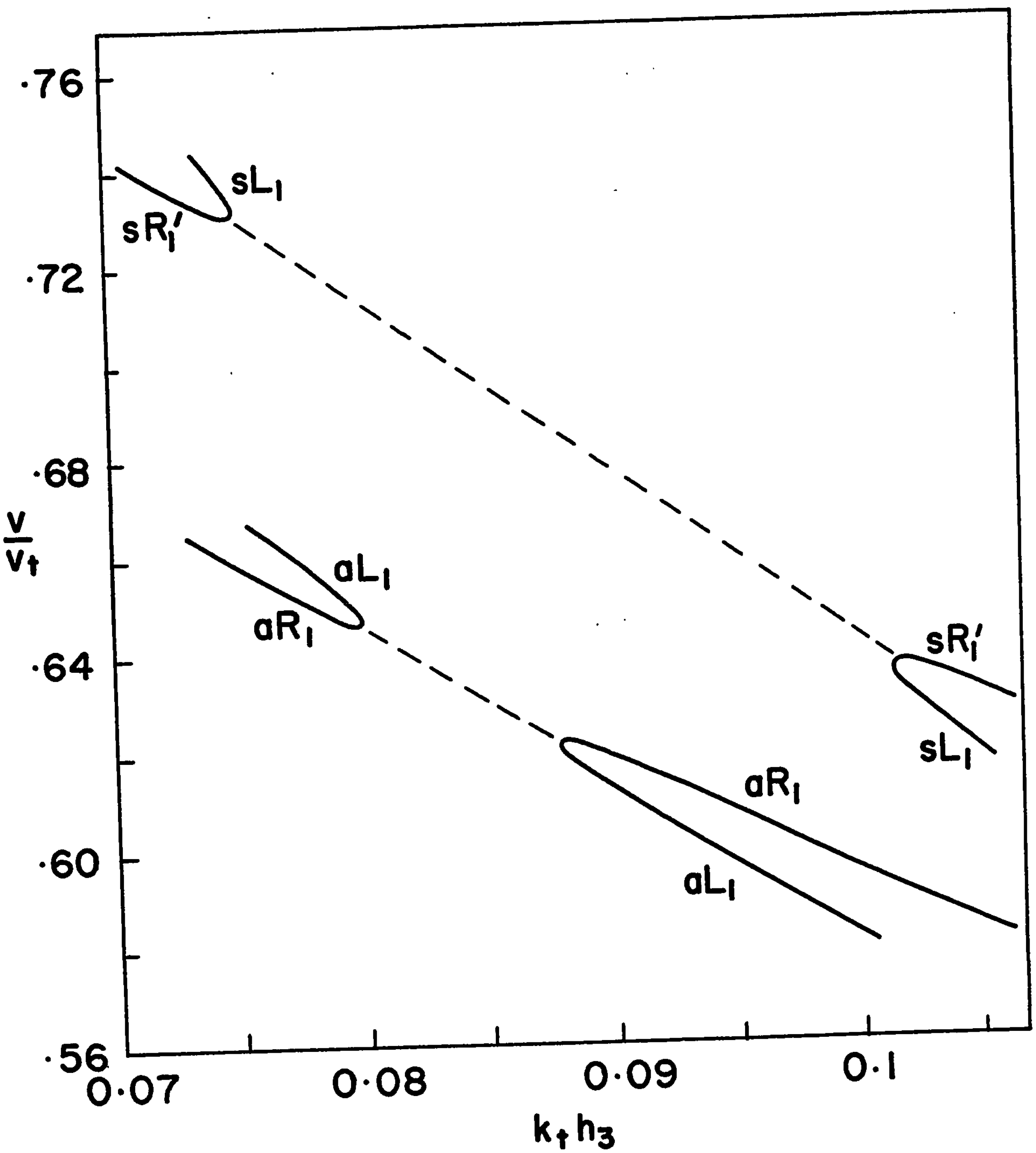

Fig. 22. Mode couplings between Rayleigh and Love modes in symmetric and antisymmetric cases, calculated with the (2,2) - approximation for $k_t h_2 = 10$.

4. Dispersion of Different Material Combinations

The results so far shown in the above sections for a gold-on-fused-quartz guide have illustrated the effects of guide thickness and provided a general overview of the application of the analysis. In this section attention is focussed on the effects which different choices of material combinations have upon the dispersion characteristics of overlay waveguides. For illustrative purposes various materials are chosen for the overlay but on a common substrate, fused quartz, and since general characteristics rather than detailed numerical values are of interest, the (1,1) - approximation has been used. The material constants selected for the comparative calculations and for the duraluminum used for the ridge waveguide in the next chapter are as follows (Mason, 1958):

Material	Lamê constants		Shear velocity	Rayleigh velocity	Density
	μ (Kbar)	λ	v_t (m/sec)	v_R (m/sec)	ρ(g/cm^3)
Fused quartz	312	161	3764	3409	2.2
Gold	285	1500	1200	1134	19.0
Gold-artificial*	71.25	375	1200	1134	4.75
Platinum	640	990	1730	1605	21.37
Nickel	800	1640	3000	2799	8.7
Polystyrene	12	34	1120	1050	1.056
Duraluninum	267	544	3130	2920	2.79

*Gold-artificial has the values of μ, λ and ρ equal to one-fourth those of real gold.

The choices of overlay material in this section fall into several different categories relative to the gold considered in detail above. Platinum has Lamé constants and density comparable to those of gold but the dispersion in the case of an infinitely wide layer of platinum on fused quartz is such that the first Rayleigh and first Love modes do not cross as they do with gold. The artificial gold is chosen to have the same Rayleigh velocity as gold and hence the same ratio of $\hat{v}_t/v_t$ but the artificial gold has smaller Lamé constants and lower density than the physical gold of the previous section. The polystyrene has much smaller Lamé constants than gold and with its very low density even less than that of the fused quartz substrate material, it gives the largest ratio of $\hat{v}_t/v_t$ of the material combinations considered. On the other hand, nickel is selected to provide an example with a relatively small ratio of $\hat{v}_t/v_t$ but with Lamé constants comparable to those of gold and platinum.

The dispersion curves of guides, made of platinum, nickel, polystyrene or gold-artificial for the overlay on a common substrate of fused quartz, are illustrated in Figures 23 to 30 with each combination having one graph for the symmetric modes and one for the antisymmetric modes. The choice of a common fused quartz substrate permits all figures to have a common uniform ordinate with the same upper-bound velocities, the shear and Rayleigh velocities of fused quartz, and the same width parameters ($k_t h_2$ = 320, 10, 1.5, 0.5 and 0.2) are used in order to obtain a better comparison between combinations. In each figure, the first Rayleigh-like (R_1) modes are plotted with solid lines, the first Love-like (L_1) modes with short broken lines. The first Love mode of the infinite layered substrate is also indicated with dots in the leaky region above Rayleigh velocity of the substrate. The same values of the adjustment parameters

r_0 and r_1 are used as shown in Section 3, Chapter IV, and the agreement between the first Love-like mode ($k_t h_2 = 320$) and the first Love mode of infinite layer is generally good.

The dispersion curves of a platinum-on-fused-quartz guide are shown in Fig. 23 and 24, and it is seen that the general shape is similar to that of the gold-on-fused-quartz guide shown in detail in the above sections. In Fig. 23 for the symmetric case, the phase velocities of the sR_1 modes approach the substrate v_R of a free surface with zero slope for decreasing values of thickness parameter, and the curves for the sR_2 modes approach with a finite slope, all analogous to the gold-overlay guide. Similarly for the antisymmetric case in Fig. 24, the curves for the aR_1 modes do not come to a common point at $k_t h_3 \rightarrow 0$ but rather appear to have a cut-off, and the aL_1 modes have cut-off and a cross-over region about $k_t h_3 = 0.17$. The zero slope of the sR_1 mode and the cut-off of all other modes is a general characteristic of the overlay waveguides seen in all of the dispersion curves calculated.

The general shape of dispersion curves of the polystyrene-overlay type in Fig. 25 and 26 are quite different from those of the platinum-overlay type in Fig. 23 and 24, here the behaviour of the sR_1 and aR_1 modes becomes quite strange in appearance and the cross-over region of the aL_1 mode has shifted upward into the leaky region above v_R. Figures 27 and 28 show the dispersion curves for an artificial-gold-overlay guide and it is readily seen that this type resembles the polystyrene-overlay guide but has the cross-over region of the aL_1 modes below v_R again. Artificial-gold is given the values of μ, λ and ρ to be one-fourth those of gold, and by such an change of material properties the dispersion structure of Fig. 23 and 24 is reshaped into that of Fig. 25 and 26 respectively.

Another category of dispersion curves is represented by a nickel-on-fused-quartz guide shown in Fig. 29 and 30 where the curves for the symmetric modes in Fig. 29 extend only over a relatively small velocity interval from 0.7 to 0.9 on the ordinate scale due to the small difference of the shear velocities of the two materials involved. Actually it can be seen that all modes in Fig. 29 and 30, except the aL_1 modes, are confined in this interval with an exact upper bound velocity v_R and with a lower bound velocity near the value $\hat{v}_R$ of the overlay. For guides of smaller Rayleigh velocity difference, the aL_1 modes spread over most of region from v_R to values far below $\hat{v}_R$, while all of the other modes are squeezed into a narrow strip between the two Rayleigh velocities; and in the limiting case of the topographic ridge guide in which the velocity difference between the overlay and the substrate becomes zero because the same material forms both overlay and substrate, all of the modes except aL_1 disappear as will be discussed in the next chapter.

The above categories of dispersion curves represented by gold, platinum, polystyrene and nickel on fused quartz are not necessarily complete in the shapes of dispersion curves which may be encountered with overlay waveguides, but they represent a wide range of possible forms. From each type of dispersion curves the frequency range of single-mode operation, the group velocity and its frequency dependence, and the mode-type for the next higher mode can be estimated before resorting to detailed calculations for a specific pair of materials.

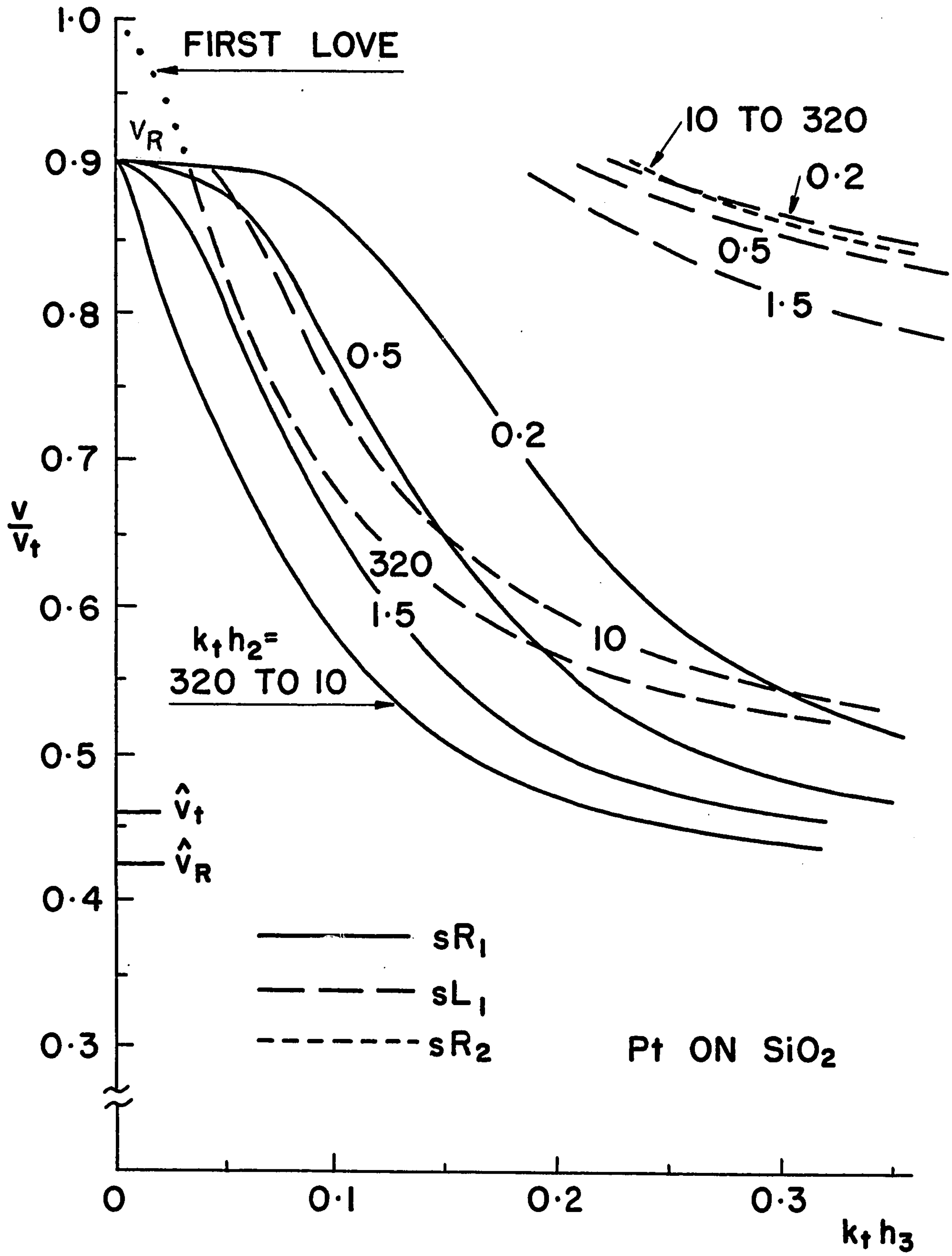

Fig. 23. Dispersion curves for symmetric modes for platinum on fused quartz from the (1,1) - approximation.

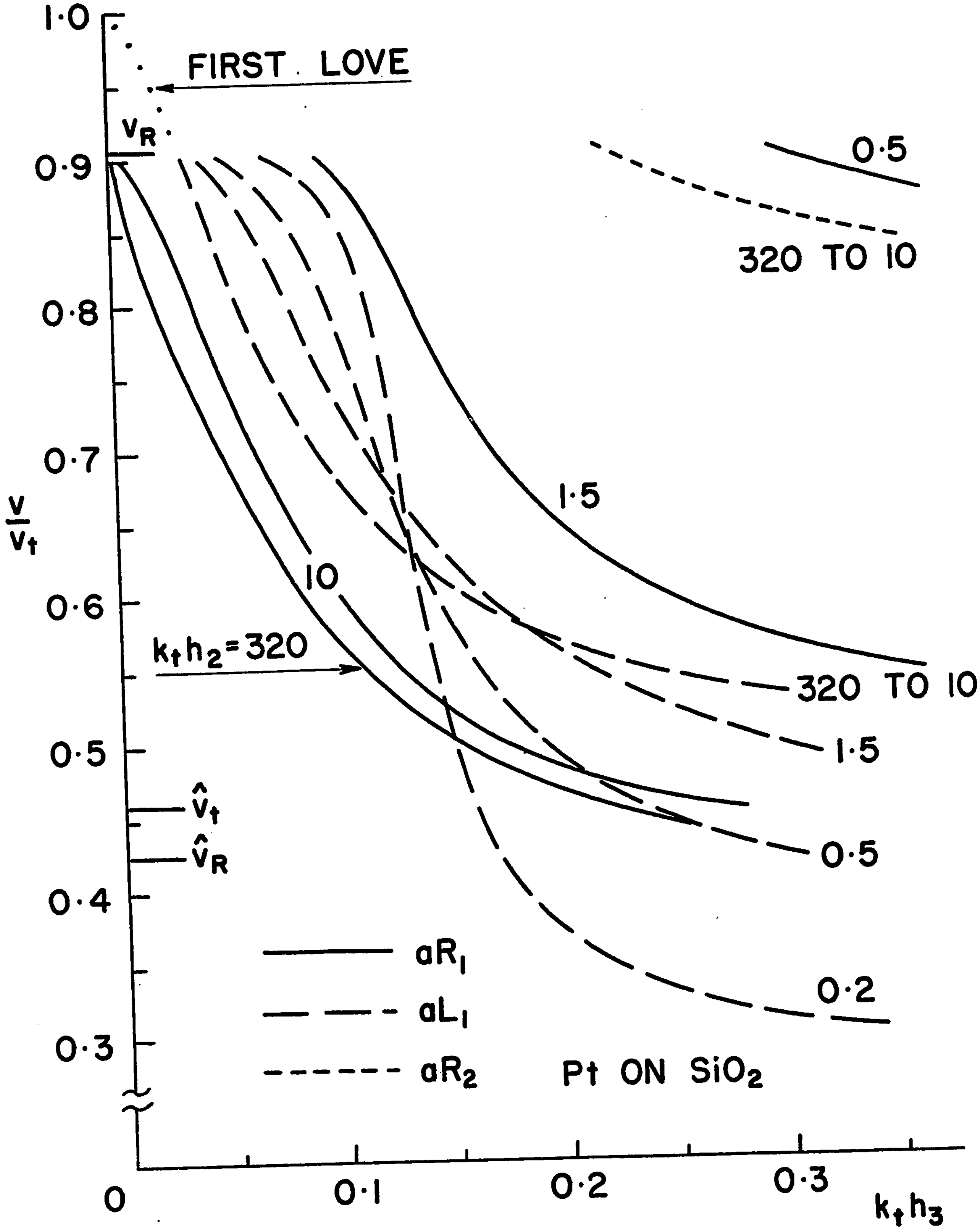

Fig. 24. Dispersion curves for antisymmetric modes for platinum on fused quartz from the (1,1) - approximation.

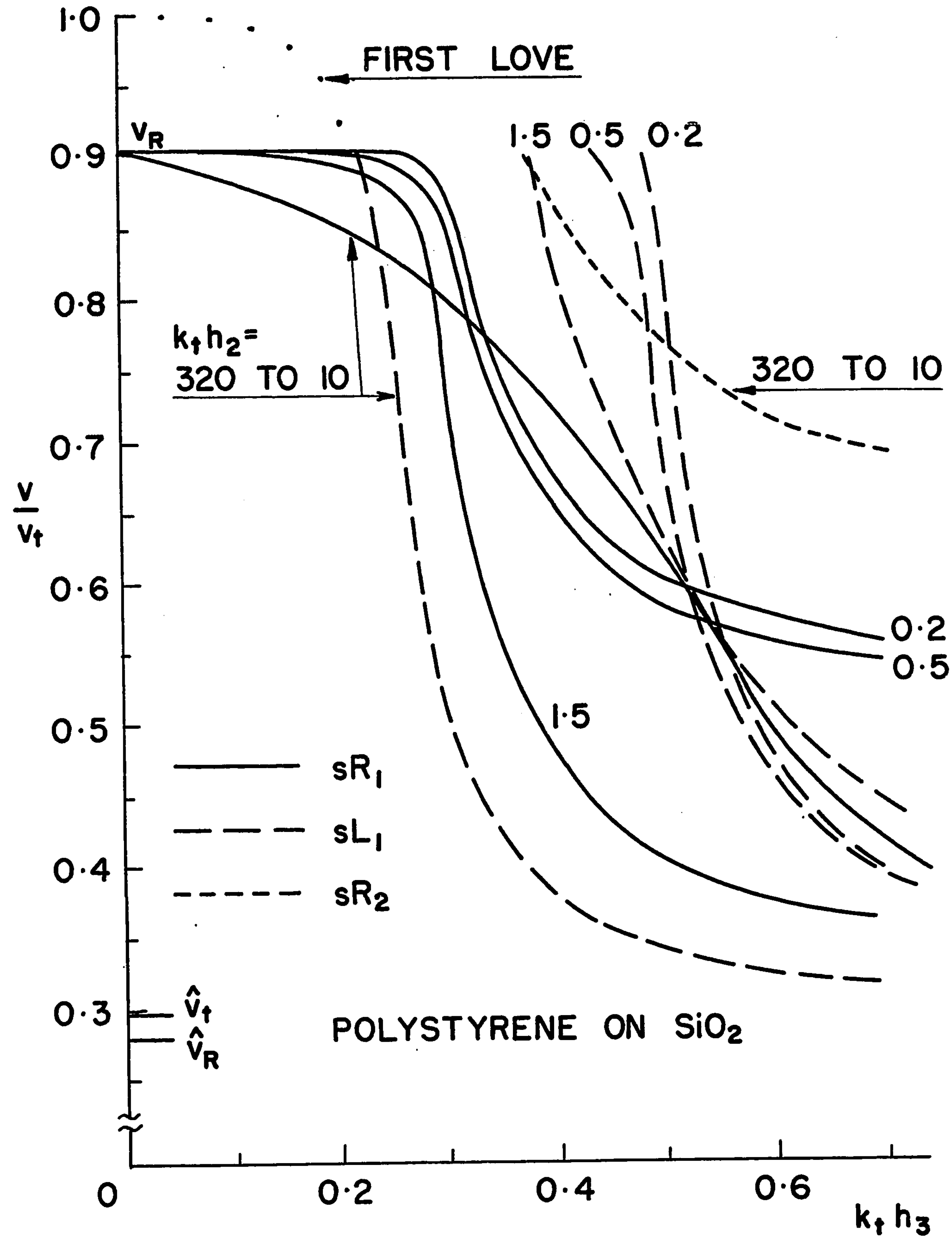

Fig. 25. Dispersion curves for symmetric modes for polystyrene on fused quartz from the (1,1) - approximation.

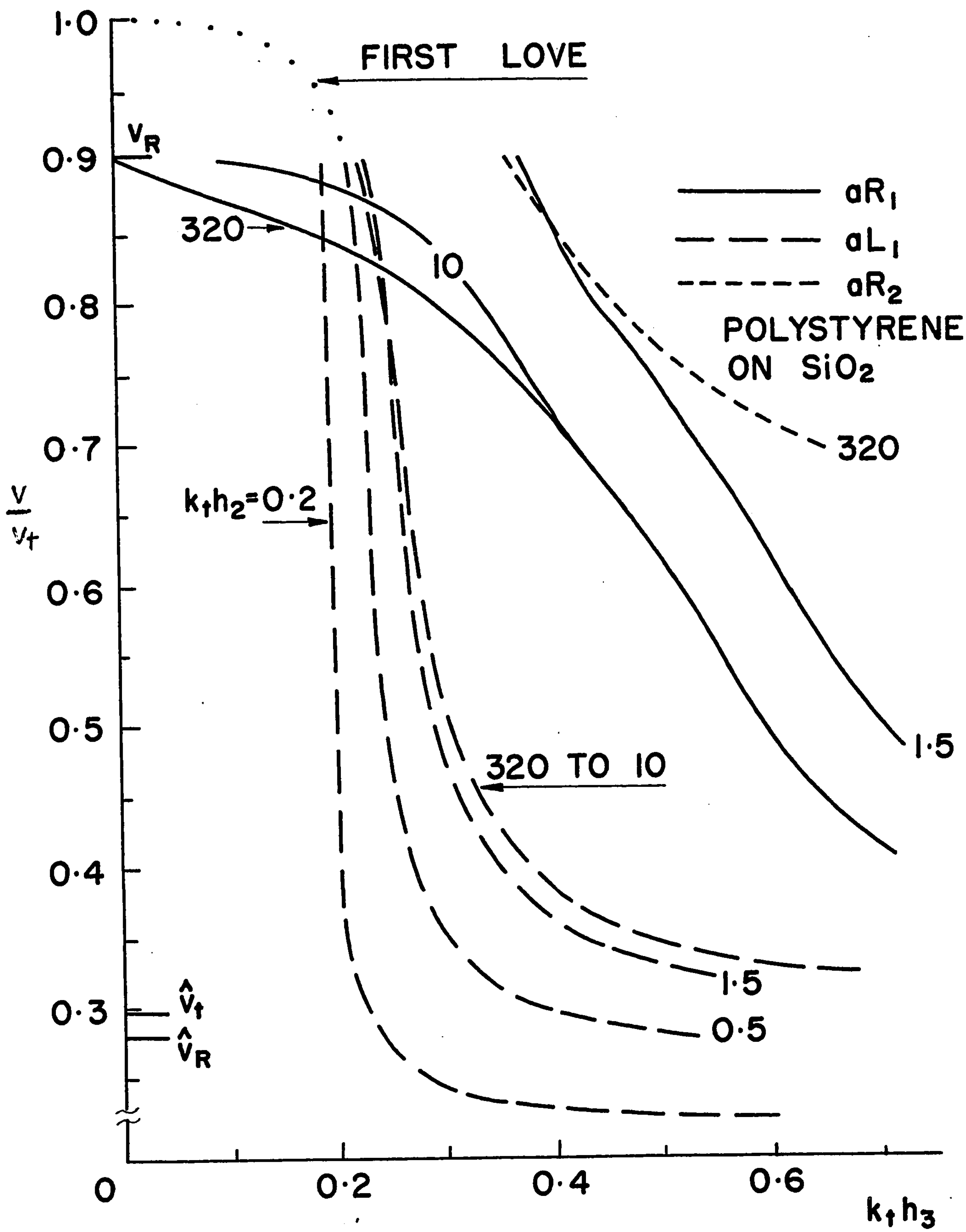

Fig. 26. Dispersion curves for antisymmetric modes for polystyrene on fused quartz from the (1,1) - approximation.

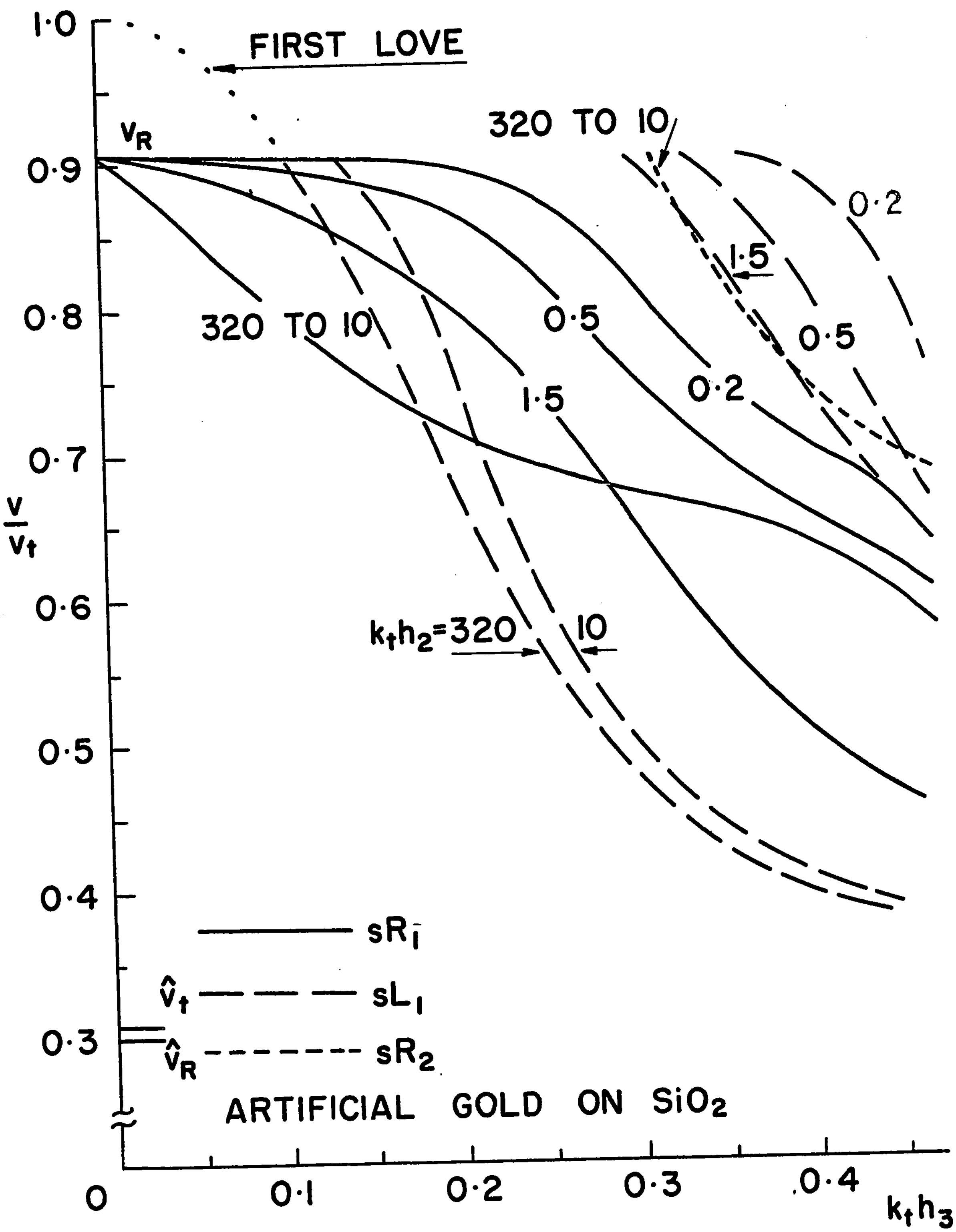

Fig. 27. Dispersion curves for symmetric modes for artificial gold on fused quartz from the (1,1) - approximation.

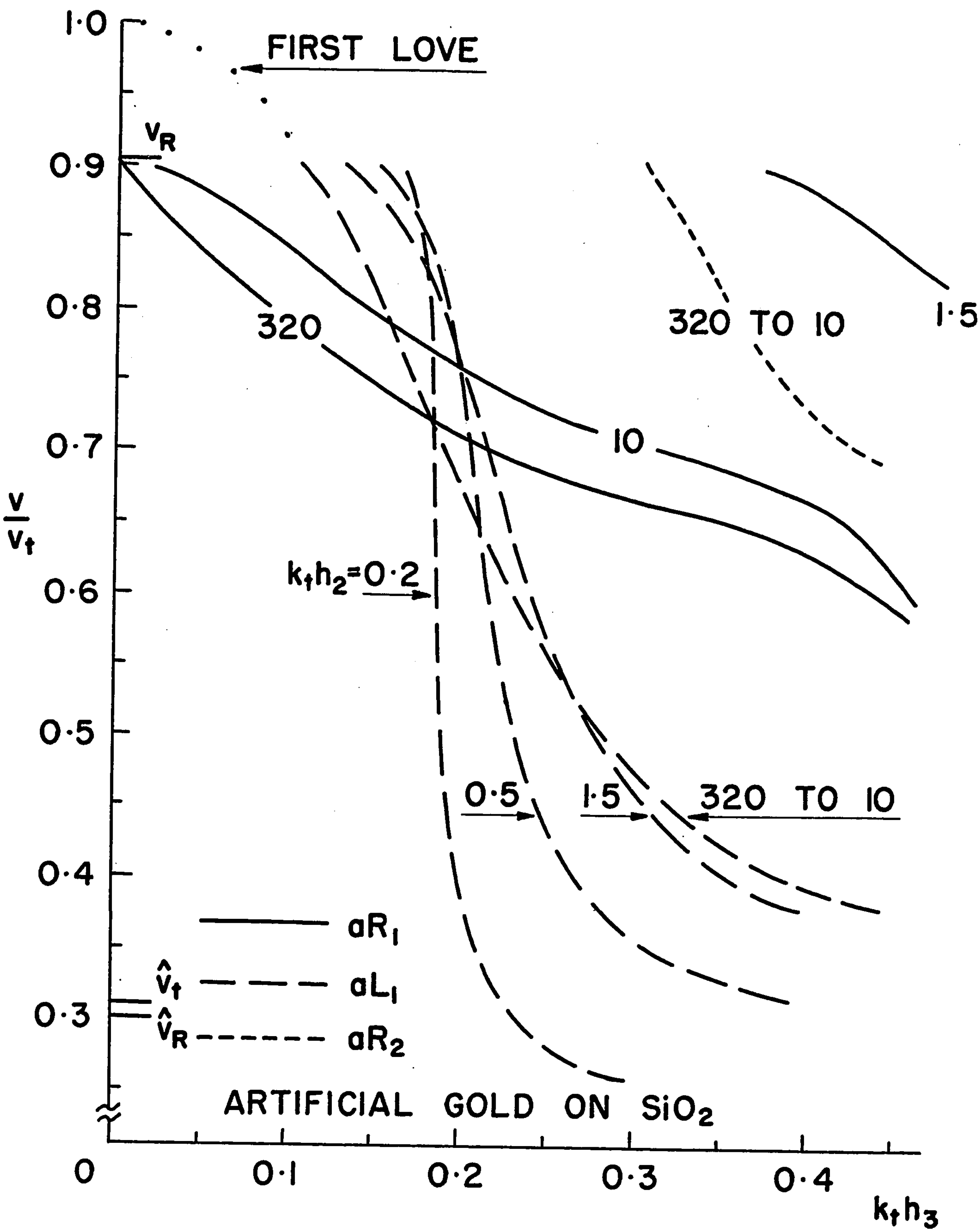

Fig. 28. Dispersion curves for antisymmetric modes for artificial gold on fused quartz from the (1,1) - approximation.

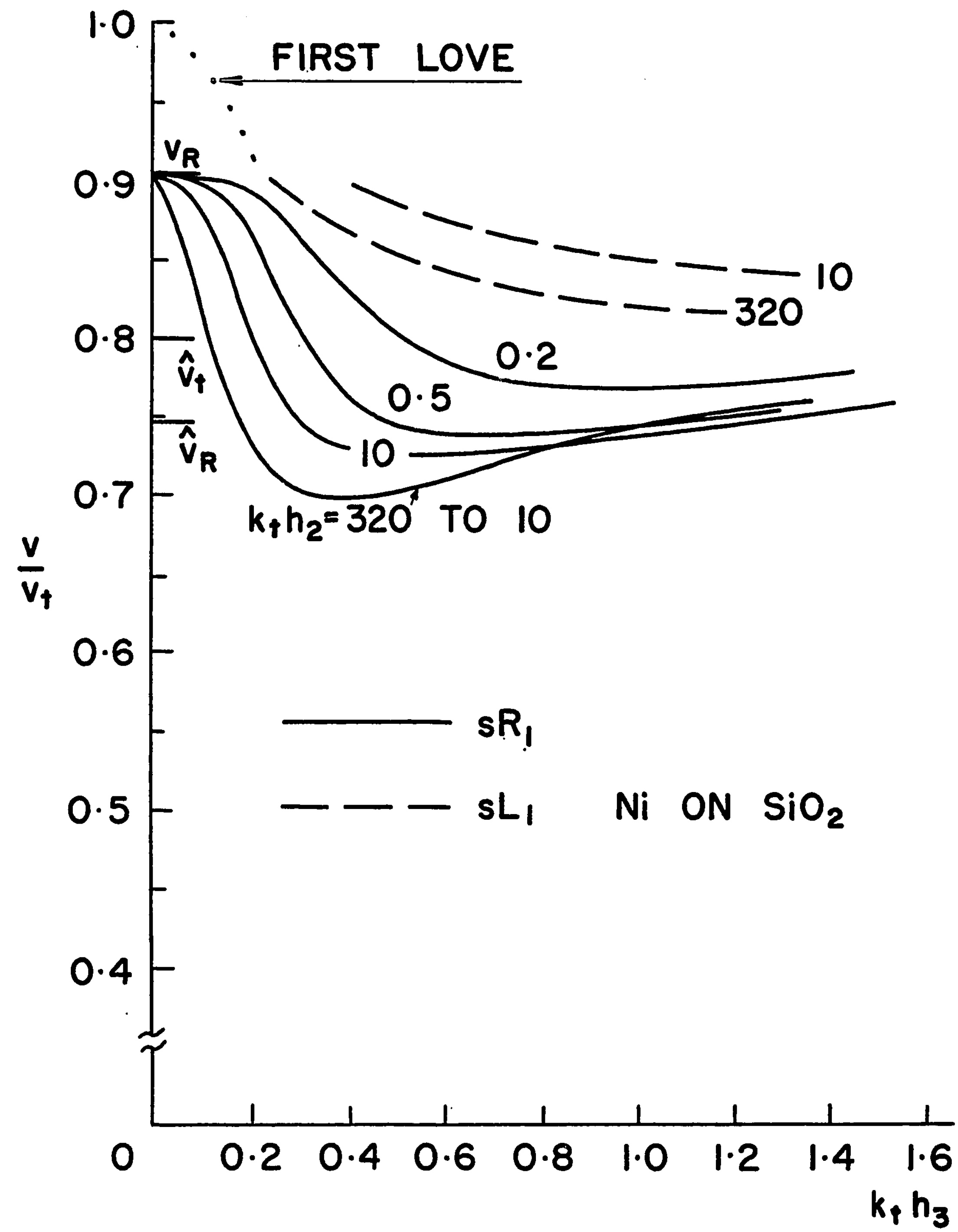

Fig. 29. Dispersion curves for symmetric modes for nickel on fused quartz from the (1,1) - approximation.

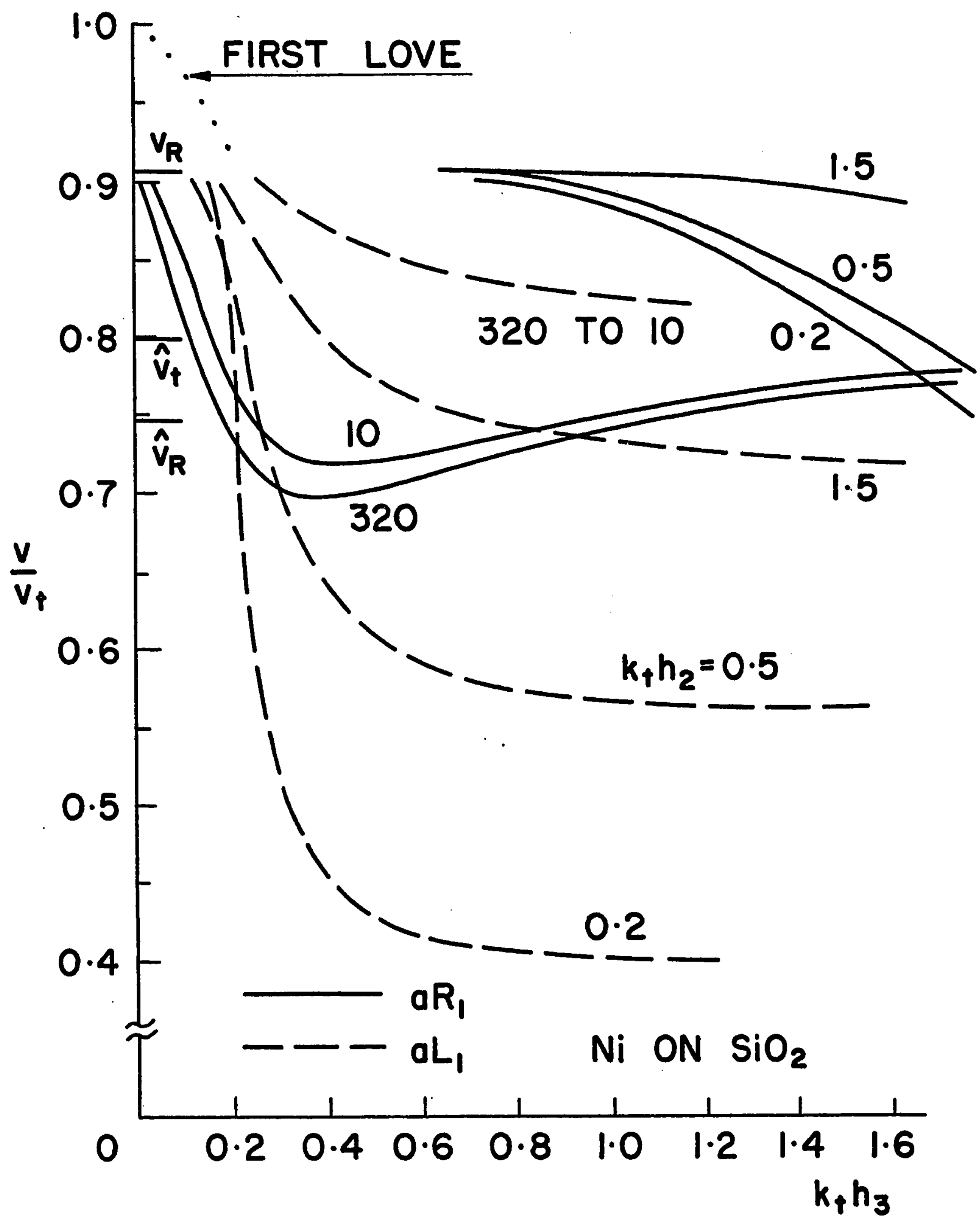

Fig. 30. Dispersion curves for antisymmetric modes for nickel on fused quartz from the (1,1) - approximation.

CHAPTER VI

ON THE TOPOGRAPHIC RIDGE WAVEGUIDES

1. General Description

As mentioned in the Introduction of Chapter I and in the Results of Chapter V, both the topographic ridge waveguides (Ash et al., 1969; Burridge and Sabina, 1971; Lagasse, 1972; Lagasse and Mason, 1972; Mason et al., 1971; Tu and Farnell, 1972a) and the rigid substrate waveguides (Waldron, 1971 and 1972) can be considered the limiting cases in the choice of material combination of this overlay-guide problem. When the material of both the overlay and the substrate is the same, the overlay guide becomes topographic ridge guide of the type suggested and first experimentally investigated by Ash et al (1969). When the substrate is assumed much more rigid than the overlay and the aspect ratio of the overlay is kept less than 0.5, we have the rigid substrate guide analyzed by Waldron (1971 and 1972).

It has been found that the theory of this analysis and as well the computation programs are readily applicable to the prediction of the propagation characteristics of the flexural mode of topographic ridge guide by using the (2,2) - approximation for antisymmetric modes (Tu and Farnell, 1972a). The results for such guide using duralumium as the propagation medium have been computed and found to be in good agreement with experimental results of Mason et al (1971).

2. Antisymmetric Modes of the Topographic Ridge Waveguides

Figure 31 shows the dispersion curves of antisymmetric modes of a rectangular ridge waveguide of height $2h_3$ and width $2h_2$ on duraluminum. For sufficiently low height, the curve for each width approaches the velocity of a simple Rayleigh wave on the undisturbed surface of the substrate half-space. In this region the decay of displacement amplitude in the transverse direction away from the guide is very slow in terms of the wavelength and the guiding action of the embossed strip is very weak. When the height becomes very large the velocity of propagation becomes independent of the height and approaches that of the first antisymmetric mode (Viktorov, 1967) of a plate of thickness $2h_2$ as marked by dashed lines on Fig. 31. The curves are essentially horizontal for h_3/h_2 ratios greater than about 3 : 1 provided the width is not less than the minimum value shown of $k_t h_2 = 0.2$.

The dispersion curves of Fig. 31 are plotted in the natural parameters of the computation and it is inconvenient to compare them directly with the corresponding experimental graphs (Mason et al., 1971), wherein the curves are plotted for fixed h_3/h_2 ratios. However comparisons without interpolation can be made for specific points and a collection of such comparisons is shown in Table I. Here the velocity and width are read from the experimental curves and the normalized height shown in the fourth column is then given by the appropriate h_3/h_2 ratio. For the same velocity and width, the guide height as calculated is given by the last column. The points selected in this table are all in the regions of Fig. 31 where there is a strong dependence of velocity on guide height and in this region the experimental and calculated values

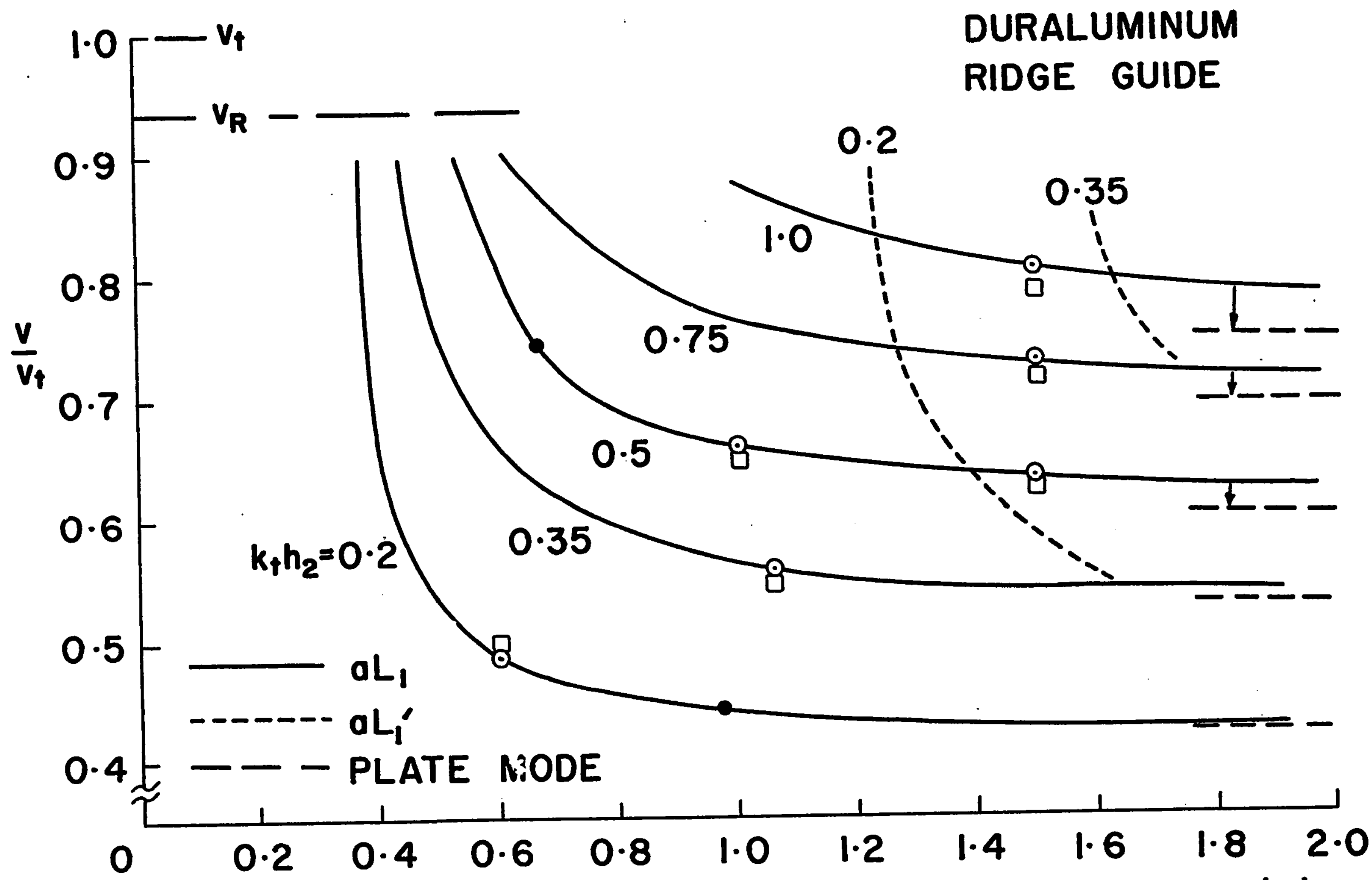

Fig. 31. Dispersion curves for antisymmetric modes for duraluminum ridge guide of width $2h_2$ and height $2h_3$. Broken asymptotes are for first antisymmetric mode of a plate of thickness $2h_2$. Squares are experimental points (Mason et al., 1971) corresponding to neighbouring calculated points marked O. Displacements for points marked with solid dots are shown in Fig. 32 and 33.

TABLE I.

COMPARISON OF SOME MEASURED AND CALCULATED RESULTS

v/v_R	v/v_t	$k_t h_2$	$k_t h_3$ measured*	$k_t h_3$ calculated
0.9	0.842	0.087	0.26	0.27
0.9	0.842	0.191	0.38	0.37
0.9	0.842	0.27	0.41	0.42
0.9	0.842	0.51	0.51	0.55
0.8	0.748	0.091	0.27	0.28
0.8	0.748	0.20	0.40	0.39
0.8	0.748	0.28	0.43	0.45
0.7	0.655	0.098	0.29	0.29
0.7	0.655	0.21	0.42	0.42
0.6	0.561	0.103	0.31	0.31
	Minima on Figure 3 of Mason et al. (1971)			
0.84	0.78	0.73	0.73	0.75
0.71	0.76	0.40	0.60	0.54
0.61	0.65	0.26	0.52	0.48
0.49	0.52	0.134	0.40	0.37

*Mason et al. (1971)

are seen to agree within ten percent. For the regions of Fig. 31 where the curves are quite horizontal, such a comparison is not meaningful because slight changes in the selected values of velocity produce large changes in the calculated height. In these regions, a more valid comparison can be made by noting the normalized height and width at specific points on the calculated curves and comparing the velocity at this point with the corresponding measured values. Such results are shown for a few pairs of points on Fig. 31 and it is seen that the agreement is again good in this flat region of the curves.

3. Displacements

Some of the details of the displacements associated with this first anti-symmetric Love-like mode are given by the remaining illustrations in the chapter. The calculated displacement components are shown as a function of depth, in Fig. 32 and 33, for the points marked with dot on the dispersion curves of Fig. 31, by the solid curves for the displacement on the central sagittal plane and by the broken curves for the vertical plane containing the side of the waveguide with abscissa x_3 in units of h_3 in order to make the thickness of overlay a constant value of 2 for different cases. As mentioned in Section 2, u_2 is the displacement component transverse to the guide, and since the mode is antisymmetric with respect to the central plane, this is the only component which exists on the central plane. On the upper corners of the guide, the sagittal components (u_1 and u_3) are appreciable so that there is a pronounced tilt to the top surface of the guide. The vertical and transverse components are in phase with each other with the sense as indicated by the relative signs of the components plotted, while the longitudinal component is in phase quadrature with the other two. In the upper parts of the guide sagittal-plane projections of the particle displacement are then progressive ellipses. Figures 32 and 33 correspond to aspect ratios ($h_3/h_2 = 1.34$ and 4.9 respectively) for the guide cross section. Since this mode corresponds to the aL_1 mode above the cross-over region of dispersion in Section 2, it can be seen again that in both cases most of the elastic energy is carried in the embossed region, though there is some displacement of the substrate material and that the penetration of the displacement pattern into the substrate of the latter case is reduced than the former. The dependence of the displacement amplitudes on the transverse dimension x_2 is generally the same as the curves shown in Fig. 15b for $v/v_t = 0.74$.

While it was noted that for large $k_t h_3$ values in Fig. 31, each of the curves approached the velocity of the first antisymmetric mode (Mason et al., 1969) of an infinite free plate of thickness $2h_2$, nevertheless the displacements do not correspond to those of such a free plate. For example, for a plate of thickness $k_t h_2 = 0.2$, the pure plate mode would have no variation of displacement in the x_3 direction, u_3 would be zero every where and the ratio of amplitudes u_1/u_2 would be 0.455. Rather, this mode becomes asymptotic to the corresponding mode of a duraluminum overlay on a semi-rigid substrate (Waldron, 1971). For example, if the overlay has the original duraluminum elastic properties, but the stiffness constants of the substrate are increased by a factor of 100 and the substrate density increased also by the same factor to maintain all the significant material velocities the same, the curves of Fig. 31 retain approximately the same shape but are translated to the right by an increment in $k_t h_3$ of the order of 0.1. In particular,

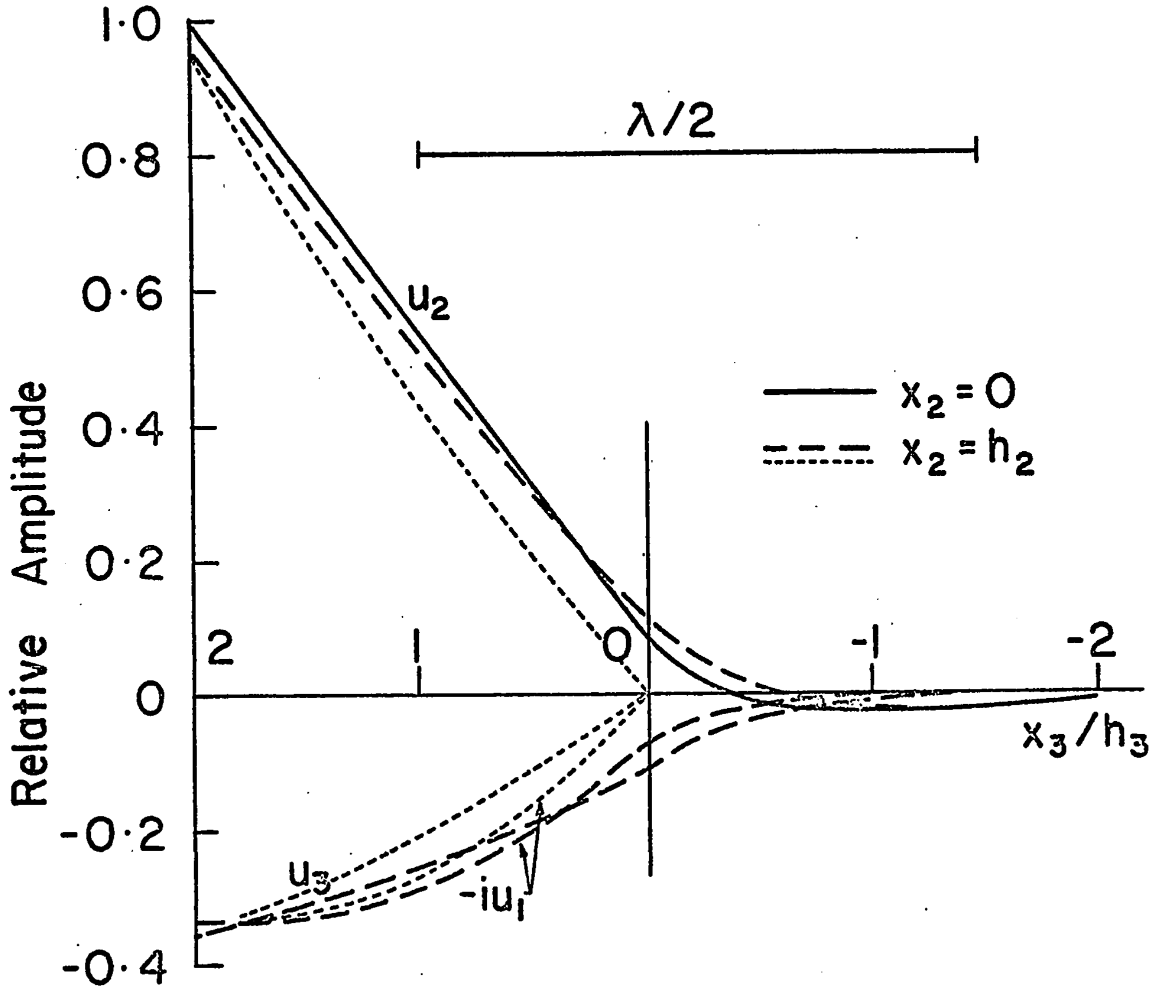

Fig. 32. Diaplacements as a function of depth on centre line ($x_2 = 0$) and on edge line ($x_2 = h_2$) for point marked with solid dot on curve $k_t h_2 = 0.5$, Fig. 31. The curves of short dashes give the edge displacements if the substrate is semi-rigid.

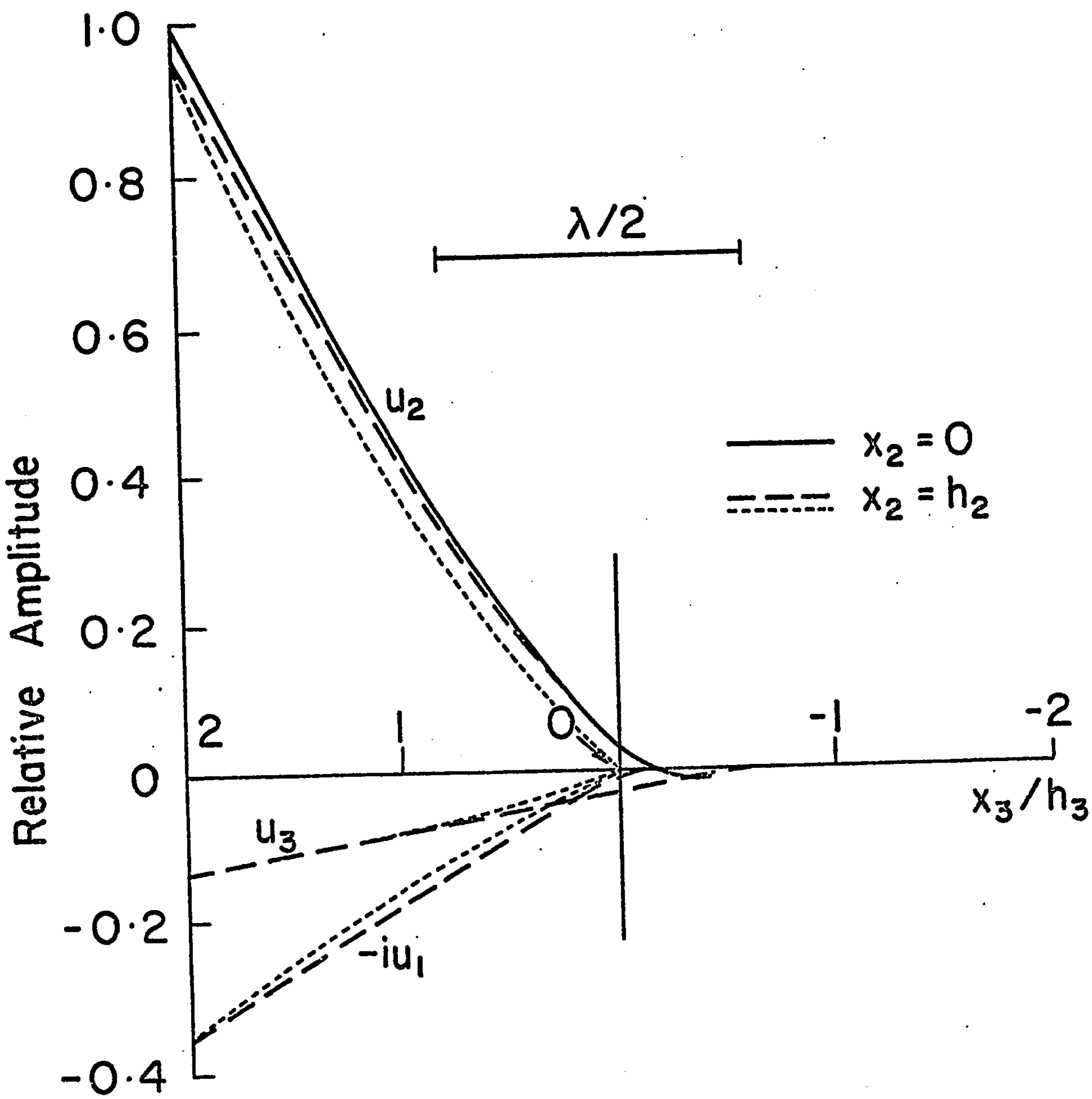

Fig. 33. Displacements as a function of depth for point on curve $k_t h_2 = 0.2$, Fig. 31, again showing edge displacements for a semi-rigid substrate.

the point marked on the $k_t h_2 = 0.5$ at $v/v_t = 0.74$ is translated from $k_t h_3 = 0.671$ to $k_t h_3 = 0.805$, and point on the curve 0.2 at $v/v_t = 0.44$, from 0.978 to 1.070; and the corresponding changes in the displacement patterns of the flexural mode for the ridge guide are similar to those of the semi-rigid substrate for the geometry, and the relative amplitudes of the components are essentially equal on the top surface.

4. Remarks

If the (2,2) - approximation for symmetric modes is used for the ridge geometry, no solution is found with velocity less than the substrate Rayleigh velocity. The reason for this, as stated in Section 1, Chapter V, is that since the same velocity constants apply to the overlay and the substrate, only the antisymmetric Love-like modes aL_1 and aL_1' have propagation velocities less than the common Rayleigh velocity and thus produce guided non-radiating waves. These modes become the "flexural modes" of the topographic ridge guides. Ash et al. (1969) reported some brief experimental results on a mode of propagation, symmetric in nature, with a velocity greater than the Rayleigh velocity and showing a leaky-wave behaviour in the side-region III of the sample. If in an analytic attempt to consider such mode we replace the transverse exponential decay of the displacements in Region III by sinusoidal functions, a solution has been found with a velocity and displacement distribution reasonable agreement with their experimental results. Since this mode radiates a Rayleigh wave and the analysis does not allow complex wave numbers, no detailed investigation of this mode of ridge propagation has been made.

In the rigid substrate waveguide suggested and analyzed by Waldron, an approximation technique originally found by Morse (1950) in an attempt at solving the rectangular bar problem, is used at the overlay surfaces $x_2 = \pm h_2$ where only the normal compressional stress is retained to satisfy the free-traction condition while the two shear stresses are ignored ; this approximation limits application to the cases having an h_3/h_2 ratio less than 0.5. In his approach, the problem was treated first by assuming the whole substrate to be perfectly rigid and then the part of substrate corresponding to Region II here was perturbed to be the almost-perfectly-rigid compared with the material of overlay. Three kinds of waves were found: shear, longitudinal and dilatational, all revealing a low-frequency cutoff. No direct comparison with his results has been made because there seems to be little interest in such extreme ratios of substrate-to-layer stiffness, and moreover it seems that in his approach, as pointed out by Oliner (1971b), some fundamental modes such as that corresponding to the first symmetric Rayleigh-like mode are missing.

CHAPTER VII

CONCLUSION

In this thesis an analytical method is developed to solve the wave propagation problem of an important type of elastic surface waveguides, namely, a rectangular overlay superimposed on a half-space substrate. Compared with other current analyses, such as that for thin-film waveguides (Tiersten, 1969; Adkins and Hughes, 1969), the transmission-network approach (Oliner, 1969), the topographic ridge waveguide (Ash et al., 1969; Mason et al., 1971; Lagasse, 1972) and the rigid substrate waveguide (Waldron, 1971), two kinds of generalization are implemented in the type of waveguide analyzed in the thesis. One is geometrical in that the thickness of the overlay as well as the width can be arbitrary and thus we can study the effects of the overlay thickness on the behaviour of such waveguides. The thin-film waveguide is contained as a limiting case. The other generalization concerns materials. The material combination of overlay and substrate is limited only by the guiding requirement that the shear velocity of overlay must be lower than or equal to that of substrate and can be freely chosen. The propagation characteristic and displacement pattern of the flexural mode for the topographic ridge guide are also contained in the analysis through the simple expedient of using the same material parameters for the overlay and substrate, and a rigid-substrate guide is approached by introducing an artificial substrate of increasing rigidity.

The analysis is basically a series expansion method and two different truncations, the (1,1) - and (2,2) - approximations, have been carried out in detail.

The algebra for the (1,1) - approximation can be done explicitly and reasonably accurate dispersion curves can be obtained for a small computation cost, while the (2,2) - approximation is quite complicated and requires iterative search techniques to determine points on the dispersion curves, however both the dispersion and displacement results are more accurate.

The fundamental derivations in the analysis are generalized so that they can be directly applied or easily converted for anisotropic materials, however the detailed exposition and application given here is for isotropic materials. The results reveal that each mode in the overlay waveguides has three components of displacement at any general point in the guided region; in other words, no mode in this waveguide is a real Rayleigh or Love mode though it approaches one or the other when the width parameter becomes infinity due to very large width relative to the wavelength. The more dispersive modes (sR_1', sR_2' and aL_1') in addition to the ordinary modes (sR_1, sR_2, sL_1, aR_1, aR_2 and aL_1) as described by the (2,2) - approximation have been discussed in some detail.

It has been found that for sufficient large values of the thickness parameter, the aL_1 mode acquires velocities much less than that of the infinitely wide layer case and this mode is identified, in the limit where the properties of the overlay and substrate materials are identical, as the first flexural mode for topographic ridge guide. The numerical results using the analysis here agree well with the accurate phase velocity measurements available for this type of guide. A further check on the analysis is provided by the agreement between the dispersion results of thin-film calculations here and the analytic and experimental results previously available for thin-film guides.

The analysis contained in this thesis allows a more complete study of the dispersion curves and displacement patterns for rectangular overlay waveguides than was previously possible. Such studies are important in determining the dispersion associated with a given mode, the material combinations suitable for a given application, the frequency range over which single-mode operation is possible, the optimum means of single-mode excitation and the geometries suitable for the elimination of undesired modes.

Mathematically, variational theories for plates and rectangular bars and the exponential-crested surface waves have been employed in the analysis together with a new procedure that treats the boundary conditions at the interfaces between regions and suggests a technique that may be applicable to other multi-connected regions. For future work, the application of the method to anisotropic materials by generalizing the part of the formulation here that applies only to isotropic materials and the extension of the analysis to piezoelectric materials may be considered.

APPENDIX A

On expanding (4.14) of Chapter III with n,m = 0,1,2, a total of 27 equations, three equations (j = 1,2,3) for every combination of n and m, are obtained for the (2,2) - approximation with the circumflex (^) omitted for c_{ijkl}, $u_k^{(n,m)}$ and ρ:

for n = 0, $d_{jk}u_k^{(0,0)} + iD_{02}c_{1jk2}u_k^{(1,0)} + iD_{03}c_{1jk3}u_k^{(0,1)} - D_{03}G_{3j}^{(0)}/2k = 0$

$$d_{jk}u_k^{(0,1)} + iD_{02}c_{1jk2}u_k^{(1,1)} + iD_{13}c_{1jk3}u_k^{(0,2)} + D_{13}G_{3j}^{(0)}/2k$$

$$- D_{13}(ic_{3jk1}u_k^{(0,0)} + D_{02}c_{3jk2}u_k^{(1,0)} + D_{03}c_{3jk3}u_k^{(0,1)}) = 0$$

$$d_{jk}u_k^{(0,2)} + iD_{02}c_{1jk2}u_k^{(1,2)} - D_{23}G_{3j}^{(0)}/2k$$

$$- D_{23}(ic_{3jk1}u_k^{(0,1)} + D_{02}c_{3jk2}u_k^{(1,1)} + D_{13}c_{3jk3}u_k^{(0,2)}) = 0$$

for n = 1, $d_{jk}u_k^{(1,0)} + i\,D_{12}c_{1jk2}u_k^{(2,0)} + iD_{03}c_{1jk3}u_k^{(1,1)} - D_{03}G_{3j}^{(1)}/2k$

$$- D_{12}(ic_{2jk1}u_k^{(0,0)} + D_{02}c_{2jk2}u_k^{(1,0)} + D_{03}c_{2jk3}u_k^{(0,1)}) = 0$$

$$d_{jk}u_k^{(1,1)} + iD_{12}c_{1jk2}u_k^{(2,1)} + iD_{13}c_{1jk3}u_k^{(1,2)} + D_{13}G_{3j}^{(1)}/2k$$

$$- D_{12}(ic_{2jk1}u_k^{(0,1)} + D_{02}c_{2jk2}u_k^{(1,1)} + D_{13}c_{2jk3}u_k^{(0,2)})$$

$$- D_{13}(ic_{3jk1}u_k^{(1,0)} + D_{12}c_{3jk2}u_k^{(2,0)} + D_{03}c_{3jk3}u_k^{(1,1)}) = 0$$

$$d_{jk}u_k^{(1,2)} + i\,D_{12}c_{1jk2}u_k^{(2,2)} - D_{23}G_{3j}^{(1)}/2k$$

$$- D_{12}(ic_{2jk1}u_k^{(0,2)} + D_{02}c_{2jk2}u_k^{(1,2)})$$

$$- D_{23}(ic_{3jk1}u_k^{(1,1)} + D_{12}c_{3jk2}u_k^{(2,1)} + D_{13}c_{3jk3}u_k^{(1,2)}) = 0$$

for n = 2, $$d_{jk}u_k^{(2,0)} + iD_{03}c_{1jk3}u_k^{(2,1)} - D_{03}G_{3j}^{(2)}/2k$$

$$- D_{22}(ic_{2jk1}u_k^{(1,0)} + D_{12}c_{2jk2}u_k^{(2,0)} + D_{03}c_{2jk3}u_k^{(1,1)}) = 0$$

$$d_{jk}u_k^{(2,1)} + iD_{13}c_{1jk3}u_k^{(2,2)} + D_{13}G_{3j}^{(2)}/2k$$

$$- D_{22}(ic_{2jk1}u_k^{(1,1)} + D_{12}c_{2jk2}u_k^{(2,1)} + D_{13}c_{2jk3}u_k^{(1,2)})$$

$$- D_{13}(ic_{3jk1}u_k^{(2,0)} + D_{03}c_{3jk3}u_k^{(2,1)}) = 0$$

$$d_{jk}u_k^{(2,2)} - D_{23}G_{3j}^{(2)}/2k$$

$$- D_{22}(ic_{2jk1}u_k^{(1,2)} + D_{12}c_{2jk2}u_k^{(2,2)})$$

$$- D_{23}(ic_{3jk1}u_k^{(2,1)} + D_{13}c_{3jk3}u_k^{(2,2)}) = 0 \qquad \text{(A.1)}$$

Here $$d_{jk} = \rho v^2 \delta_{jk} - c_{1jk1}, \quad D_{n2} = 2/C_n kh_2 \text{ and } D_{n3} = 2/C_n kh_3 \qquad \text{(A.2)}$$

serving only to simplify the expression.

APPENDIX B

The overlay partial matrices f_S and f_A to be used in (5.3) and (5.4) have the non-zero elements given by the following relations. For the symmetric modes the diagonal elements are :

$$
\begin{array}{l|l|l}
f_{11} = V_{00}^2 - \delta & f_{22} = V_{00}^2 - 1 & f_{33} = V_{01}^2 - \delta - 3/H_3^2 \\
f_{44} = V_{01}^2 - 1 - 3\delta/H_3^2 & f_{55} = V_{02}^2 - \delta - 15/H_3^2 & f_{66} = V_{02}^2 - 1 - 15\,\delta/H_3^2 \\
f_{77} = V_{10}^2 - 1 - 3\delta/H_2^2 & f_{88} = V_{11}^2 - 1 - 3\delta/H_2^2 - 3/H_3^2 & f_{99} = V_{12}^2 - 1 - 3\delta/H_2^2 - 15/H_3^2 \\
f_{10,10} = V_{20}^2 - \delta - 15/H_2^2 & f_{11,11} = V_{20}^2 - 1 - 15/H_2^2 & f_{12,12} = V_{21}^2 - \delta - 15/H_2^2 - 3/H_3^2 \\
f_{13,13} = V_{21}^2 - 1 - 15/H_2^2 - 3\delta/H_3^2 & f_{14,14} = V_{22}^2 - \delta - 15/H_2^2 - 15/H_3^2 & f_{15,15} = V_{22}^2 - 1 - 15/H_2^2 - 15\delta/H_3^2
\end{array}
\tag{B.1}
$$

where $\delta = (\hat{\lambda} + 2\,\hat{\mu}) / \hat{\mu}$, $H_2 = k\,h_2$, $H_3 = k\,h_3$ and the normalized velocity with the truncation correction factors included is represented by $V_{nm}^2 = r_n\, r_m\, (v / \hat{v}_t)^2$. While the non-zero off-diagonal elements for the symmetric modes are :

$$
\begin{aligned}
& f_{14} = -f_{41}/3 = f_{36}/3 = -f_{63}/5 = f_{10,13} = -f_{13,10}/3 = f_{12,15}/3 = -f_{15,12}/5 = i\,\hat{\lambda} / \hat{\mu}\,H_3 \\
& f_{23} = -f_{32}/3 = f_{45}/3 = -f_{54}/5 = f_{11,12} = -f_{12,11}/3 = f_{13,14}/3 = -f_{14,13}/5 = i / H_3 \\
& f_{17} = -f_{71}/3 = f_{38} = -f_{83}/3 = f_{59} = -f_{95}/3 = i\,\hat{\lambda} / \hat{\mu}\,H_2 \\
& f_{47} = f_{74} = 3\,f_{68}/5 = f_{86}/3 = -3\,\hat{\lambda} / \hat{\mu}\,H_2\,H_3 \\
& f_{7,10} = -3\,f_{10,7}/5 = f_{8,12} = -3\,f_{12,8}/5 = f_{9,14} = -3\,f_{14,9}/5 = 3\,i / H_2 \\
& f_{8,11} = 9\,f_{11,8}/5 = 9\,f_{9,13}/15 = 9\,f_{13,9}/15 = -9 / H_2\,H_3
\end{aligned}
\tag{B.2}
$$

For the antisymmetric modes, the diagonal elements are :

$$
\begin{array}{lll}
f_{11} = V_{00}^2 - 1 & f_{22} = V_{01}^2 - 1 - 3/H_3^2 & f_{33} = V_{02}^2 - 1 - 15/H_3^2 \\
f_{44} = V_{10}^2 - \delta - 3/H_2^2 & f_{55} = V_{10}^2 - 1 - 3/H_2^2 & f_{66} = V_{11}^2 - \delta - 3/H_2^2 - 3/H_3^2 \\
f_{77} = V_{11}^2 - 1 - 3/H_2^2 - 3\delta/H_3^2 & f_{88} = V_{12}^2 - \delta - 3/H_2^2 - 15/H_3^2 & f_{99} = V_{12}^2 - 1 - 3/H_2^2 - 15\delta/H_3^2 \\
f_{10,10} = V_{20}^2 - 1 - 15\delta/H_2^2 & f_{11,11} = V_{21}^2 - 1 - 15/H_2^2 - 3/H_3^2 & f_{12,12} = V_{22}^2 - 1 - 15\delta/H_2^2 - 15/H
\end{array}
\tag{B.3}
$$

using the same parameters as in (B.1) ; and the non-zero off-diagonal elements are :

$$
\begin{aligned}
f_{14} &= -f_{41}/3 = f_{26} = -f_{62}/3 = f_{38} = -f_{83}/3 = i/H_2 \\
f_{25} &= f_{52} = 3 f_{37}/5 = f_{73}/3 = -3/H_2 H_3 \\
f_{47} &= -f_{74}/3 = f_{69}/3 = -f_{96}/5 = i\,\hat{\lambda}/\hat{\mu} H_3 \\
f_{56} &= -f_{65}/3 = f_{78}/3 = -f_{87}/5 = i/H_3 \\
f_{4,10} &= -3 f_{10,4}/5 = f_{6,11} = -3 f_{11,6}/5 = f_{8,12} = -3 f_{12,8}/5 = 3 i\,\hat{\lambda}/\hat{\mu} H_2 \\
f_{7,10} &= 9 f_{10,7}/5 = 3 f_{9,11}/5 = 3 f_{11,9}/5 = -9\,\hat{\lambda}/\hat{\mu} H_2 H_3 \,.
\end{aligned}
\tag{B.4}
$$

REFERENCES

Achenbach, J.D. and Epstein, H.I., (1967), "Dynamic interaction of a layer and a half-space," Proc. ASCE, EM 5, pp. 27-42.

Adkins, L.R. and Hughes, A.J., (1969), "Elastic surface waves guided by thin films : gold on fused quartz," IEEE Trans. on Microwave Theory and Techniques, MTT-17, pp. 904-911.

Ash, E.A., De La Rue, R.M. and Humphreys, R.F., (1969), "Microsound surface waveguides," IEEE Trans. on Microwave Theory and Techniques, MTT-17, pp. 882-892.

Burridge, R. and Sabina, F.J., (1971), "Theoretical computations on ridge acoustic surface waves using the finite-element method," Electronics Lett., 7, pp. 720-722.

Cauchy, A.L., (1828), "Sur l'Equilibre et le Mouvement d'une Plaque Solid," Exercices de Mathematique, 3, pp. 328-355.

Churchill, R. V., (1963), Fourier Series and Boundary Value Problems, McGraw-Hill Book Co., 2nd ed., pp. 200-211.

Eshbach, J.R., (1962), "Spin wave propagation and the magnetoelastic interaction in yttrium iron granet," Phys. Rev. Lett., 8, pp. 357-359.

Farnell, G.W. and Adler, E.L., (1972), "Elastic wave propagation in thin layers," to appear Physical Acoustics, edited by Mason, W.P. and Thurston, R.N., Vol. 9, Academic Press.

Frazer, W.B., (1969), "Stress wave propagation in rectangular bars," Int. J. Solids Structures, 5, pp. 379-397.

Goldren, L.A., (1971), "Monolithic acoustic amplifiers," IEEE Ultrasonics Symposium, Miami Beach, U.S.A., paper F-2.

Gordon, E.I., (1966), "A review of acoustooptical deflection and modulation devices," Proc. IEEE, 54, pp. 1391-1401.

Kirchhoff, G., (1850), "Uber das Gleichgewicht und die Bewegung einer Elastichen Scheibe," Crelles Journal, 40, pp. 51-88.

Lagasse, P.E., (1972), "A higher order finite element analysis of topographic guides supporting elastic surface waves," to appear J. Acous. Soc. Am.

Lagasse, P.E. and Mason, I.M., (1972) "Analysis of propagation in ridge guides for acoustic surface waves," Electronics Lett., 8, pp. 82-84.

Lamb, H., (1917), "On waves in an elastic plate," Proc. Roy. Soc., A93, pp.114-128.

Lim, T.C. and Farnell, G.W., (1968), "Search for forbidden directions of elastic surface-wave propagation in anisotropic crystals," J. App. Phys., 39, pp.4319-4325.

Mason, I.M., De La Rue, R.M., Schmidt, R.V., Ash, E. S. and Lagasse, P.E., (1971), "Ridge guides for acoustic surface waves," Electronics Lett., 7, pp. 395-397.

Mason, W.P., (1958), Physical Acoustics and the Properties of Solids, Van Nostrand, New York, p.17.

Medick, M.A., (1966), "One-dimensional theory of wave propagation and vibrations in elastic bars of rectangular cross section," J. App. Mech., 33, No. 3, pp. 489-496.

- (1968), "Extensional waves in elastic bars of rectangular cross section," J. Acous. Soc. Am., 43, No. 1, pp. 152-161.

Meeker, T.R. and Meitzler, A.H., (1964), "Guided wave propagation in elongated cylinders and plates," in Physical Acoustics, edited by Mason, W.P., 1A, Academic Press, pp. 130-141.

Mindlin, R.D., (1955), "An Introduction to the Mathematical Theory of Vibrations of Elastic Plates," Monograph for U.S. Army Corps Engineering Laboratories, Fort Monmouth, N.J., Signal Corps Contract DA-36-039 SC-56772.

Mindlin, R.D. and Medick, M.A., (1959), "Extensional vibrations of elastic plates," J. Appl. Mech., 26, pp. 561-569.

Morse, R.W., (1950), "The velocity of compressional waves in rods of rectangular cross-section," J.Acous. Soc. Am., 22, pp. 219-223.

Nigro, N.J., (1966), "Steady-state wave propagation in infinite bars of noncircular cross-section," J. Acous. Soc. Am., 40, pp. 1501-1508.

- (1968), "Wave propagation in anisotropic bars of rectangular cross section. I. Longitudinal wave propagation, "J. Acous. Soc. Am., 43, pp 958-965.

- (1969), "II. Flexural wave propagation," J. Acous. Soc. Am., 46, part 2, pp. 639-642.

Oliner, A.A., (1969), "Microwave network methods for guided elastic waves," IEEE Trans. on Microwave Theory and Techniques, MTT-17, pp. 812-826.

- (1971a), "Surface waveguides and waveguide components," IEEE Ultrasonics Symposium, Miami Beach, U.S.A., paper D-1 .

- (1971b), private communication.

Poisson , S.D., (1829), "Memoire sur l'Equilibre et le Mouvement des Corps Elastiques," Memoires de l'Academie des Sciences, series 2, 8, pp. 357-570.

Rayleigh, Lord, (1887), "On waves propagated along the plane surface of an elastic solid," Proc. London Math. Soc., 17, pp.4-11.

- (1889), "On the free vibrations of an infinite plate of homogeneous isotropic elastic matter," Proc. London Math. Soc., 20, pp. 225-234.

Shaw, H.J., (1971), "Long time delays with surface waves," IEEE Ultrasonics Symposium, Miami Beach, U.S.A., paper K-1 .

Stern, E., (1969), "Microsound components, circuits, and applications," IEEE Trans. on Microwave Theory and Techniques, MTT-17, pp.835-844.

Tiersten, H.F., (1969), "Elastic surface waves guided by thin films," J. Appl. Phys., 40, pp. 770-789.

Tu, C.C. and Farnell, G.W., (1971a), "Thick overlay elastic waveguides," European Microwave Conference, Stockholm, Sweden, paper C7.

- (1971b), "Thickness effects in overlay elastic waveguides," IEEE Ultrasonics Symposium, Miami Beach, U.S.A., paper D-3.

- (1972a), "Flexural mode of ridge guides for elastic surface waves," Electronics Lett., 8, pp. 68-70.

- (1972b), "Thickness effects in overlay guides for elastic surface wave," to appear IEEE Trans. on Sonics and Ultrasonics.

Viktorov, I.A., (1967), Rayleigh and Lamb Waves, Plenum Press, New York, Chapter II.

Volterra, E., (1961), "Second approximation of method of internal constraints and its applications," Int. J. Mech. Sci., 3, pp. 47-67.

Love, A.E.H., (1959), A Treatise on the Mathematical Theory of Elasticity, Cambridge University Press and Macmillan Co., 4th ed.

Waldron, R.A., (1969), "Sonic problems in the theory of guided microsonic waves," IEEE Trans. on Microwave Theory and Techniques, MTT-17, pp. 893-904.

- (1971), "Mode spectrum of a microsound waveguide consisting of an isotropic rectangular overlay on a perfectly rigid substrate," IEEE Trans. on Sonics and Ultrasonics, SU-18, pp.8-20.

- (1972), "Microsound waveguides and waveguide components," to be published.

White, D.L., (1962), "Amplification of ultrasonic waves in piezoelectric semi-conductors," J. Appl. Phys., 33, pp. 2547-2554.

- (1967) "Sonic circuits : A waveguide system for ultrasonic surface waves," Symposium on Sonics and Ultrasonics, Vancouver, Canada, paper N1.

White, R.M., (1970), "Surface elastic waves," Proc. IEEE, 58, No. 8, pp. 1238-1276.